



室蘭工業大学

学術資源アーカイブ

Muroran Institute of Technology Academic Resources Archive



## 単調および繰返し載荷条件下での人工軽量盛土材・標準砂混合材料の強度・変形挙動に関する研究

メタデータ	言語: English 出版者: 公開日: 2022-06-30 キーワード (Ja): キーワード (En): 作成者: ジャオ, ヤフエイ メールアドレス: 所属:
URL	<a href="https://doi.org/10.15118/00010861">https://doi.org/10.15118/00010861</a>

**STUDY ON STRENGTH-DEFORMATION BEHAVIOR OF  
ARTIFICIAL LIGHTWEIGHT GEOMATERIALS WITH SAND  
UNDER MONOTONIC AND CYCLIC LOADING CONDITIONS**

**By**

**YAFEI ZHAO**

**A DISSERTATION SUBMITTED TO THE FACULTY OF THE  
MURORAN INSTITUTE OF TECHNOLOGY IN PARTIAL  
FULFILLMENT OF THE REQUIREMENTS FOR THE DEGREE OF  
DOCTOR OF ENGINEERING**



**DIVISION OF CIVIL AND ENVIRONMENTAL ENGINEERING  
MURORAN INSTITUTE OF TECHNOLOGY  
February 2022**



## Acknowledgments

I would like to express my deepest gratitude and sincere appreciation to my supervisor, Professor Dr. Yukihiro Kohata, for his continuous support on my research, giving me the opportunity to perform this research and for his professional supervising, fruitful discussions and constructive suggestions throughout the course of this research. Thank you for your endless guidance and putting up with my frustration.

I also wish to thank Professor Dr. Shima Kawamura and Associate Professor Dr. Noriyuki Sugata, my committee members, for their precious comments and invaluable advices helping me improve the quality of my research.

Special I am grateful to Dr. Yuan Lili for her introduction and recommendation to Muroran Institute of Technology and Professor Kohata before applied for doctor course here.

My sincere thanks are due to Ms. Kozue Takekawa and all the staffs of the Centre for International Relations for making my life in Hokkaido really comfortable and enjoyable. They always extended instant help whenever I needed. Especially thanks to Professor Naoko Yamaji' teaching, my Japanese has been improved much.

The author would like to thankfully appreciate Mr. Kota Takahashi, Mr. Shinpei Yamaji and all our lab group members, Mr. Hiroki Endo, Ms. Rise Ouchi, Ms.Huang Tianxing and Mr. naominzhure as well for their cooperation in experimental works.

I also would like to thankfully appreciate Mr. Masanori Sugawara and Mr. Kiyokatu Sasaki (Koen engineering Co., Ltd.) for their preliminary experiment.

I am indeed indebted to my friends who assisted in life during three years of my doctor course, Mr. Li dongdong, Mr. Zhang shaowei, Ms. Mitsuya, Mr. Ilagaqi, Ms. Ruan Lili, Mr. Zhao yao and Mr. Wang Xinzheng friends here. Thanks to everyone.

Finally, I would like to express sincere thanks to my wife, Ms. Chen Feng for her unlimited patience, understanding, encouragement, and love during three years of research in Japan. Without her continuous support this work would not have been completed. Special thanks to my family members in China for their support and encouragement.



## ABSTRACT

Residual settlement often appears in the soft foundation, which affects the road performance and impact on the normal operation. One way to reduce the effects of residual settlement is reducing the weight of the subbase course. Therefore, the objective of this study is to develop a new lightweight subbase course material to replace the commonly used upper subbase course material. A series of monotonic and cyclic triaxial tests were conducted to investigate the strength and deformation characteristics of the materials.

1. Through the monotonic triaxial tests were conducted under the exhaust and drainage conditions at a constant rate of 0.18 mm/min. The cyclic triaxial tests of specimens were conducted under 10,000 cycles of vertical loading at a frequency of 0.125 Hz, where the vertical stress was changed between  $49.4 \pm 10$  kPa in a sinusoidal wave.

2. Experimental research on the effects of cyclic loading on the strength and deformation under three confining pressures (29.4, 49.0, and 68.6 kPa) of the specimen are analyzed by monotonic triaxial test. The test results revealed that the maximum deviator stress  $q_{max}$  and the initial young's modulus  $E_0$  of specimen increase with the increase of confining pressure. After cyclic loading, the strength and stiffness of specimen becomes greater. It also increases cohesion and decreases friction angle in the specimen.

3. Experimental research on the effects of moisture on the strength and deformation of the specimen are analyzed by monotonic triaxial test. From the results of specimens studied with moisture and without moisture, it was found that maximum deviator stress  $q_{max}$ , the tangential deformation modulus  $E_{tan}$  and the  $E_0$  of the dry specimen were greater than the case of the wet specimen. The moisture also increases the cohesion and decreases the friction angle in the specimen, which reduces the strength and stiffness of the specimen.

4. The effects of moisture, confining pressure and number of cyclic loadings on the deformation characteristics of specimen are analyzed. The results revealed that under three confining pressures (29.4, 49.0, and 68.6 kPa), it was found that the confining pressure has a greater impact on the equivalent young's modulus  $E_{eq}$  of specimen. In addition, the moisture reduces the friction between the particles and the skeleton structure becomes unstable. The  $E_{eq}$  of dry specimen is greater than the case in the wet specimen. The  $E_{eq}$  maintains stable with number of loading cycles of the specimens, all specimens belong to range A in the shakedown range boundaries. It was also found that the Poisson's ratio fluctuates with the increase of loading cycles and the fluctuation range is within 0.05 under the same condition.

**Keywords:** residual settlement, subbase course material, cyclic loading, young's modulus, stiffness, triaxial test, strength, Poisson's ratio



## TABLE OF CONTENTS

TABLE OF CONTENTS .....	I
LIST OF TABLES .....	V
LIST OF FIGURES .....	VI

### CHAPTER 1 INTRODUCTION

1.1 Background .....	1
1.2 Literature Review of lightweight fill materials .....	3
1.2.1 Expanded Polystyrene (EPS) blocks .....	4
1.2.2 EPS bead mixture .....	5
1.2.3 Lightweight air-mixed soil (LWS) .....	7
1.2.4 Rubber-soil mixtures .....	8
1.2.5 Lightweight aggregates(LWA) .....	11
1.3 Objective and scopes .....	14
1.4 Organization of thesis .....	14
References: .....	16

### CHAPTER 2 TSETING MATERIALS, APPARATUS AND METHODS

2.1 Introduction .....	21
2.2 Materials .....	21
2.2.1 Cement standard sand .....	21
2.2.2 Artificial lightweight coarse aggregate .....	22
2.2.3 Testing materials .....	24
2.3 Testing apparatus .....	27
2.3.1 The schematic diagram of the test apparatus .....	27

2.3.2 The medium-size triaxial apparatus .....	28
2.3.2.1 Triaxial cell .....	28
2.3.2.2 Load testing equipment.....	28
2.3.3 Measuring devices .....	30
2.3.3.1 Axial stress measuring device (Load cell) .....	30
2.3.3.2 Apparatus for measuring strain.....	31
2.4 Specimen preparation.....	37
2.4.1 Top-loading vibrator apparatus.....	37
2.4.2 Preparation method .....	37
2.5 Testing scheme design .....	38
2.5.1 Monotonic triaxial tests.....	38
2.5.2 Cyclic triaxial tests.....	40
References:.....	41

**CHAPTER 3 EFFECT OF CYCLIC LOADING ON STRENGTH DEFORMATION OF SPECIMEN**

3.1 Introduction.....	43
3.2 Test principle .....	43
3.3 Relationship between deviator stress and axial strain.....	44
3.3.1 Under dry condition .....	44
3.3.2 Under optimum moisture content condition .....	47
3.4 The maximum deviator stress and Mohr's circle.....	49
3.4.1 Under dry condition .....	49
3.4.2 Under optimum moisture content condition .....	50
3.5 Initial Young's modulus and Tangent Young's modulus.....	52
3.5.1 Definition of the Young's modulus .....	52
3.5.2 Under dry condition .....	53

3.5.3 Under optimum moisture content condition .....	56
3.6 Summary .....	57
References: .....	58

**CHAPTER 4 EFFECT OF MOISTURE ON STRENGTH DEFORMATION OF SPECIMEN**

4.1 Introduction.....	60
4.2 Relationship between deviator stress and axial strain.....	61
4.2.1 Without loading history .....	61
4.2.2 With loading history .....	63
4.3 The maximum deviator stress and Mohr's circle.....	65
4.3.1 Without loading history .....	65
4.3.2 With loading history .....	67
4.4 The Initial deformation modulus and Tangent deformation modulus.....	68
4.4.1 Without loading history .....	68
4.4.2 With loading history .....	70
4.5 Summary .....	71
References: .....	72

**CHAPTER 5 DEFORMATION CHARACTERISTICS OF SPECIMEN UNDER CYCLIC LOADING**

5.1 Introduction.....	74
5.2 Test principle .....	76
5.3 The deformation under cyclic loading .....	77
5.4 Relationship between deviator stress and axial strain.....	80
5.4.1 Under dry condition .....	80
5.4.2 Under optimum moisture content condition .....	82
5.5 Equivalent young's modulus and number of loading cycles .....	83
5.6 Relationship between radial strain and axial strain.....	85

5.6.1 Under dry condition .....	85
5.6.2 Under optimum moisture content condition .....	88
5.7 Poisson's ratios and number of loading cycles .....	88
5.8 Relationship between volumetric strain and axial strain.....	90
5.8.1 Under dry condition .....	90
5.8.2 Under optimum moisture content condition .....	93
5.9 Dilatancy properties under cyclic loading.....	95
5.10 Summary .....	96
References:.....	97

## **CHAPTER 6 CONCLUSIONS**

6.1 Introduction.....	102
6.2 Effect of cyclic loading on strength deformation of specimen (Chapter 3) .....	102
6.3 Effect of dry and wet state on strength deformation of specimen (Chapter 4).....	102
6.4 Deformation characteristics of specimen under cyclic loading (Chapter 5) .....	103
6.5 Recommendations.....	103

## LIST OF TABLES

Table 2.1 The grading requirements of EN 196-1 and of ISO 679: 2009 .....	22
Table 2.2 Physical properties of cement standard sand .....	22
Table 2.3 Chemical composition of cement standard sand, unit (%).....	22
Table 2.4 Particle passing rate of the artificial lightweight coarse aggregate .....	24
Table 2.5 Physical properties of the artificial lightweight coarse aggregate.....	24
Table 2.6 Physical properties of the testing materials.....	25
Table 2.7 The initial conditions of all specimens for monotonic triaxial test .....	39
Table 2.8 The initial conditions of all specimens for cyclic triaxial test.....	41
Table 5.1 The dilatancy properties under different numbers of cyclic loading.....	95



## LIST OF FIGURES

Figure 1.1 Pavement system .....	2
Figure 1.2 A crack and differential settlement in the road.....	2
Figure 1.3 Recurring failure in repair area.....	3
Figure 1.4 EPS blocks.....	4
Figure 1.5 EPS bead mixture .....	6
Figure 1.6 Lightweight air-mixed soil .....	7
Figure 1.7 Rubber-soil mixtures .....	9
Figure 1.8 Lightweight aggregates.....	12
Figure 1.9 Flow chart of this dissertation.....	15
Figure 2.1 Cement standard sand.....	21
Figure 2.2 Grain-size distribution of sand.....	21
Figure 2.3 The artificial lightweight coarse aggregate.....	23
Figure 2.4 Grain-size distribution of coarse aggregate .....	23
Figure 2.5 The manufacturing process of artificial lightweight coarse aggregate .....	23
Figure 2.6 The testing materials.....	25
Figure 2.7 Grain-size distribution of testing materials.....	25
Figure 2.8 The compaction curve of the testing materials by vibrating compaction .....	26
Figure 2.9 Grain-size distribution of testing materials before and after triaxial testing.....	26
Figure 2.10 The schematic diagram of the test apparatus .....	27
Figure 2.11 A schematic of the triaxial cell .....	28
Figure 2.12 Load testing equipment .....	30
Figure 2.13 Calibration result of the load cell (Ch.1) .....	30
Figure 2.14 Calibration result of the dial gauge (Ch.2) .....	32
Figure 2.15 Calibration result of the LDT1 (Ch.3) .....	34
Figure 2.16 Calibration result of the LDT2 (Ch.4) .....	34

Figure 2.17 Calibration result of the horizontal gap sensor (Ch.7).....	35
Figure 2.18 Calibration result of the horizontal gap sensor (Ch.8).....	35
Figure 2.19 Calibration result of the horizontal gap sensor (Ch.9) .....	36
Figure 2.20 Calibration result of the horizontal gap sensor (Ch.10) .....	36
Figure 2.21 Top-loading vibrator apparatus.....	37
Figure 2.22 Specimen preparation .....	38
Figure 2.23 Sinusoidal waveform loading curve for cyclic triaxial test .....	40
Figure 3.1 Mohr stress circles and stress path in constant confining pressure failure tests .....	44
Figure 3.2 The stress-strain behavior of the specimens under the dry condition without cyclic loading .....	46
Figure 3.3 The stress-strain behavior of the specimens under the dry condition with cyclic loading .....	46
Figure 3.4 The stress-strain behavior of the specimens under the wet condition without cyclic loading .....	48
Figure 3.5 The stress-strain behavior of the specimens under the wet condition after cyclic loading .....	48
Figure 3.6 The peak strength-confining pressure behavior of the specimens under dry condition.....	49
Figure 3.7 The Mohr's circles in peak stress state under dry condition .....	50
Figure 3.8 The peak strength-confining pressure behavior of the specimens under optimum moisture content condition .....	51
Figure 3.9 The Mohr's circles in peak stress state under optimum moisture content condition .....	52
Figure 3.10 Definition of different Young's modulus.....	53
Figure 3.11 Initial Young's modulus calculation method .....	53
Figure 3.12 The relationship between confining pressure and initial deformation modulus under dry condition .....	55
Figure 3.13 The relationship between axial strain and tangential deformation modulus without cyclic loading .....	55
Figure 3.14 The relationship between the axial strain and tangential deformation modulus after cyclic loading .....	55
Figure 3.15 The relationship between confining pressure and initial deformation modulus under optimum moisture content condition.....	56

Figure 3.16 The relationship between axial strain and tangential deformation modulus without cyclic loading	57
Figure 3.17 The relationship between the axial strain and tangential deformation modulus after cyclic loading	57
Figure 4.1 The stress-strain behavior of the specimens without loading history under dry condition	63
Figure 4.2 The stress-strain behavior of the specimens without loading history under wet condition	63
Figure 4.3 The stress-strain behavior of the specimens with loading history under dry condition	64
Figure 4.4 The stress-strain behavior of the specimens with loading history under wet condition	64
Figure 4.5 The peak strength-confining pressure behavior of the specimens without loading history	65
Figure 4.6 The Mohr's circles in peak stress state without loading history	66
Figure 4.7 The peak strength-confining pressure behavior of the specimens with loading history	67
Figure 4.8 The Mohr's circles in peak stress state with loading history	68
Figure 4.9 The relationship between confining pressure and initial deformation modulus without loading history	69
Figure 4.10 The relationship between the axial strain and tangential deformation modulus under dry condition	69
Figure 4.11 The relationship between axial strain and tangential deformation modulus under wet condition	69
Figure 4.12 The relationship between confining pressure and initial deformation modulus with loading history	70
Figure 4.13 The relationship between the axial strain and tangential deformation modulus under dry condition	71
Figure 4.14 The relationship between axial strain and tangential deformation modulus under wet condition	71
Figure 5.1 Stress regimes experienced by a pavement element under a moving wheel load	74
Figure 5.2 Schematic representation of triaxial stress system	77
Figure 5.3 Hysteresis loop of different number of loading cycles	78
Figure 5.4 Strains in the testing materials during one load cycle	79

Figure 5.5 The stress-strain behavior of the specimens in the dry condition under different confining pressure .....	81
Figure 5.6 The stress-strain behavior of the specimens in optimum moisture content condition under different confining pressure.....	82
Figure 5.7 The relationship between number of loading cycles and equivalent young's modulus .....	85
Figure 5.8 The lateral strain-axial strain behavior of the specimens in dry condition under different confining pressure .....	86
Figure 5.9 The lateral strain-axial strain behavior of the specimens in optimum moisture content condition under different confining pressure .....	87
Figure 5.10 The relationship between number of loading cycles and Poisson's ratios .....	90
Figure 5.11 The volumetric strain-axial strain behavior of the specimens in dry condition under different confining pressure.....	92
Figure 5.12 The volumetric strain-axial strain behavior of the specimens in optimum moisture content condition under different confining pressure .....	94

**CHAPTER 1**  
**INTRODUCTION**



## 1.1 Background

The road network of a developed country is a valuable asset that supports the economy, freight transportation, and level of living of the country. Around the world, road networks, which serve as a framework for infrastructure, are fueling economic development. Road systems are said to cover more than 14 million km of worldwide land area (e.g., Strano, et al., 2017; Wang et al., 2021), and the total length of new roads is predicted to increase by 25 million km by 2050, which is more than 60 percent more than in 2010 (William, et al., 2014). Nowadays, the world's roads must transport at least nine trillion tons kilometers of freight and fifteen trillion kilometers of passengers each year (e.g., Neff, et al., 2010; Iaych, 2010), implying that a country's prosperity is tightly linked to its road network construction (e.g., Laurance et al., 2009; Richard et al, 2013). With 6.85 million kilometers of road, the United States now boasts the world's largest road network, while Japan ranks sixth with 1.22 million kilometers (Contributors et al., 2019).

For the next ten years, the majority of the roads and bridges were built during Japan's boom phase and will be 50 years old. However, with aging road and bridge infrastructure, restoration of old, deteriorated highways is becoming more necessary (Huang, Y., 1993). There are two types of road pavements: flexible pavements and rigid pavements. Bituminous (or asphalt)-coated pavements are known as flexible pavements. A top layer of Portland cement concrete is used to create rigid sidewalks (Road Bureau, 2018). Flexible pavements are often used due to many years of knowledge and experience. The typical flexible pavement structure consists of a surface course, base course and subbase course, as shown in **Fig. 1.1**. Surface course is the top layer and the layer in contact with traffic. It can consist of one or more different hot mix asphalt sub-layers. Base course is the layer directly under the hot-mix asphalt layer and usually consists of aggregates. Subbase course is the layer (or layers) below the base course and above the subgrade. The base course and the subbase course play a crucial role in absorbing the loads, especially traffic loads, and distributing them over the subgrade.

In a flexible road system, the base and subbase layers are the main layers that bear the load. These layers can provide as a working platform for an asphalt surface layer, as well as providing structural stability. The wheel load is dispersed across a broader area on the subgrade by densely graded unbound granular materials in the base course substructure. Subbase course in Japan is divided into two parts: upper subbase base course and lower

subbase base course. The stiffness and strength requirements of the upper subbase course are higher than those of the lower subbase course because it directly bears the stresses transmitted from the base course (Rodriguez et al., 1988).

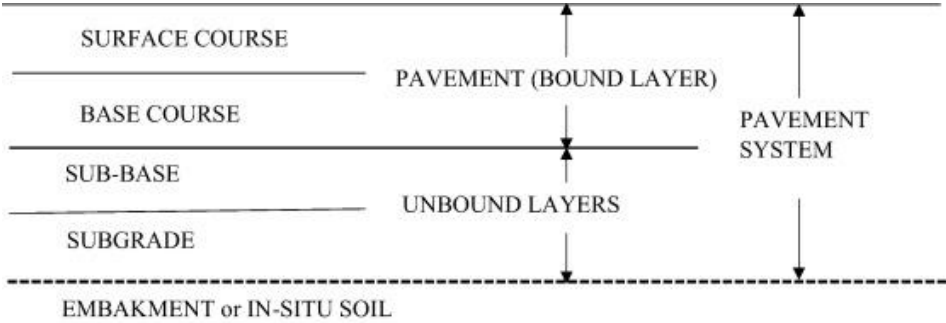


**Fig. 1.1** Pavement system (Gautam et al., 2018)

When roads, motorways, and railways are built on top of soft soils, inadequate bearing capacity and excessive settlement are very common and serious problems. Unbound granular material layers, as is widely known, play the most essential structural role in road pavements since, in most situations, the soil subgrade ensures enough bearing capacity. As traffic volumes and weights increase, the base and subbase gradually deteriorate due to cyclic traffic loadings and changes in the surrounding environment, rutting occurs on the surface layer, resulting in pavement depression and progressive fatigue cracking of bituminous layers (e.g., Erlingsson et al., 2013; Saberian et al., 2019; Chen et al., 2019), which causes problems that can significantly affect safety operations, as shown in **Fig. 1.2**.

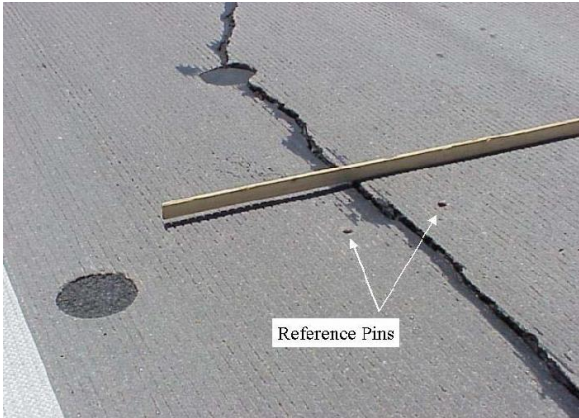


**Fig. 1.2** A crack and differential settlement in the road (Ardani. A. et al., 2003)

It is vital to repair and resurface this aged infrastructure in order to ensure its safety. The most common way of restoration is to excavate and resurface the sinking area of the pavement. To decrease the negative impact of repaving on the usual traffic of the road and to shorten the repaving period, the pavement will be restored directly without digging out the damaged pavement on routes with high traffic flow and only local settlement. The weight load absorbed by the road foundation will increase for some roads built on soft soil layers as the pavement thickness increases after repaving. As demonstrated in **Fig. 1.3**, the pavement frequently creates rutting and cracking of the bituminous layers, resulting in recurring failure in the repair region, reducing the road service length and increasing road maintenance expenses.



**Fig. 1.3** Recurring failure in repair area (Chen et al., 2013)

## 1.2 Literature review of lightweight fill materials

The size of primary settlements induced by embankments erected on soft soil layers is a function of increased vertical tension caused by the embankment. As a result, using lighter materials in the embankment minimizes the size of these communities. Chipped bark, natural lightweight aggregate (i.e. pumice), dried peat, shredded tires, cinders, slag, fly ash, sawdust, cellular (foamed) concrete, and expanded polystyrene have all been utilized in embankment and fill construction (geofoam or EPS). Expanded clay, slate, and shale, and tire-derived aggregate, "ash-rock" aggregate made entirely of coal ash have all grown in popularity due to their low cost (Holtz and Schuster, 1996).

The following mainly reviews the five most commonly used types of lightweight subgrade backfill materials.

### 1.2.1 Expanded polystyrene (EPS) blocks

In geotechnical engineering, the ASTM D6817 (2007) Standard defines EPS as a planar or block rigid cellular foam polymeric material. Expanded polystyrene (EPS) is a type of foamed plastic created by the expansion of polystyrene resin beads during the molding process. EPS is made in the form of a block with certain dimension tolerances (UNI EN 13163, 2009). Water absorption is roughly 2-5 % of the specimen volume, with bulk density ranging from 10 to 40 KN/m<sup>3</sup>. The first successful use of EPS blocks as an experimental lightweight geo-material was in Norway, where they were utilized as backfill in an embankment on soft ground, effectively lowering the upload (Preber et al., 1995). From 1985 to 1997, Japan was the largest market for geofoam applications, with over 1.7 million m<sup>3</sup> of EPS blocks used for airport taxiways (see **Fig. 1.4**). (e. g. Aytekin, 1997; Horvath, 1997; Beinbrech and Hillmann, 1997) have undertaken numerous investigations on the properties of EPS blocks and the related design difficulties.



**Fig. 1.4** EPS blocks

According to Montepara et al. (2000), geofoam is an acceptable alternative to natural aggregates for the construction of an embankment on a soft subgrade. EPS blocks allow for a very light structure while eliminating all of the issues associated with embankment foundation settlement. This is especially true when speedy road reconstruction is required to address the serious issues caused by landslides.

EPS blocks have a high compressive resistance and may thus support traffic loadings on minor and interstate highways. EPS also removes the requirement for compaction and fill testing, shortens construction time, and lowers the impact on existing roadways, surrounding structures, and subsurface utilities (El-Didamony et al., 1997).

Horvath (1994) and Stark et al. (2004) address the many advantages of employing EPS block geofoms in depth. However, there are several drawbacks to using ESP blocks in applications. These include: (1) the ESP blocks must be prefabricated off-site, requiring transportation; (2) the ESP blocks must be made into regularly shaped blocks, preventing them from being easily used to fill an irregular volume; and (3) the stiffness and properties of EPS cannot be easily changed to suit the soil properties on-site.

### **1.2.2 EPS bead mixture**

The EPS beads are made from expandable polystyrene resin beads with microscopic cells filled with a blowing agent and a diameter of less than 3 mm (usually pentanes or butanes). Adjusting the EPS to other materials ratio (such sand, soil, cement) can readily vary the density and other attributes of the EPS beads mixed lightweight fill (e.g., Takashi et al., 2001; Nicholas et al., 2013 and Edinçliler et al., 2014). The wet density of lightweight soil in the field is in the range of 1.0-1.2 g/cm<sup>3</sup>, but the similar range in the laboratory is 0.7-1.3 g/cm<sup>3</sup>. As a result, as illustrated in **Fig. 1.5**, the goal of reducing self-weight and applied forces caused by embankment on soft ground is easily realized. Lightweight fill materials formed by mixing EPS beads with dirt and cement can be used as a substitute to EPS blocks when their use becomes impractical. It's very well suited to filling voids, irregularly shaped subsurface entrances, and rehabilitation projects. Another advantage of EPS beads mixed lightweight fill over EPS blocks is that it can be employed in circumstances that need higher compressive pressures than EPS blocks can give.



**Fig. 1.5** EPS bead mixture

Some researchers blended EPS particles with sand to make a lightweight fill and used direct shear and triaxial compression tests in the lab to determine the stress–strain characteristics of the amended soils (e.g., Liu et al., 2006; Deng et al., 2010). Recent studies and applications of EPS beads mixed lightweight fill include the use of lightweight fill made by mixing dredged mud with EPS beads and cement for reclamation (e.g., Tsuchida et al., 2001; Yoonz et al., 2004), the use of EPS beads mixed lightweight fill for embankment on a soft foundation (Sato et al., 2001), and the use of EPS beads mixed lightweight fill for embankment on a hard foundation (Ma, 2003). Liu et al. (2006) published a laboratory investigation on the effects of varied compositions and ratios of EPS beads and soil, cement and soil, water and soil on the density, compressive strength, and deformation of the lightweight fill.

The mechanical characteristics of a lightweight EPS bead mixture under static loading were explored by Minegishi et al. (2002) and Chun et al. (2004). Under dynamic loading, Gao et al. (2011) investigated the mechanical characteristics of a lightweight EPS bead mixture. Empirical and analytical methodologies are used to create a unified deformation-strength framework. At the same time, cyclic stress–strain equations and Modulus Reduction Curves for EPS bead mixtures with various mixture ratios are discussed.

Dredged sand was combined with EPS beads and Portland cement by Miao et al. (2012). They carried out a variety of geotechnical studies to see if they may be used to mitigate settlement issues associated with bridge approach embankments in soft soil. Padade and Mandal (2014) suggested a geomaterial made of fly ash, EPS beads, and cement instead of soil. The compressive strength of an EPS bead mixture increases significantly when

cement-to-fly ash ratios of 10%, 15%, and 20% are utilized, according to compression experiments.

For a single type of EPS bead–sand mixture, Deng and Xiao (2009, 2010) investigated the stress–strain behavior of EPS–sand. With increasing EPS content, they demonstrated a systematic decline in drained strength.

### 1.2.3 Lightweight air-mixed soil (LWS)

Air bubbles and water are mixed with construction waste or in-situ soils and cement to create a lightweight air-mixed soil (LWS). The density of soil slurry can be adjusted in the range of roughly  $10 \text{ kN/m}^3$ , but due to the effect of quality control variables, density control may be limited to meet the needed parameters (for instance, compression strength, slump, and dissipation air bubbles). LWS has a number of benefits. First, because it is lighter than dirt, it may lower the strain on the ground, and because of its great fluidity, it can be moved by pumping. It's also simple to put together because it doesn't require any compaction, as seen in **Fig. 1.6**. It has long been recognized as a useful material for soft ground banking, backfilling retaining walls, backfilling structures, and stuffing settlement ground, among other applications (e.g., Kim and Lee, 2002; Kim et al., 2007). It has a wide range of potential applications as a result of these benefits (e.g., Hayashi et al., 2002; Miki et al., 2003; Jamnongpipatkul et al., 2009).



**Fig. 1.6** Lightweight air-mixed soil

Because it is a combination material, past studies on LWS have found that the compression strength of LWS

is influenced by the initial moisture content of the soil sample, the cement percentage, the air bubble percentage, and the curing technique (Kim and Lee, 2002). By examining the elements impacting quality, Yoon and Kim (2004) established a method to estimate the unconfined compression strength of LWS in line with the mixing combination. They developed a regression equation for the unconfined compression strength represented as a normalized coefficient in terms of the initial moisture content of in-situ soil, cement percentages, and air bubble percentages. The normalized coefficient was also shown to be strongly dependent on the soil utilized to prepare the lightweight air-mixed soil in this investigation. Because the elements of the in-situ soil were different, the unconfined compression strength of LWS varied. If the in-situ soil's coefficient of curvature grows, the density and strength differential between the upper and lower parts of the constructed LWS increases. When the coefficient of curvature varies dramatically, the fraction of coarse-grained soils increases, and the rate of air bubble dissipation increases. When employing such a soil, it was advised that construction be limited to specified in-situ soils (Song et al., 2008). Other researchers conducted similar investigations focusing on the strength in the laboratory (Hayashi et al., 2002; Yajima and Mydin, 2006). Kim et al.(2013) investigated the unconfined compression strength and capillary rise of lightweight soil, as well as the settlement of soft ground, and discovered that the unconfined compression strengths of samples cured at the site for 1 or 5 months met the required goal strength of 500 kPa.

#### **1.2.4 Rubber-soil mixtures**

Waste tire rubber and sand mixtures have been progressively employed as a new type of subgrade filler in highway and railway engineering (Bosscher et al., 1997 ; Krystyna, 2007), due to their low unit weight, strong linear elastic deformation ability, good durability, and high energy dissipation (Garga et al., 2000 ). Many studies have been interested in the mechanical properties of waste tire rubber-sand combinations, as seen in **Fig. 1.7**.



**Fig. 1.7** Rubber-soil mixtures

By adding flexible tire shred to the sand, Zornberg et al., (2004) discovered that the ductility of tire shred-sand mixes can be increased; the shear strength of the mixtures scaled nonlinearly with the rubber tire shred content, with an ideal tire shred content of roughly 35 %. Bergado et al., (2005) studied the effect of rubber tire chips content on the shear behavior of flat rubber tire chip-sand mixes and discovered that as the rubber tire chips content grew, the shear strength of the mixtures dropped. According to Noorzad and Raveshi (2017) research, the shear strength of tire-sand mixes dropped as the tire crumb content increased. Other relevant research, such as (Foose et al., 1996; M.F. Attom, 2006), suggested that altering the waste tire composition might greatly improve the shear strength of waste tire and sand combinations.

Mashiri et al. (2016) observed that a tire chip content of 20 % to 40 % lowered the liquefaction potential of sand-tire chip mixtures. The dynamic properties and strength characteristics of rubber-soil mixes can be modified through the proportion of rubber content for different design applications, according to Anastasiadis et al. (2012) findings also showed that waste tire rubber might lower dynamic pore water pressure and improve saturated sand liquefaction resistance. On the other hand, found that adding rubber granules to saturated sand boosted its liquefaction potential. (Senetakis et al., 2012 ; Kaneko et al., 2013) investigated the features of the shear modulus and damping ratio with varying tire rubber content at modest strain levels, concluding that the shear modulus fell and the damping ratio rose as tire rubber content increased. Their findings support the use of tire rubber as an energy dissipation and vibration isolation material. Sotiris et al. (2016) discovered that using rubberised backfill reduces backfill settlements, bridge deck horizontal displacements, residual horizontal displacements of

the top of the abutment, and pressures acting on the abutment by up to 55, 18, 43, and 47 percents, respectively, when compared to using clean sand backfill.

Under four levels of normal stress, Ali et al. (2021) conducted direct shear tests to examine the strength and deformation properties of two types of gravel-granulated tyre rubber (G-GTR) mixtures (6.5, 30, 60, and 100 kPa). Using a combination of small and large rubber particles combined with a rounded uniform gravel, mixtures with varied volumetric rubber content (VRC) of 0 percent, 10%, 25%, 40%, and 100% were created. The findings revealed that VRC and normal stress are the most important factors influencing the mechanical behavior of G-GTR mixes, with rubber size having a greater impact at lower VRC. A framework with compressibility and strength performance-based criteria for the selection of G-GTR mixtures as structural fillers for geotechnical applications is proposed based on the experimental data. Manohar and Anbazhagan (2021) used an Unconsolidated Undrained (UU) triaxial test to explore the shear strength characteristics of a geosynthetic-reinforced rubber-sand mixture (RSM). RSM reinforced with geosynthetic has higher peak strength, failure strength, and axial strain at failure, according to the findings. For dry combinations of sand/rubber (SRM) and gravel/rubber (GRM), Senetakis et al.(2012) provide general normalized shear modulus and damping ratio against shearing strain amplitude curves suitable for engineering practice. Finally, they describe prior investigations' analytical equations for small-strain shear modulus and damping ratio for SRM and GRM. Zhuo et al. (2021) presented a technique for analyzing the macroscopic and micromechanical parameters of LFM through stress–strain change and contact force chain distribution by combining numerical simulation and model testing. The model test takes into account some characteristics that affect earth pressure, structural deformation, and soil settlement, such as the LFM fill height and embedding depth. The results show that when the rubber fraction by volume (RF) is between 30 and 45 percent, the LFM deformation and load-bearing capability are the most stable. Furthermore, the stress concentration at the top center of the CCT can be minimized by choosing a suitable rubber percent by volume (RF = 40%) and backfill height (between 0.63 and 0.83 times the height of the CCT).

Saeed et al. (2020) used dynamic hollow cylinder tests to study various aspects of dynamic behavior of sand-rubber mixtures over a wide range of shear strains. The impacts of numerous parameters such as relative density,

rubber content, confining tension, and rubber particle size were explored in depth for this aim. The findings showed that rubber content and confining stress values influenced the dynamic properties of sand-crumb rubber mixtures the most, whereas relative density and rubber particle size were less effective. Furthermore, it was discovered that the dynamic behavior of the mixtures was completely strain-dependent, with an increase in rubber content leading to higher damping ratios at strain ranges lower than a threshold value, which was determined by the applied confining stress, while a reverse trend was observed at strain levels higher than the threshold value.

### **1.2.5 Lightweight aggregates(LWA)**

Lightweight aggregates (LWA) (Ayati et al., 2018) are minerals, natural rock materials, rock-like products, and manufacturing process by-products used as bulk fillers in lightweight structural concrete, concrete building blocks, precast structural units, road surfacing materials, plaster aggregates, and insulating fill in lightweight structural concrete, concrete building blocks, precast structural units, road surfacing materials, and insulating fill. LWA are granulated materials (Mason et al., 1994) mainly obtained directly from natural resources, like pumice, perlite, volcanic scoria, and ashes (Bogas and Cunha, 2017), manufactured by firing in a kiln raw materials with expansive properties like vermiculite, shale, clay or secondary materials (like waste glass, sewage sludge ash, incinerator bottom ash, mining residues), at temperatures from 1,000 °C to 1,300 °C (rapid sintering) (Dondi et al., 2016; Quina et al., 2014) as shown in **Fig. 1.8**. LWA was first manufactured from clay and shale sintered in a rotary kiln in 1917. Under high-temperature heating, certain elements present in the raw materials expand, thus forming a hard vitrified layer on the surface (Short and Kinniburgh, 1976). Since then, sintering of LWA has mainly been performed in a rotary kiln. Sintering sewage sludge ash (SSA) at 1040 ~ 1100 °C, Bhatta and Reidt (1989) had successfully manufactured LWA with bulk density of 0.8~1.4 g/cm<sup>3</sup> in large quantity and at low cost.



**Fig. 1.8** Lightweight aggregates

Manosa et al.(2021) make lightweight aggregates by substituting sludge for expanded clay up to 50% by weight. The physical properties of lightweight aggregates were investigated, including bloating index, density, and porosity. The use of expanded clay and water treatment sludge to make lightweight aggregates with low replacement percentages is demonstrated (up to 15 wt percent of sludge). Lytag is the most popular LWA in the UK, and it's made from sintered fly ash (pulverized fuel ash), a by product of coal-fired power plants (Owens, 1993). The influence of glass addition on the processing, physical characteristics, and microstructure of lightweight aggregate formed from lignite coal fly ash from the Megalopolis power station in Greece was examined by Kourti and Cheeseman (2010). Megalopolis fly ash coupled with waste glass can be utilized to make lightweight aggregate with qualities equal to commercially available materials, according to the research. Fly ash and glass, which are currently waste products in Greece, are potential resources. Ducman et al. (2002) looked into the possibility of using discarded glass to make lightweight aggregate. By granulating waste glass with an expanding agent and heating the material to 880 °C in a rotating kiln, a lightweight aggregate based on powdered waste glass was created.

Cheeseman and Viridi (2005) studied the characteristics of lightweight aggregate (LWA) made from ash produced by sewage sludge incineration in a fluidized bed. The ash was combined with a clay binder, shaped into roughly spherical pellets, and sintered quickly in a rotary tube furnace at temperatures ranging from 1020 to 1080 °C. The density (apparent specific gravity), water absorption, and compressive (crushing) strength of sintered ash pellets relevant to their use as lightweight aggregate have all been determined.

Chiou et al. (2006) used sewage sludge ash (SSA), which has properties similar to expansive clay, as the main material and sewage sludge (SS) as an admixture to sinter lightweight aggregate and investigate the effects of raw material composition on pelletizing, sintering effect, and aggregate properties. The results demonstrated that both SS and SSA may be sintered separately or in combination to form synthetic aggregates.

Huang et al. (2007) looked into the production of artificial lightweight aggregate (LWA) using recycled materials. Mining waste, incinerator fly ash, and electronic waste water plant heavy metal sludge were blended into raw aggregate pellets and put into a tunnel kiln to be sintered and quickly cooled. The impact of different feeding and sintering temperatures on the extent of vitrification on the aggregate surface was investigated. Toxicity characteristic leaching procedure (TCLP) and microstructural analyses were also carried out. The results reveal that sintering at 1150 °C for 15 minutes with raw aggregate pellets fed at 750 °C is the best condition for LWA fabrication.

Gennaro et al. (2004) look into the possibility of using Italian zeolitic rocks to make lightweight aggregates. The expansion at high temperatures as well as the technological characteristics of burnt products were studied in particular. The study included fifteen zeolite-bearing volcanoclastites from Northern Sardinia, as well as three zeolitized tuffs from Campania and Tuscany (Sorano and Campanian ignimbrites, and Neapolitan Yellow Tuff). The results reveal that some products are extremely water resistant (water absorption less than 1%), have a large fire expansion (>100% in volume), a low bulk density (0.5–0.7 gcm<sup>3</sup>), and good technical qualities (loose weight and strength of particles). These zeolitic rocks from Italy can be utilized to make lightweight aggregates.

Sugawara et al. (2019) used a physical experiment to investigate the possibilities of adopting a lightweight geo-material as a subbase course material. This material's coarse aggregate is constructed of expanded shale that has been fired and foamed expansively at a high temperature. The weight of lightweight geo-material is 2/3 that of standard material, according to the findings. As a subbase course material for asphalt pavement, the percentage of wear is 25.8%, which meets the specified standards. The frost heave rate is 0.2 to 0.3 percent, and the material is non-frost heaving. The triaxial shear property of this lightweight geo-material was investigated by Kohata et al. (2019). The maximum deviator stress of this material is 60 percent that of typical materials, according to the data. The internal friction angle is 39 °, which meets the standards for use as a subbase course material for asphalt

pavement. Sugawara et al. (2020) investigated the strength of this lightweight geomaterial following particle crushing. The breakage rate is 4.5%, according to the findings. The sample's maximal deviator stress before and after crushing is almost unchanged. The internal friction angle before and after crushing is 42° degrees, which meets the standards for use as a subbase course material for asphalt pavement. Sugawara et al. (2021) investigated the foundation of a man-made lightweight geomaterials-standard sand mixed soil. This material's coarse aggregate is formed of expanded shale and sewage sludge that has been fired and foamed expansively at high temperatures. The results suggest that the breakage rate is ten percent. At a compaction degree of 95%, the CBR is 50%.

### **1.3 Objective and scopes**

The residual settlement issues that would be imposed by traditional soil fill loads, the use of lightweight fill material is an effective solution. The purpose of this study is to develop a new lightweight subbase course material to replace the commonly used upper subbase course material, which can reduce the load borne by the road subgrade. The strength and deformation characteristics are analyzed by monotonic triaxial test and cyclic triaxial test, the objectives in this study are shown follows.

- (1) To examine the effect of cyclic loading on strength and deformation characteristics of the lightweight subbase course material by the monotonic triaxial test.
- (2) To examine the effect of moisture on strength and deformation characteristics of the lightweight subbase course material by the monotonic triaxial test.
- (3) To examine the effect of moisture, confining pressure and number of cyclic loadings on the deformation characteristics of the lightweight subbase course material during cyclic loading.

### **1.4 Organization of thesis**

This thesis introduces effects of cyclic loading on the strength and deformation characteristics of the lightweight subbase course material by the monotonic triaxial test, along with deformation characteristics influenced by moisture during cyclic loading. The layout of the research approach is described in **Fig. 1.9**.

The thesis is divided into 6 chapters. A brief summary of the chapters is as follows.

Chapter 1 presents the research background, literature review related to the lightweight fill material and objectives of this thesis.

Chapter 2 is devoted to describing the testing material and testing methods.

Chapter 3 presents the effect of cyclic loading on the test results of monotonic triaxial tests.

Chapter 4 presents the effect of moisture on the test results of monotonic triaxial tests.

Chapter 5 discusses the effect of moisture on deformation characteristics of specimen during cyclic loading.

Chapter 6 summarizes all of the findings in this study and provides suggestions for the future work.

The following is this thesis structure:

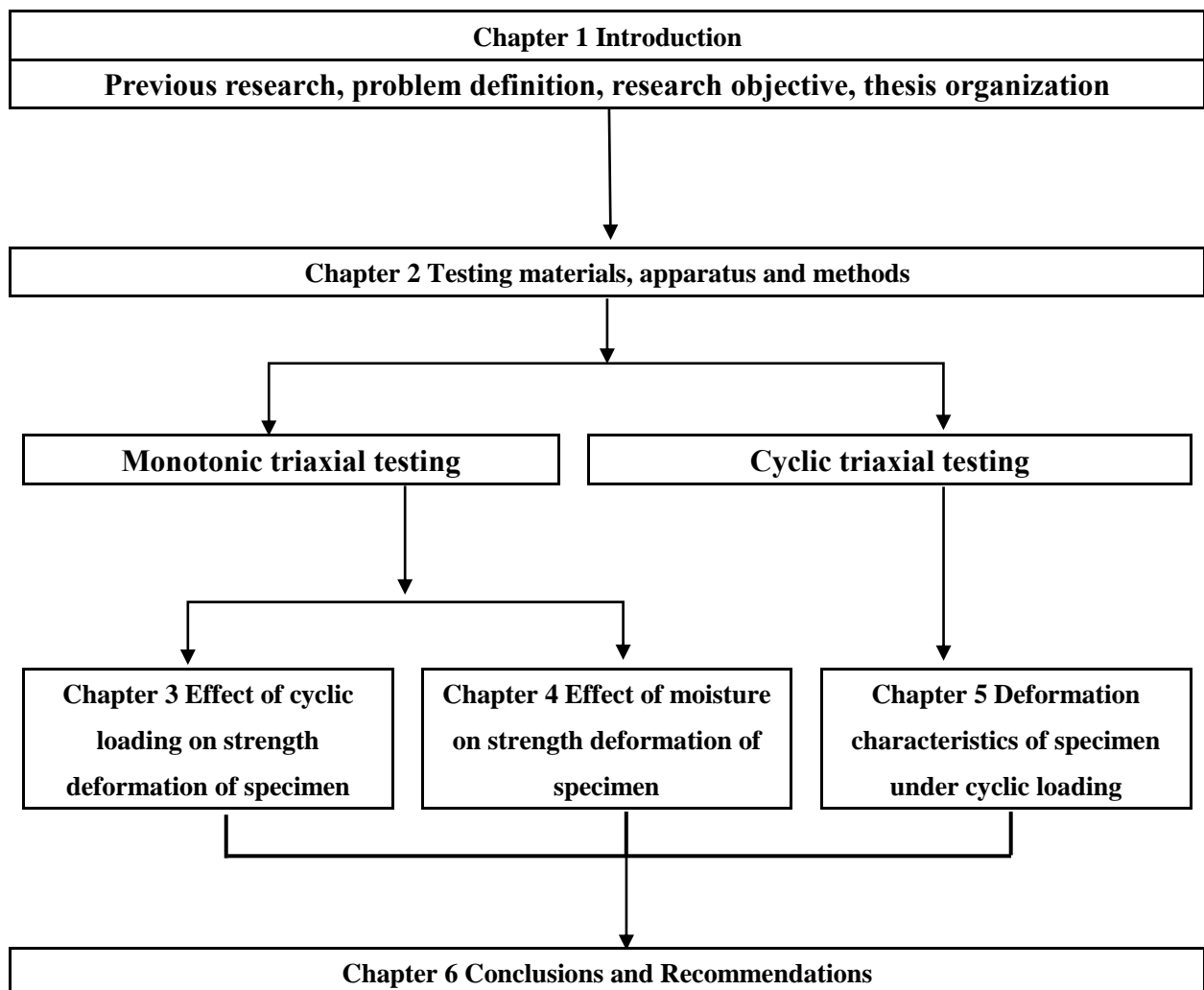


**Fig. 1.9** Flow chart of this dissertation

## References:

- Ali, T., Gabriele, C., Laura, B. and Alessandro, P., 2021. Experimental investigation of the mechanical behaviour of gravel-granulated tyre rubber mixtures, *Construction and Building Materials* Volume 273.
- Anastasiadis, A., Senetakis, K. and Pitolakis, K., 2012. Small-strain shear modulus and damping ratio of sand-rubber and gravel-rubber mixtures. *Geotech Geol Eng* 30(2):363-382.
- ASTM D6817 (2007). Standard Specifications for Rigid Cellular Polystyrene Geof foam.
- Attom, M.F., 2006. The use of shredded waste tires to improve the geotechnical engineering properties of sands, *Environ. Geol.*, 49 (4), pp. 497-503.
- Ayati, B., Ferrández-Mas, V., Newport, D. and Cheeseman, D., 2018. Use of clay in the manufacture of lightweight aggregate, *Constr. Build. Mater.*, 162, pp. 124-131.
- Aytekin, M., 1997. Numerical modeling of EPS geof foam used with swelling soil, *Geotextiles and Geomembranes*, 15 (1-3), pp. 133-146.
- Beinbrech, G. and Hillmann, R., 1997. EPS in road construction—Current situation in Germany, *Geotextiles and Geomembranes*, 15 (1-3), pp. 39-57.
- Bergado, D.T., Youwai, S. and Rittirong, A., 2005. Strength and deformation characteristics of flat and cubical rubber tyre chip-sand mixtures, *Géotechnique*, 55 (8), pp. 603-606.
- Bhatty, J.I. and Reidt, K.J., 1989. Moderate strength concrete from lightweight sludge ash aggregate, *Cement Compos. Lightweight Concrete* 11(3), pp. 179-187.
- Bogas, J.A. and Cunha, D., 2017. Non-structural lightweight concrete with volcanic scoria aggregates for lightweight fill in building's floors, *Constr. Build. Mater.*, 135, pp. 151-163.
- Bosscher, P.J., Edil, T.B. and Kuraoka, S., 1997. Design of highway embankments using tyre chips, *J. Geotech. Geoenviron. Eng.*, 123 (4), pp. 295-304.
- Cheeseman, C.R. and Viridi, G.S., 2005. Properties and microstructure of lightweight aggregate produced from sintered sewage sludge ash, *Resour. Conserv. Recy.*, pp. 18-30.
- Chen, W.B., Feng, W.Q., Yin, J.H., Borana, L. and Chen, R.P., 2019. Characterization of permanent axial strain of granular materials subjected to cyclic loading based on shakedown theory, *Constr. Build. Mater.*, 198, pp. 751-761.
- Chiou, I.J., Wang, K.S., Chen, C.H. and Lin, Y.T., 2006. Lightweight aggregate made from sewage sludge and incinerated ash, *Waste Manage.*, pp. 1453-1461.
- Chun, B.S., Lim, H., Sagong, M., and Kim, K., 2004. Development of a hyperbolic constitutive model for expanded polystyrene (EPS) geof foam under triaxial compression tests, *Geotextiles and Geomembranes*, 22, pp. 223-237.
- Contributors, W., 2019. List of countries by road network size, Wikipedia.
- Deng, A and Yang, X., 2009. Modeling stress-strain behavior of sand-EPS beads lightweight fills based on cam-clay models, In *Recent Advancement in Soil Behavior, in Situ Test Methods, Pile Foundations, and Tunneling@ Selected Papers From the 2009 GeoHunan International Conference*, pp. 55-61.
- Deng, A. and Yang, X., 2010. Measuring and modeling proportion-dependent stress-strain behavior of EPS-sand mixture 1, *Int. J. Geomech.*, 10 (6), pp. 214-222.

- Dondi, M., Cappelletti, P., Amore M.D., Gennaro, R.D., Graziano, S.F., Langella, A., Raimondo, M. and Zanelli, C., 2016. Lightweight aggregates from waste materials: Reappraisal of expansion behavior and prediction schemes for bloating, *Constr. Build. Mater.*, pp. 394-409.
- Ducman, V., Mladenovic, A. and Suput, J.S., 2002. Lightweight aggregate based on waste glass and its alkali-silica reactivity, *Cem. Conc. Res.*, pp. 223-226.
- El-Didamony, H., Abo El-Enein, A.A., Ali, A.H. and Sakkary, T.M., 1997. Recycling of cement kiln dust in slag cement. Proceeding of the 7th International Conference on Environment Protection, May 20-22 Alexandria, Egypt, pp. 587-603.
- Erlingsson, S. and Rahman, M., 2013. Evaluation of permanent deformation characteristics of unbound granular materials by means of multistage repeated load triaxial tests, *Transport. Res. Rec.*, 2369, pp. 11-19.
- Foose, G.J., Benson, C.H. and Bosscher, P.J., 1996. Sand reinforced with shredded waste tires, *J. Geotech. Eng.*, 122 (9), pp. 760-767.
- Gao, Y.F., Wang, S.M. and Chen, C.B., 2011. A united deformation-strength framework for Lightweight Sand-EPS Beads Soil (LSES) under cyclic loading, *Soil Dynamics and Earthquake Engineering*, Volume 31, Issue 8, pp. 1144-1153.
- Garga, V.K. and O'Shaughnessy, V., 2000. Tire-reinforced earth-fill. Part 1: Construction of a test fill, performance, and retaining wall design, *Can. Geotech. J.*, 37 (1), pp. 75-96.
- Gennaro, R., Cappelletti, P., Cerri, G., Gennaro, M., Dondi, M. and Langella, A., 2004. Zeolitic tuffs as raw materials for lightweight aggregates, *Appl. Clay Sci.*, pp. 71-81.
- Hayashi, Y., Suzuki, A. and Matsuo, A., 2002. Mechanical properties of air-cement-treated soils, *Ground Improvement*, 6 (1), pp. 69-78.
- Holtz, R.D. and Schuster, R.L., 1996. Stabilization of soil slope. In: Turner, A.K., Schuster R.L., (Eds), *Landslides: Investigation and Mitigation*. Transportation Research Board, Special Report 247, National Academy Press, Washington DC, pp. 439-473.
- Horvath, J.S., 1994. Expanded polystyrene (EPS) geofilm: an introduction to material behavior, *Geotextiles and Geomembranes*, 13 (4), pp. 263-280.
- Horvath, J.S., 1997. The compressible inclusion function of EPS geofilm, *Geotextiles and Geomembranes*, 15 (1-3), pp. 77-120.
- Huang, S.C., Chang, F.C., Lo, S.L., Lee, M.Y., Wang, C.F. and Lin, J.D., 2007. Production of lightweight aggregates from mining residues, heavy metal sludge, and incinerator fly ash, *J. Hazard. Mater.*, pp. 52-58.
- Huang, Y., 1993. *Pavement analysis and design*, Prentice-Hall, Englewood Cliffs, NJ.
- Iaych, K., 2010. *IRF World Road Statistics, Data 2003-2008*.
- Jamnongpipatkul, P., Dechakulsom, M. and Sukolrat, J., 2009. Application of air foam stabilized soil for bridge-embankment transition zone in Thailand, Printed in *Geotechnical Special Publication No. 190*, pp. 181-193.
- Kaneko, T., Orense, R.P. and Hyodo, M., 2013. Seismic response characteristics of saturated sand deposits mixed with tire chips, *J. Geotech. Geoenviron. Eng.*, 139 (4), pp. 633-643.
- Kim, J.C., and Lee, J.K., 2002. Mechanical characteristics of light-weighted foam soil consisting of dredged soils, *Journal of Korean Geotechnical Society*, 18 (4), pp. 309-317.
- Kim, J.C., Jang, J.K. and Lee, S.W., 2007. Application of lightweight foam mixed soil method, *Proceeding of Autumn Conference of Korean Geotechnical Society*.

- Kim,T.H., Kim,T.H. and Kang,G.C., 2013. Performance evaluation of road embankment constructed using lightweight soils on an unimproved soft soil layer, *Engineering Geology*, Volume 160, pp. 34-43.
- Kohata,Y. and Wakatsuki,H., 2019. Triaxial shear property of man-made lightweight geomaterials-clinker soil, *The 59th of Japanese Geotechnical Society Hokkaido Branch Technical Report Collection* (in Japanese).
- Kourti,I. and Cheeseman,C., 2010. Properties and microstructure of lightweight aggregate produced from lignite coal fly ash and recycled glass, *Resources, Conservation and Recycling*, Volume 54, Issue 11, pp. 769-775.
- Krystyna,K.F., 2007. Influence of geosynthetic reinforcement on the load-settlement characteristics of two-layer subgrade, *Geotext. Geomembr.*, 25 (6), pp. 366-376.
- Laurance,W.F., Goosem,M. and Laurance,S.G., 2009. Impacts of roads and linear clearings on tropical forests, *Trends Ecol*, 24 (12), pp. 659-669.
- Liu,H.L., Deng,A. and Chu,J., 2006. Effect of different mixing ratios of polystyrene pre-puff beads and cement on the mechanical behaviour of lightweight fill, *J. Geotext. Geomembr.*, 24 (6), pp. 331-338.
- Ma,S., 2003. Stability and settlement of embankment filled with stabilized light soil, *Rock and Soil Mechanics*, 24 (3), pp. 331-334.
- Manohar,D.R. and Anbazhagan,P., 2021. Shear strength characteristics of geosynthetic reinforced rubber-sand mixtures, *Geotextiles and Geomembranes*, Volume 49, Issue 4, pp. 910-920.
- Manosa,J., Formosa,J., Giro-Paloma,J., Maldonado-Alameda,A., Quina,M.J. and Chimenos,J.M., 2021. Valorisation of water treatment sludge for lightweight aggregate production, *Construction and Building Materials*, Volume 269.
- Mashiri,M.S., Vinod,J.S. and Sheikh,M.N., 2016. Liquefaction potential and dynamic properties of sand-tyre chip (STCh) mixtures, *Geotech. Test. J.*, 39 (1), pp. 69-79.
- Mason,B., 1994. Lightweight aggregates, from industrial minerals and rocks, 6th ed. Society for Mining, Metallurgy, and Exploration, pp. 343-350.
- Miao,L.C., Wang,F., Han,J., Lv,W.H. and Li, J., 2012. Properties and applications of cement-treated sand-expanded polystyrene bead lightweight fill, *J. Mater. Civ. Eng.*, 25 (1), pp. 86-93.
- Miki,H., Mori,M. and Chida,S., 2003. Trial embankment on soft ground using lightweight-foam-mixed in-situ surface soil, *Proc. XXIIInd PIARC World Road Congress*, Durban.
- Minegishi,K., Makiuchi,K. and Takahashi,R., 2002. Strength-deformation characteristics of EPS beads-mixed lightweight geomaterial subjected to cyclic loadings. In: *Proceedings of the international workshop on lightweight geo-materials*. Tokyo; pp. 119-250.
- Montepara,A. and Giuliani,F., 2000. Design of road embankments lightened by Expanded Polystyrene (EPS) laying on low-bearing capacity grounds. *Proceedings of the 10th REAA Conference, Road Development for 21st Century*. Tokyo, Japan.
- Neff,J. and Dickens,M., 2010. A.P.T. Association, Public transportation fact book.
- Nicholas,T., Rocco and Ronaldo,L., 2013. Mixtures of clay/EPS particulates and undrained shear strength, *Geo-Congress 2013 Stability and Performance of Slopes and Embankments III*, pp. 2059-2068.
- Noorzad,R. and Raveshi,M., 2017. Mechanical behavior of waste tire crumbs-sand mixtures determined by triaxial tests, *Geotech. Geol. Eng.*, 35 (4), pp. 1793-1802.
- Owens P.L., 1993. Lightweight aggregates for concrete. 2nd ed. in: Clarke JL, Blackie, editors. *Structural*

Lightweight Aggregate Concrete. pp. 1-18

Padade,A. and Mandal,J., 2014. Expanded polystyrene-based geomaterial with fly ash, *Int. J. Geomech.*, 14 (6).

Preber,T., Bang,S., Chung,J. and Cho,Y.,1995. Behavior of expanded polystyrene blocks, *Transportation Research Record*, 1462, pp. 36-46.

Richard,T.T.F., Daniel,S., John,A.B., Anthony,P.C., Carol,D.C., Virginia,H.D., Lenore,F., Robert, L.F., Charles,R.G., Kevin,H., Julia,J., Frederick,S., Thomas,T. and Thomas,C.W., 2013. *Road ecology: science and solutions*, Island press.

Road Bureau, 2018. Ministry of Land, Infrastructure, Transport and Tourism, *Roads in Japan*.

Rodriguez,A.R., Castillo,H. and Sowers,G.F., 1988. *Soil mechanics in highway engineering*, Trans Tech Publications, Germany.

Quina,M.J., Bordado,J.M. and Quinta-ferreira,R.M., 2014. Recycling of air pollution control residues from municipal solid waste incineration into lightweight aggregates, *Waste Manag.*, pp. 430-438.

Saberian,M., Li,J. and Setunge,S., 2019. Evaluation of permanent deformation of a new pavement base and subbase containing unbound granular materials, crumb rubber and crushed glass, *J. Clean. Prod.*, 230, pp. 38-45.

Saeed,S., Ali, K., Peiman, Z. and Abbas,G., 2020. Dynamic behavior of sand-rubber mixtures based on hollow cylinder tests, *Construction and Building Materials*, Volume 251, 118948.

Satoh,T., Tsuchida,T., Mitsukuri,K. and Hong,Z., 2001. Field placing test of lightweight treated soil under seawater in Kumamoto Port, *Soils and Foundations*, 41 (5), pp. 145-154.

Senetakis,K., Anastasiadis,A. and Pitilakis,K., 2012. Dynamic properties of dry sand/rubber (SRM) and gravel/rubber (GRM) mixtures in a wide range of shearing strain amplitudes, *Soil Dyn. Earthquake Eng.*, 33 (1), pp. 38-53.

Short, A. and Kinniburgh,W., 1976. *Lightweight Concrete*, Building Research Establishment. Garston Watford. UK.

Song,J.H., Im,J.C. and Hong,S.W., 2008. Analysis of compressive strength of lightweight air-mixed soil according to the properties of soil, *Journal of Korean Geotechnical Society*, 24 (11), pp. 1-10.

Sotiris,A., Anastasia,P., Stergios,M. and Dimitris, P., 2016. Use of rubberised backfills for improving the seismic response of integral abutment bridges, *Bulletin of Earthquake Engineering* volume 14, pp. 3573-3590.

Stark,T.D., Arellano,D., Horvath,J.S. and Leshchinsky,D., 2004. *Geofoam applications in the design and construction of highway embankments*. NCHRP Web Document, vol. 65, Transportation Research Board, USA.

Strano,E., Giometto,A., Shai,S., Bertuzzo,E., Mucha,P.J. and Rinaldo,A., 2017. The scaling structure of the global road network, *Royal Society open science*, 4 (10). <https://doi.org/10.1098/rsos.170590>

Sugawara,M., Sasaki,K. and Kohata,Y., 2019. Investigation on applicability of lightweight geo-materials for roadbeds, *The 59th of Japanese Geotechnical Society Hokkaido Branch Technical Report Collection*, pp. 256-262. (in Japanese).

Sugawara,M., Sasaki,K., Kaihui,T., Yuki,K. and Kohata,Y.,2020. Strength after particle crushing of man-made lightweight geomaterials - clinker ash mixed soil, *The 60th of Japanese Geotechnical Society Hokkaido Branch Technical Report Collection* (in Japanese).

Sugawara,M., Sasaki,K., Kaihui,T., Yuki,K. and Kohata,Y.,2021. Base examination of man-made lightweight geomaterials- standard sand mixed soil, *The 61th of Japanese Geotechnical Society Hokkaido Branch Technical*

Report Collection (in Japanese).

Takashi,T., Ali,P. and Nobuyuki,Y., 2001. Development of a geomaterial from dredged bay mud, *J. Mater. Civ. Eng.*, 13 (2), pp. 152-160.

Tsuchida,T., Porbaha,A., Yamane,N., 2001. Development of a geomaterial from dredged bay mud, *Journal of Materials in Civil Engineering, ASCE*, 13 (2), pp. 152-160.

UNI EN 13163 (2009). *Prodotti di Polistirene Espanso Ottenuti in Fabbrica.*

Wang,F. S., Xie,J., Wu,S.P., Li,J.S., Barbieri,D.M. and Zhang,L., 2021. Life cycle energy consumption by roads and associated interpretative analysis of sustainable policies, *Renewable and Sustainable Energy Review Volume 141*.

William,F.L., Gopaldasamy,R.C., Sean,S., Christine,S., O'Connell, Nathan,D.,Mueller, Miriam Goosem, Oscar Venter, David P. Edwards, Ben Phalan, Andrew Balmfords and Rodney Van Der, 2014. A global strategy for road building, *Nature* 513,229-232.

Yajima,J. and Mydin,S.H., 2006. Mechanical properties of the unsaturated foam composite light-weight soil, *Geotechnical Special Publication No. 147*, pp. 1639-1650.

Yoonz,G., Jeon,S., and Kim,B., 2004. Mechanical characteristics of light-weighted soils using dredged materials, *Marine Georesources and Geotechnology*, 22 (4), pp. 215-229.

Yoon,G.L. and Kim B.T., 2004. Compressibility and strength characteristics of light-weighted foam soil, *Journal of Korean Geotechnical Society*, 20 (4), pp. 5-13.

Zhuo,B., Zhu,M.Y., Fang,Y., Wang,F.Y, Yao,Y.X. and Li,S., 2021. Numerical and experimental analyses for rubber-sand particle mixtures applied in high-filled cut-and-cover tunnels, *Construction and Building Materials*, Volume 306, 1, 124874.

Zornberg,J.G., Cabral,A.R. and Viratjandr,C., 2004. Behaviour of tire shred-sand mixtures, *Can. Geotech. J.*, 41 (2), pp. 227-241.

## **CHAPTER 2**

### **TSETING MATERIALS, APPARATUS AND METHODS**



## 2.1 Introduction

In this study, an artificial lightweight material widely used in Japan is used as fill material, which is made by firing and foaming expanded shale and sewage sludge at high temperatures. Since the particle gradation of a single coarse aggregate is not good and it is difficult to be compacted during use, another type of fine aggregate is used in a combination with it, which is a cement standard sand. This chapter introduces the testing materials and testing methods.

## 2.2 Materials

### 2.2.1 Cement standard sand

Cement standard sand (ISO standard sand) is a natural sand, which is siliceous particularly its finest fractions. It is clean, the particles are generally isometric and rounded in shape. It is dried, screened and prepared in a modern workshop which offers every guarantee in terms of quality and consistency, the maximum moisture content is 0.2 %. The sand is portioned in bags of 1,350 ( $\pm 5$ ) g, as shown in **Fig. 2.1**. The characteristic of cement standard sand is its specific grain size distribution. It ranges between 0.08 and 2.00 mm. The grain size distribution of cement standard sand is drawn in the **Fig. 2.2**. The grading, measured by sieving, complies with the requirements of EN 196-1 and of ISO 679: 2009 and listed in the **Table 2.1**, **Table 2.2** and **Table 2.3** show physical property and chemical composition of the cement standard sand.



**Fig. 2.1** Cement standard sand

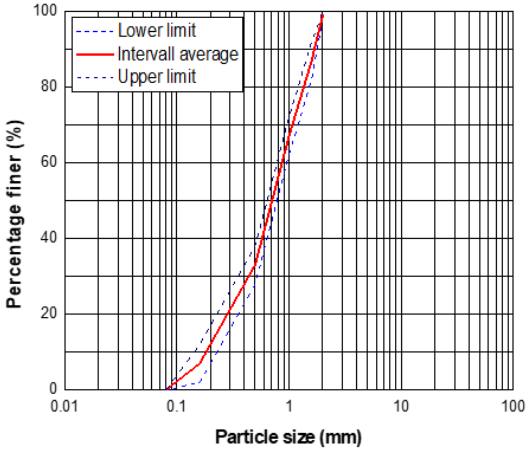


**Fig. 2.2** Grain-size distribution of sand

**Table 2.1** The grading requirements of EN 196-1 and of ISO 679: 2009

Mesh size (mm)	Lower limit (%)	Interval average (%)	Upper limit (%)
2	0	0	0
1.6	2	7	12
1.0	28	33	38
0.5	62	67	72
0.16	82	87	92
0.08	98	99	100

**Table 2.2** Physical properties of cement standard sand

Testing project	Testing value
Specific gravity in oven dried condition (JIS A 1109)	2.67
Percentage of absorption (%) (JIS A 1109)	0.42
Weight per unit volume (kg/L) (JIS A 1104)	1.76
Solid content in aggregate (%) (JIS A 1104)	66.7
Organic impurities (JIS A 1105)	light
Nature moisture content (%)	0.0
Gravel (%)	0.0
Sand (%)	99.2
Fines (%)	0.8

**Table 2.3** Chemical composition of cement standard sand, unit (%)

Ig. loss	SiO <sub>2</sub>	Al <sub>2</sub> O <sub>3</sub>	Fe <sub>2</sub> O <sub>3</sub>	CaO	MgO	Na <sub>2</sub> O	K <sub>2</sub> O
0.00	98.40	0.40	0.40	0.20	0.00	0.01	0.01

### 2.2.2 Artificial lightweight coarse aggregate

Sintering and cold-bonding are two widely-recognized methods to produce artificial lightweight aggregates (Qian et al., 2020; Tajra et al., 2019). Sintering highly relies on the use of elevated temperature, which is commonly higher than 1000 °C (to crystallize the raw materials), while the traditional cold-bonding method usually utilizes cementitious pastes to bind the raw materials together.

In this study, the artificial lightweight coarse aggregate is made of expanded shale mined in Chiba Prefecture and sludge generate from water treatment plants and sewage treatment plants in Tokyo, Chiba and other

prefectures, as shown in the Fig. 2.3. The grain size distribution of artificial lightweight coarse aggregate is drawn in the Fig. 2.4. It is an "eco-recycled product" made by firing and foaming at about 1,100 °C. The manufacturing process is shown in the Fig. 2.5. Table 2.4 and Table 2.5 show the particle passing rate and physical property of the artificial lightweight coarse aggregate.

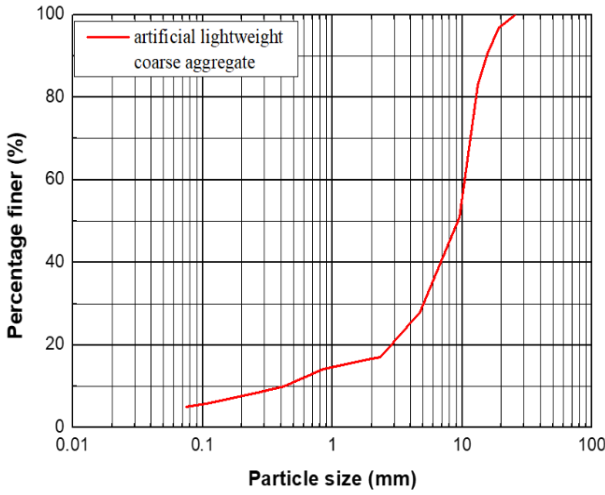


Fig. 2.3 The artificial lightweight coarse aggregate

Fig. 2.4 Grain-size distribution of coarse aggregate

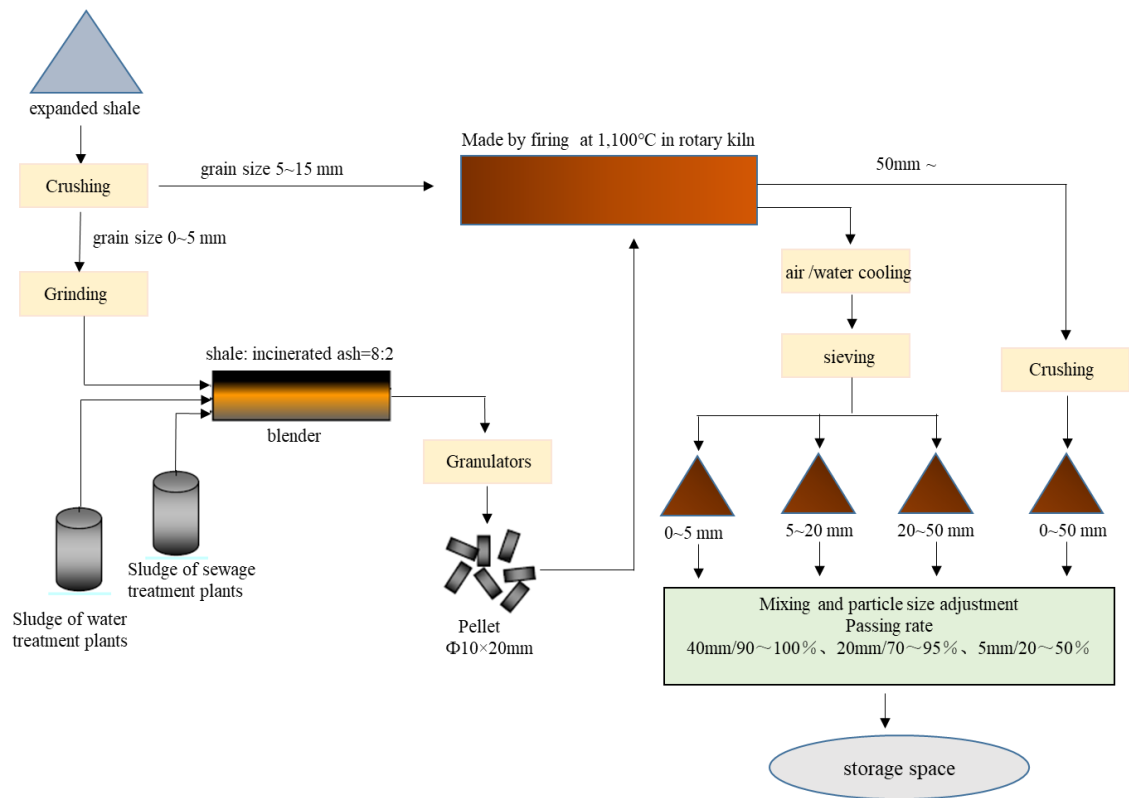


Fig. 2.5 The manufacturing process of artificial lightweight coarse aggregate

**Table 2.4** Particle passing rate of the artificial lightweight coarse aggregate

Mesh size (mm)	Lower limit (%)	Upper limit (%)
40	90	100
20	70	95
5	20	50

**Table 2.5** Physical properties of the artificial lightweight coarse aggregate

Testing project	Testing value
Density (g/cm <sup>3</sup> )	1.20
Maximum dry density (g/cm <sup>3</sup> ) (wet condition)	1.098
Maximum dry density (g/cm <sup>3</sup> ) (dry condition)	0.892
CBR (%)	> 20
Weight per unit volume (kg/L) (wet condition)	1.05 ± 0.10
Weight per unit volume (kg/L) (dry condition)	0.90 ± 0.10
Angle of friction (°)	40
hydraulic conductivity (cm/s)	1.05
Percentage of absorption (%) (JIS A 1109)	15.27
Point load strength (MN/m <sup>2</sup> )	2.0
Nature moisture content (%)	10
Gravel (%)	83.6
Sand (%)	12.1
Silt (%)	4.2
Clay (%)	0.1

### 2.2.3 Testing materials

In this study, the testing material is made by mixing cement standard sand and the artificial lightweight coarse aggregate in a 1 to 1 ratio by weight under dry condition, as shown in the **Fig 2.6**. The grain size distribution of testing material is drawn in the **Fig. 2.7**. **Table 2.5** shows physical properties of the testing material.

**Fig. 2.8** shows the compaction curve of the testing materials by vibrating compaction. Generally, a dry density for compaction curve of soil under a constant energy decreases when a water content is decreased from optimum moisture content. However, for a cohesionless soil like sand, a minimum dry density is taken at some water content so that a dense state of soil particle is resisted due to the capillary tension of the pore water. This

phenomenon is known as the bulking of sand. And more, when a water content is decreased, the capillary tension of the pore water becomes weak, soil particles come close. Consequently, a dry density increases again (Raj, 2008; Hilf, 1991). Thus, a dry density at  $w = 0\%$  indicates the relatively large value. It is considered that this tendency becomes more remarkable for a vibrating compaction.

The effect of particle crushing by the triaxial testing under confining pressure 29.4kPa on the grain size distribution was found to be insignificant. The grain size distribution curves of specimen measured before and after triaxial testing are shown in Fig. 2.9. According to the method of Marsal (1967), the breakage rate of the testing materials was calculated, and it was found that the breakage rate was about 1.3% after each testing.



Fig. 2.6 The testing materials

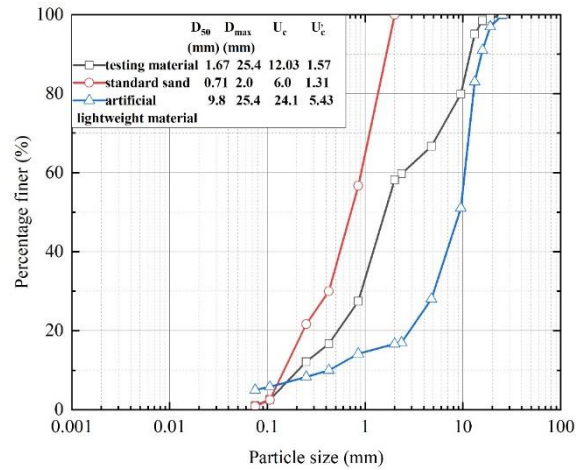


Fig. 2.7 Grain-size distribution of testing materials

Table 2.6 Physical properties of the testing materials

Testing project	Testing value
The particle density ( $\text{g}/\text{cm}^3$ )	2.126
Natural water content (%)	9.5
Percentage of absorption (%) (JIS A 1109)	24.43
CBR (%)	50
Volume weight ( $\text{kg}/\text{m}^3$ )	14
Particle breaking rate (%) (After the proctor compaction by JIS A 1201 E-b)	10
Nature moisture content (%)	9.5
Gravel (%)	39.1
Sand (%)	58.4
Fines (%)	2.5

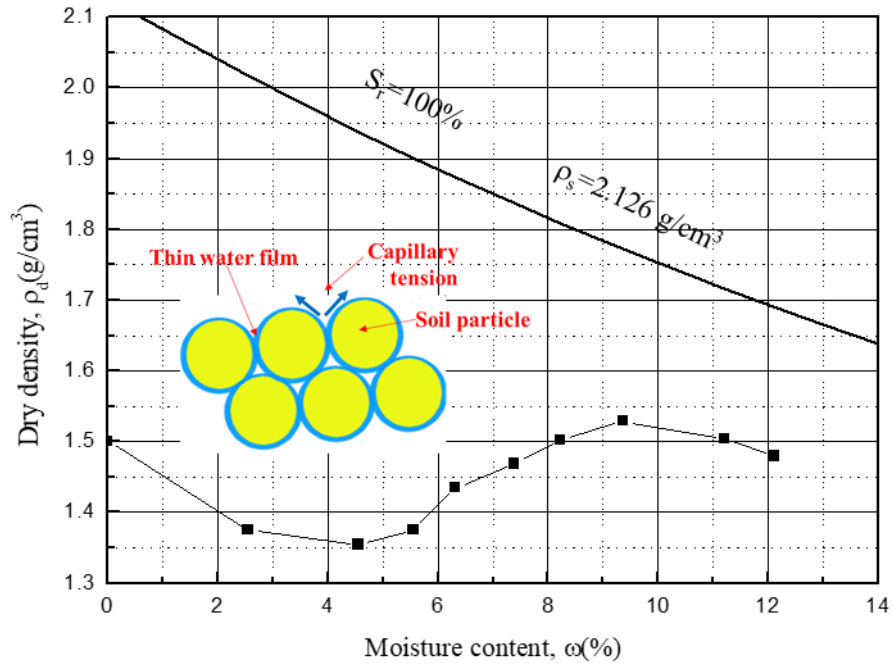


Fig. 2.8 The compaction curve of the testing materials by vibrating compaction

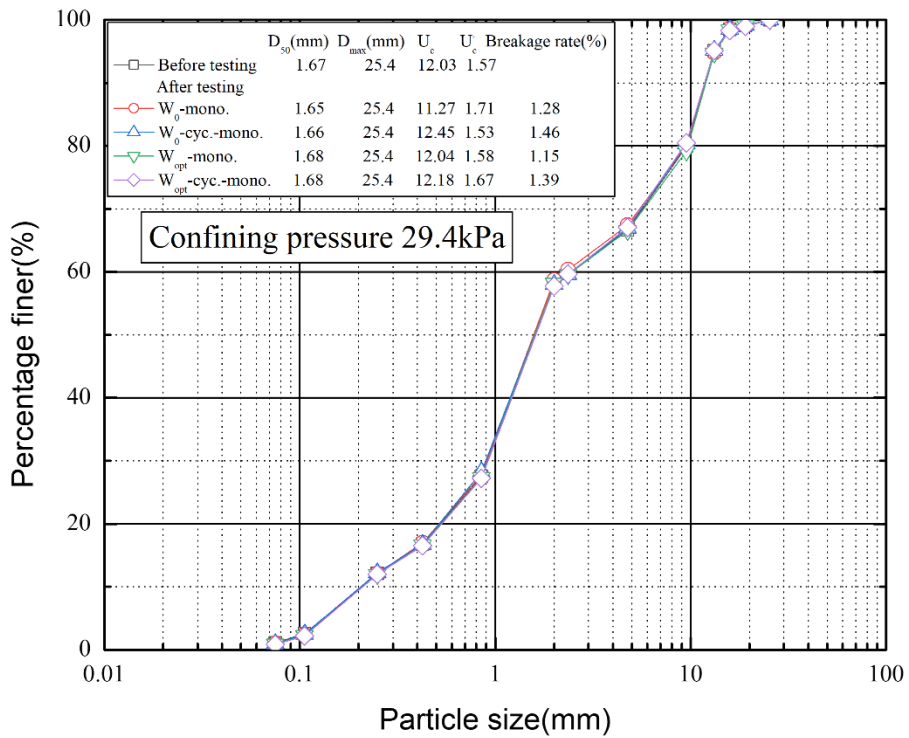


Fig. 2.9 Grain-size distribution of testing materials before and after triaxial testing

## 2.3 Testing apparatus

### 2.3.1 The schematic diagram of the test apparatus

The medium-size triaxial apparatus, which was developed by Shimadzu Corporation, was used in this study. The apparatus equipped with a hydraulic servo control system by the feedback control method so that it can apply a high precision axial load to the specimen by stress control method and strain control method. The size of specimen was 300 mm in height and 150 mm in diameter. The schematic diagram of the testing apparatus is shown in **Fig. 2.10**. This medium-sized triaxial test apparatus consists of a monotonic loading test apparatus, non-contact displacement transducer (GAP sensor) for measuring lateral displacement and an axial load measuring apparatus (Load cell).

The three projects to be measured are axial load, specimen axial displacement and specimen lateral displacement. The data measured by each measuring device are converted into digital data by a 12-bit 16-channel A/D converter through a dynamic strainmeter and a general-purpose DC amplifier or transducer, and recorded in a computer.

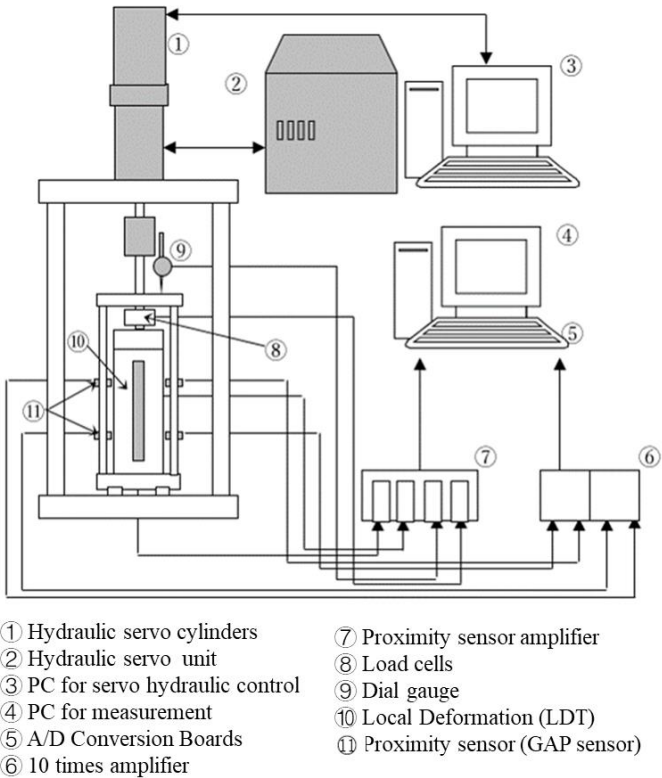


**Fig. 2.10** The schematic diagram of the test apparatus

### 2.3.2 The medium-size triaxial apparatus

#### 2.3.2.1 Triaxial cell

A schematic of the triaxial cell is shown in **Fig. 2.11**. The triaxial cell consists of a lower plate and an upper plate. In the center of the lower panel is a cylindrical pedestal, and a specimen covered with a membrane is placed on top for testing. The pedestal is surrounded by three pillars on which the non-contact displacement transducer (GAP sensor) is mounted. On the top panel there is a load cell, a cap and a loading rod. The load rod runs through the center and the vertical movement is facilitated by ball bearings. For triaxial tests, the loading rod is connected to the loading device and the cap is placed.

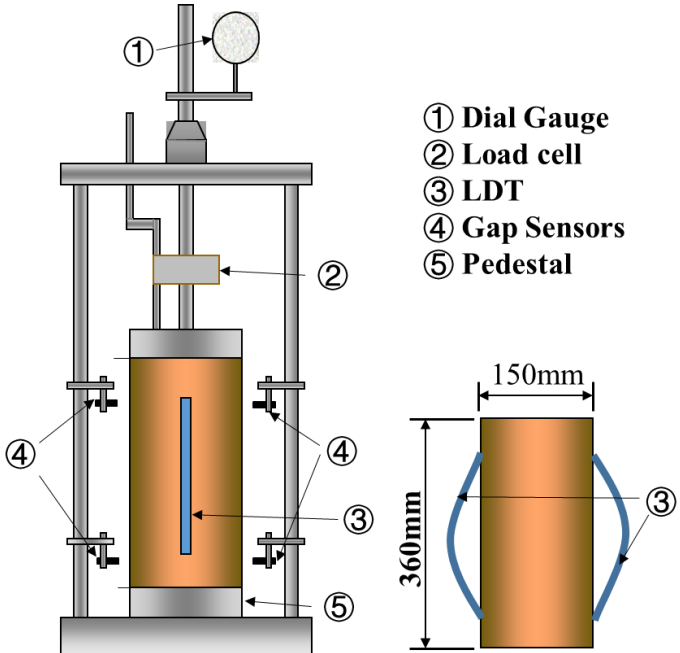


**Fig. 2.11** A schematic of the triaxial cell

#### 2.3.2.2 Load testing equipment

The test apparatus is shown in **Fig. 2.12**. In the load testing apparatus, the load shaft is raised and lowered by hydraulic pressure to load the specimen. The positioning is carried out by sending certain commands from a PC to the drive unit.

- Crosshead, table and pillar

The frame is composed of a frame that receives reaction forces. The frame is designed to have high rigidity and minimal deformation under load. The wide table is T-slotted for easy mounting of the specimen.

- Dust seal for pillar

Prevents dust and other debris from getting between the crosshead and the strut, causing poor movement and scratching.

- Lifting jacks

Hydraulic jacks for lifting and lowering crossheads.

- Clamp jacks

Hydraulic clamps for fixing the crosshead.

- Auxiliary clamping bottle

Bolts to assist clamping of the crosshead. Tighten when using low oil pressure or when securing the crosshead for a long period of time to assist the clamping force of the crosshead.

- Actuator

Hydraulic cylinder for generating test forces. Incorporates a high precision piston displacement detector.

- Servo valves

High performance servo valves for controlling the movement of actuators. The opening degree is adjusted according to the control signal to control the movement of the actuator with high precision.

- Accumulator

The accumulator is filled with high-pressure nitrogen gas to eliminate pulsations in the hydraulic pump and to store hydraulic pressure to assist in the hydraulic pressure reduction.



**Fig. 2.12** Load testing equipment

### 2.3.3 Measuring devices

#### 2.3.3.1 Axial stress measuring device (Load cell)

The axial stress was measured by means of a load cell mounted between the cap of the loading rod and the top plate. The load cell has a capacity of 2 t. The basic principle is that when a load is applied, the body of the load cell is elastically deformed and the strain gauge inside the load cell measures the amount of deformation, thus measuring the load. **Fig. 2.13** shows the calibration result.

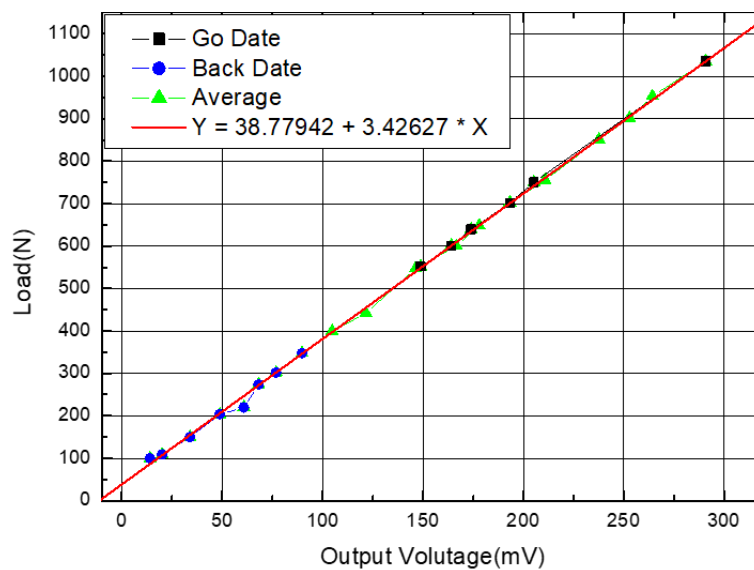


**Fig. 2.13** Calibration result of the load cell (Ch.1)

### 2.3.3.2 Apparatus for measuring strain

The axial strains of the specimens were measured by means of dial gauges, relative displacement of mega torque motor and a Local Deformation Transducer (LDT) (Goto et al., 1991). The LDT is capable of measuring axial strains of less than 2 %. However, the LDT can only measure axial strains up to less than 2 %. In this study, axial strains exceeding this level were measured using a mega torque motor and a dial gauge, and the values were corrected by subtracting the amount of bedding error. (Burland, 1989; Dawson and Gillett, 1998).

#### ※ **Bedding error**

Bedding error is a measurement error in the "axial strain calculated from the axial displacement of the cap or loading piston" caused by loose deformation around the top and bottom edges of the specimen or incomplete contact between the specimen and the capped pedestal surface. Specifically, it is caused by the following three factors.

(1) Poor smoothness at the top and bottom edges of the specimen and parallelism with the cap and pedestal excessive deformation is caused by imperfect contact.

(2) When an undisturbed specimen of hard ground material (hard clay, sand, gravel, cement improved soil, soft rock, etc.) is shaped, a thin layer of disturbed material is formed on its top and bottom edges. This layer is much more compressible than the main body of the specimen, which leads to bedding errors.

(3) When filter paper or a friction-reducing layer is used on the top and bottom edges of the specimen, these areas are subject to compressive deformation, resulting in bending errors.

#### **a) Dial gauge**

In this study, the displacement of a metal plate attached perpendicular to the loading rod of the upper panel was measured by a dial gauge. The maximum measuring range is 50 mm. The piston displacement of the dial gauge is converted into an electrical signal and recorded on a PC. **Fig. 2.14** shows the calibration results.

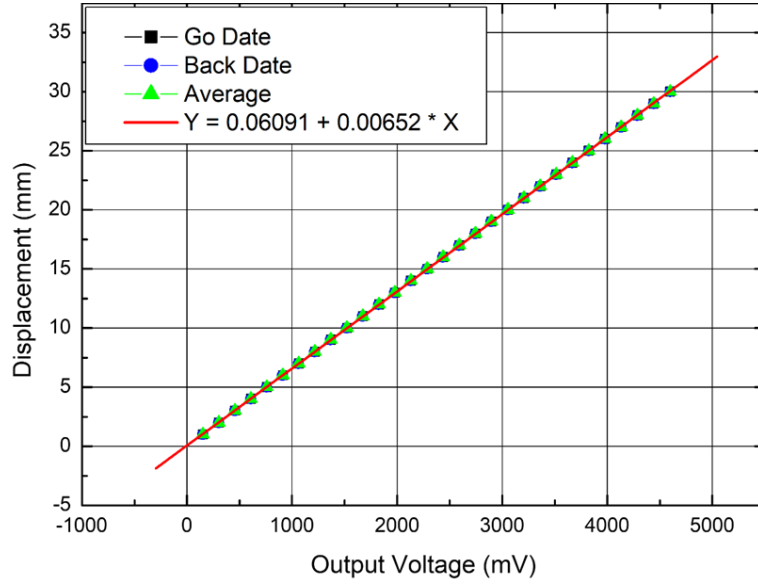


**Fig. 2.14** Calibration result of the dial gauge (Ch.2)

### b) Local Deformation Transducer

The Local Displacement Transducer (LDT) was used to precisely measure the axial strain without the effect of bending errors from less than 0.001% to about 2%. In this study, two LDTs were set diagonally on the left and right sides of the specimen and the average of the measured values was taken as the axial strain. The measuring principle of the LDT is as follows.

It is suppose that LDT is a plate in a straight line of length  $L_0$ . This is bent by the compression of the specimen and displaced relative to the vertical by  $\Delta L$  to form an arc of radius  $R$ . The geometrical conditions allow the following equation to be established.

$$\frac{dX}{R} = \frac{dX + \Delta dX}{R + Y}$$

$$\varepsilon_x = \frac{\Delta dX}{dX} = \frac{Y}{R} \quad (2.1)$$

$$L_0 = R\theta = const \quad (2.2)$$

$$L_0 - \Delta L_0 = 2R \sin \frac{\theta}{2} \quad (2.3)$$

dX: Length of the microelement at the part with the strain gauge

$\Delta dX$ : Amount of change in dX due to change in plate

R: Radius of the arc of a circle

Y: 1/2 of the thickness of the plate

In this case, the axial strain of the specimen is as follow.

$$\varepsilon_1 = \frac{\Delta L}{L_0} \quad (2.4)$$

After Eliminating R and  $\theta$  from (2.1) to (2.4),

$$\varepsilon_1 = 1 - \frac{2Y \sin \left( \frac{L_0 \varepsilon_x}{2Y} \right)}{L_0 \varepsilon_x} \quad (2.5)$$

Formula (2.5) is calculated by Taylor Formula and omit the fourth order and above,

$$\varepsilon_1 = \frac{1}{6} \cdot \left( \frac{\varepsilon_x L_0}{2Y} \right)^2$$

The relationship between the strain of the plate and the strain gage can be obtained. It can be seen that the strain  $\varepsilon_1$  of the specimen is represented by the square of the strain gage  $\varepsilon_x$ . The calibration results are shown in **Fig. 2.15** and **Fig. 2.16**.

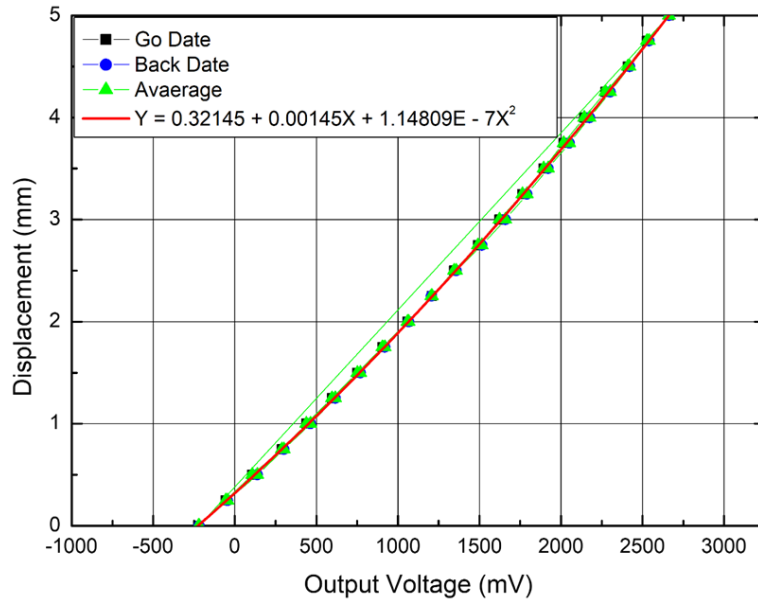


**Fig. 2.15** Calibration result of the LDT1 (Ch.3)

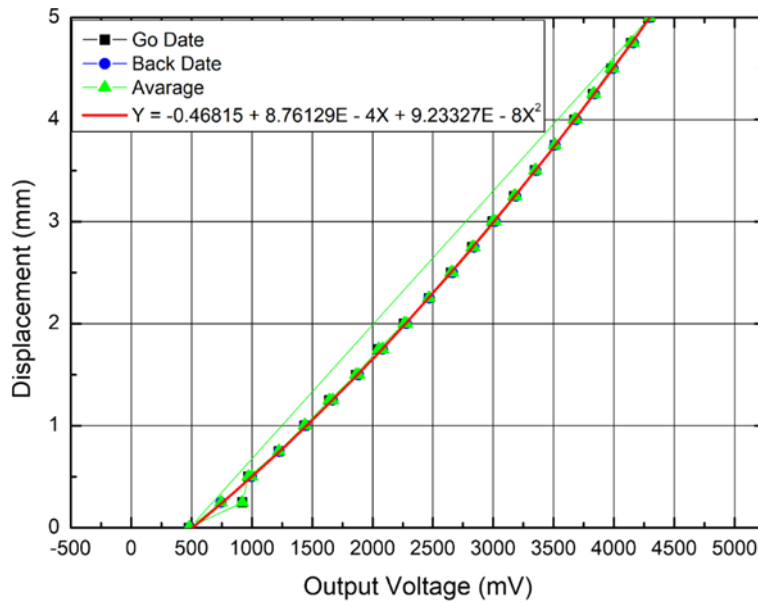


**Fig. 2.16** Calibration result of the LDT2 (Ch.4)

**c) Horizontal gap sensor**

A non-contact displacement transducer was used to measure the lateral strain of the specimen (Tatsuoka et al., 1994). A magnetic field is generated at the tip (probe) of the non-contact displacement transducer, and as the distance to the target changes, the voltage changes. The amount of change in the voltage can be used to determine

the amount of change in the distance to the target. The capacity of this non-contact displacement transducer is 4 mm, and the target is a 40 x 50 mm aluminium foil attached to a membrane by vacuum grease at a height of 12 mm and 24 mm from the bottom edge of the specimen. Four targets are installed, two on each side, diagonally opposite to the specimen. The calibration results are shown in **Fig. 2.17**, **Fig. 2.18**, **Fig. 2.19** and **Fig. 2.20**.

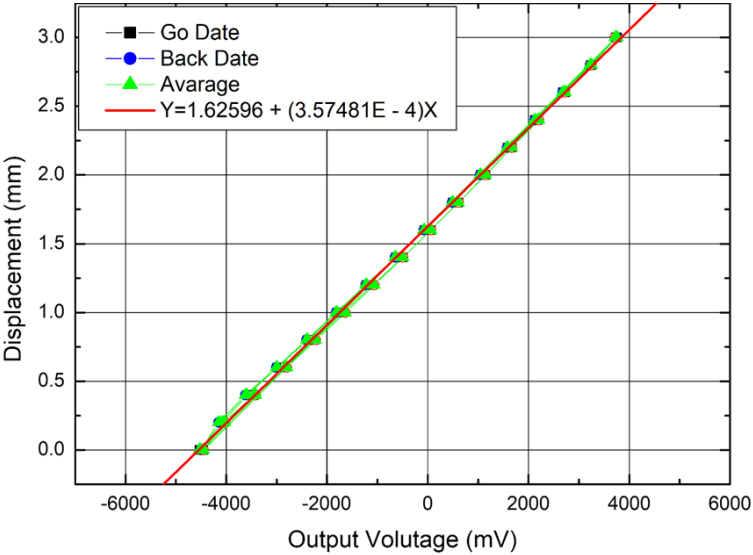


**Fig. 2.17** Calibration result of the horizontal gap sensor (Ch.7)

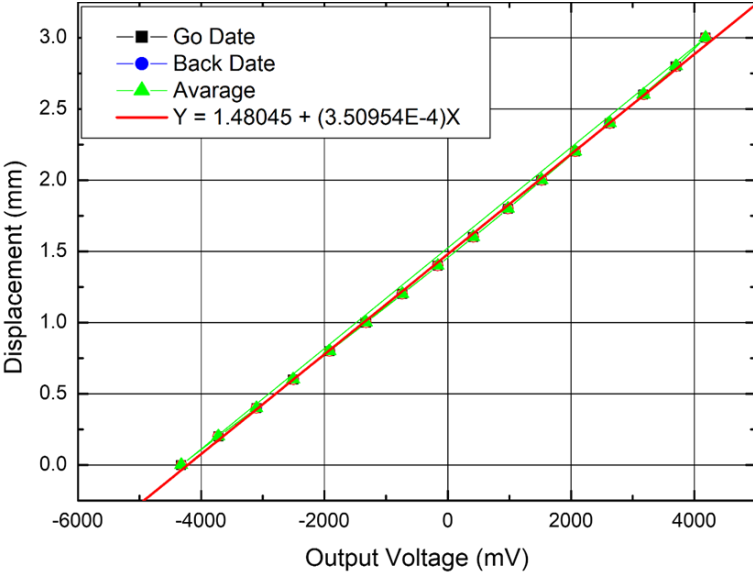


**Fig. 2.18** Calibration result of the horizontal gap sensor (Ch.8)

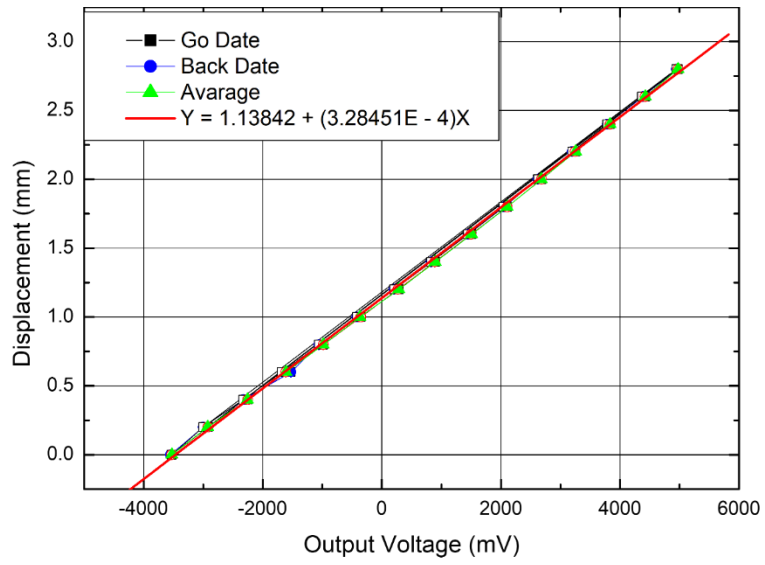


**Fig. 2.19** Calibration result of the horizontal gap sensor (Ch.9)

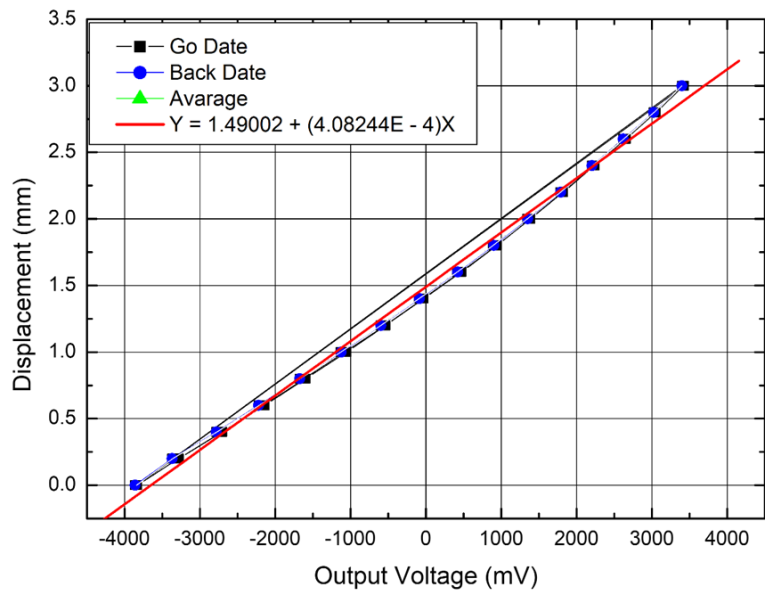


**Fig. 2.20** Calibration result of the horizontal gap sensor (Ch.10)

## 2.4 Specimen preparation

### 2.4.1 Top-loading vibrator apparatus

Top-loading vibrator is used for compaction during the preparation of the specimen. On top of the vibrator there is a device called a spring balancer (Endo Kogyo Co., Ltd.). This allows the position of the vibrator to be fixed and the weight of the specimen to be adjusted during compaction weight adjustment range (30-40 kg). It is also possible to change the vibration frequency of the vibrator by means of a controller. Top-loading vibrator is shown in **Fig. 2.21**.



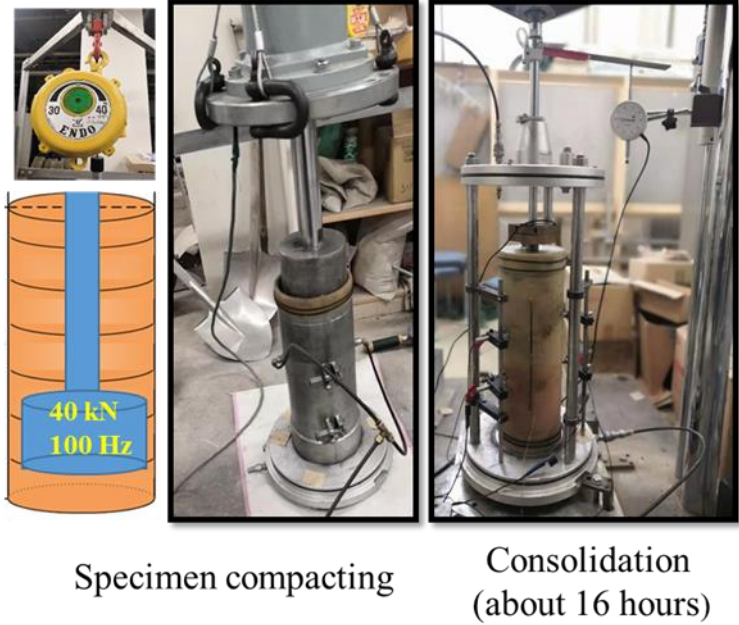
**Fig. 2.21** Top-loading vibrator apparatus

### 2.4.2 Preparation method

A medium-scale triaxial test apparatus is used in this study. Because the size of the specimens should be no less than 5 times the maximum particle size (Erlingsson et al., 2002; Lennart et al., 2014), the test specimens of this study have a diameter of 150 mm and a height of 360 mm.

The specimen is compacted by a top-loading vibrator. The weight of the vibrator is 40 kN, and the vibration

frequency by controllers is adjusted 100 Hz. Each specimen is loaded with seven layers. The compaction time of the first six layers is 10 min, and that of the last layer is 5 min, because it will give the best compaction effect on the test specimens by the top-loading vibrator, as shown in **Fig. 2.22**. Before placing the material for the next layer, the surface of the previously compacted layer was scraped by a depth of about 2 cm to ensure good interlocking between the vertically adjacent layers (Burland, 1989; Thakur et al., 2013; Duong et al., 2013). After the specimens are made, it is ready for the triaxial test that an isotropic confining pressure is consolidated to the specimens for 16 hours.



Specimen compacting

Consolidation  
(about 16 hours)

**Fig. 2.22** Specimen preparation

**2.5 Testing scheme design**

**2.5.1 Monotonic triaxial tests**

In order to analyze the effects of confining pressure, cyclic loading history and moisture on the strength and deformation of the specimen, the monotonic triaxial test were carried out for 12 sets of specimen. The monotonic triaxial test is performed in the displacement controlled mode under the exhaust and drainage conditions at a constant displacement rate of 0.18 mm/min to simulate failure loading rates under moving wheel loads. In the

displacement controlled mode the load magnitude is applied which is required to maintain a constant displacement rate. This has the advantage over force controlled test that the load reduces as the specimen fails while the test extends after failure. From **Table 2.7**, it can be seen that the initial conditions of all specimens. The objectives in this testing are shown follows.

- (1) To analyze the behavior of stress-strain of the specimen under differential conditions.
- (2) To analyze the behavior of maximum deviator stress-confining pressure of the specimen under differential conditions.
- (3) To analyze the behavior initial deformation modulus-confining pressure of the specimen under differential conditions.
- (4) To analyze the behavior of the Mohr's circles in peak stress state of the specimen under differential conditions.
- (5) To analyze the tangential deformation modulus of the specimen under differential conditions.

**Table 2.7** The initial conditions of all specimens for monotonic triaxial test

Specimen material state	Design moisture content (%)	Cyclic loading	Symbol	Confining pressure (kPa)	Dry density $\rho_d$ (g/cm <sup>3</sup> )
Dry condition (W <sub>0</sub> )	0	without	W <sub>0</sub> -mono	29.4	1.459
				49	1.452
				68.6	1.461
		with	W <sub>0</sub> -cyc-mono	29.4	1.462
				49	1.475
				68.6	1.458
Optimum moisture content (W <sub>opt</sub> )	9.38	without	W <sub>opt</sub> -mono	29.4	1.356
				49	1.362
				68.6	1.359
		with	W <sub>opt</sub> -cyc-mono	29.4	1.361
				49	1.365
				68.6	1.363

## 2.5.2 Cyclic triaxial tests

In order to analyze the effects of confining pressure, moisture and number of cyclic loading on the deformation of the specimen during cyclic loading, the cyclic triaxial test were carried out for 6 sets of specimen. 10,000 cycles of vertical loading at a frequency of 0.125 Hz were performed for the specimen, where the vertical stress was changed between  $49.4 \pm 10$  kPa in a sinusoidal wave, as shown in the **Fig. 2.23**. Measurement readings are taken during conditioning at load cycle numbers 0-200, 400-600, 900-1100, 4900-5100 and 9800-10000. The initial conditions of all specimens are shown in **Table 2.8**. The objectives in this testing are shown follows.

- (1) To analyze the deviator stress-axial strain relations of the specimen under differential condition.
- (2) To analyze the lateral strain-axial strain relations of the specimen under differential condition.
- (3) To analyze the volumetric strain-axial strain relations of the specimen under differential condition.
- (4) To analyze the Equivalent Young's modulus of the specimen under differential condition.
- (5) To analyze the Poisson's ratios of the specimen under differential condition.
- (6) To analyze the dilatancy properties of the specimen under differential condition.

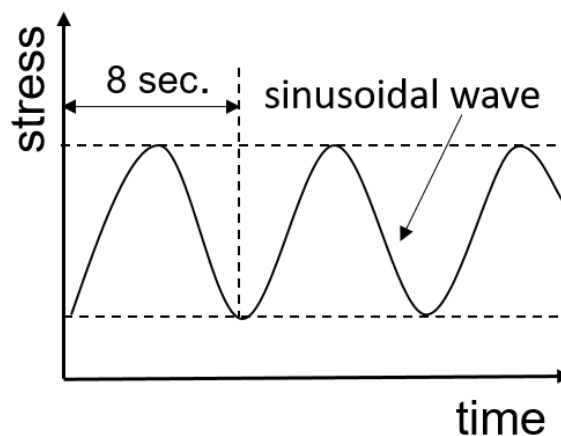


**Fig.2.23** Sinusoidal waveform loading curve for cyclic triaxial test

**Table 2.8** The initial conditions of all specimens for cyclic triaxial test

Specimen material state	Design moisture content (%)	Symbol	Confining pressure (kPa)	Dry density $\rho_d$ (g/cm <sup>3</sup> )
Dry condition ( $W_0$ )	0	$W_0$ -cyc-mono	29.4	1.462
			49	1.475
			68.6	1.458
Optimum moisture content ( $W_{opt}$ )	9.38	$W_{opt}$ -cyc-mono	29.4	1.361
			49	1.365
			68.6	1.363

## References:

Burland, J.B., 1989. Ninth Laurits Bjerrum Memorial Lecture: Small is beautiful-the stiffness of soils at small strain, Canadian geotechnical journal. Vol. 26, Issue 4, pp. 499-516.

Dawson, A.R. and Gillett, S.D., 1998. Assessment of on-sample instrumentation for repeated load triaxial tests, Transp. Res. Record: J. Transp. Res. Board. Vol. 1614, pp. 52-60.

Duong, T.V., Tang, A.M., Cui, Y.J., Trinh, V.N., Dupla, J.C., Calon, N., Canou, J. and Robinet, A., 2013. Effects of fines and water contents on the mechanical behavior of interlayer soil in ancient railway sub-structure, Soils and Foundations. Vol. 53, Issue 6, pp. 868-878.

Erlingsson, S. and Magnusdottir, B., 2002. Dynamic triaxial testing of unbound granular base course materials, In: Proceedings of the 6th International Conference on the Bearing Capacity of Roads, Railways and Airfield, Lisbon, pp. 989-1000.

Goto, S., Tatsuoka, F. and Shibuya, S., 1991. A simple gauge for local small strain measurements in the laboratory[J], Soils and foundations, Vol. 31, Issue 4, pp. 169-180.

Hilf, J.W., 1991. "Compacted Fill". In H.-Y. Fang (Ed.), Foundation Engineering Handbook, 2nd Edition, New York: Van Nostrand Reinhold, pp. 249-316.

Lennart, S., Koseki, J., Miyashita, Y. and Sato, T., 2014. Large-scale triaxial tests of dense gravel material at low confining pressures, Soils Found, Vol. 54, Issue 1, pp. 45-55.

Marsal,R.J., 1967. Large-scale testing of rockfill material [J], Journal of the Soil Mechanics and Foundation Division, American Society of Civil Engineering, Vol.93, Issue 2, pp. 27-43.

Qian,L.P., Wang,Y.S., Alrefaei,Y. and Dai,J.G., 2020. Experimental study on full-volume fly ash geopolymer mortars: sintered fly ash versus sand as fine aggregates J. Clean. Prod.

Raj,P.P., 2008. Soil Mechanics and Foundation Engineering, Dorling Kindersley, pp. 87-88.

Tajra,F., Abd,E.M. and Stephan,D., 2019. The production and properties of cold-bonded aggregate and its applications in concrete: a review, Construct. Build. Mater, pp. 29-43.

Tatsuoka,F., Teachavorasinskun,S., Dong, J., Kohata,Y. and Sato,T., 1994. Importance of measuring local strains in cyclic triaxial tests on granular materials. In Dynamic geotechnical testing II, ASTM, STP 1213, pp. 288-302.

Thakur,P.K., Vinod,J.S. and Indraratna,B., 2013. Effect of confining pressure and frequency on the deformation of ballast, Geotechnique, Vol. 63, Issue 9, pp. 786-790.

## **CHAPTER 3**

### **EFFECT OF CYCLIC LOADING ON STRENGTH DEFORMATION OF SPECIMEN**



### 3.1 Introduction

It is generally accepted that the deformation induced by long-term traffic loads is an important part of the total subgrade settlement. To understand traffic-related deformation, many experimental studies have been carried out (e.g., Seed and McNeill, 1956; Hyde et al., 1993; Moses and Rao, 2003; Wang et al., 2013). Due to its cyclical load history, the nature of a soil (i.e. number, orientation and shape of the particle contacts) changes as well as the distribution of interparticle forces. The stress curve effects occur as a result of progressive compaction and particle rearrangement with repeated loading.

The monotonous triaxial test is a common method for measuring the mechanical properties of many deformable solids, especially soils (like, sand and clay) and rock and other granular materials or powders. In this chapter, the effects of cyclic loading on the strength and deformation of specimens are analyzed by the monotonic triaxial test. The changes of deviator stress - axial strain relationship, Mohr circle, initial elastic modulus and tangent deformation modulus with or without loading history are compared.

### 3.2 Test principle

In the monotonic triaxial test a granular material is subjected to a controlled constant confining pressure. Apart from the all-around confining stress the material is also subjected to an increasing additional axial stress which leads to failure. Failure is defined as the level at which no further increase in axial stress is required to obtain an increase of axial deformation or strain. At failure, the axial stress can be expressed as a shear stress ( $\tau$ ) or a major principal stress ( $\sigma_{1,f}$ ) and the confining stress as a normal stress ( $\sigma_c$ ) or a minor principal stress ( $\sigma_3$ ).

By performing a failure test at a minimum of two or three confining stress levels the stress dependency of the failure behavior of a granular material can be established. This is described by the well-known Mohr-Coulomb failure criterion in equations (3.1):

$$\tau = c + \sigma * \tan\varphi \quad (3.1)$$

Where:

$\tau$ , shear stress at failure (kPa)

$\sigma$ , normal stress at failure (kPa)

$c$ , cohesion (kPa)

$\phi$ , angle of internal friction ( $^{\circ}$ )

The Mohr-Coulomb failure criterion can be expressed in principal stresses as in equation 3.2 and schematically illustrated for constant confining pressure in **Fig. 3.1**:

$$\sigma_{1,f} = \frac{(1 + \sin\phi) * \sigma_{3,f} + 2c * \cos\phi}{1 - \sin\phi} = A * \sigma_{3,f} + B \quad (3.2)$$

Where:

$\sigma_{1,f}$  = major principal stress at failure (kPa)

$\sigma_{3,f}$  = minor principal stress at failure (kPa)

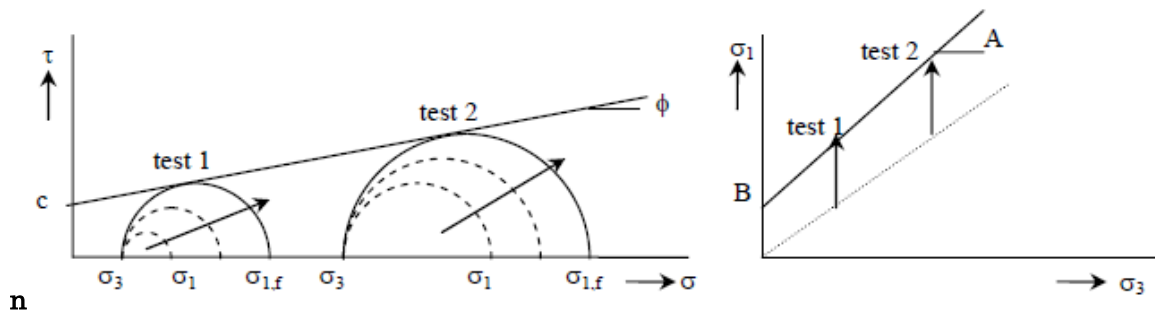


**Fig. 3.1** Mohr stress circles and stress path in constant confining pressure failure tests

### 3.3 Relationship between deviator stress and axial strain

#### 3.3.1 Under dry condition

**Fig.3.2 (a)** and **3.3 (a)** show that the deviator stress and axial strain relations of all test case under absolute dry condition in this study. It is seen that the stress reduces with increasing of strain in these stress-strain curves after the peak. This behavior is typical of dense granular materials and is commonly characterized as strain softening (Van et al., 1998; Akke et al., 2005). The strain-softening process is concomitant with the generation

of large deformations, which causes geometrically non-linear effects to become important. When the specimen is in a dense state, particles of different sizes fill each other dense, so that the particles squeezed tight, so in the shear increased the friction between the particles. And the particles in the shear band move or roll in the process of shear damage, then, stress-dilatancy is bound to occur. After the peak, because of the increase of stress-dilatancy behavior, the particles from the dense state gradually become loose state, the force on engagement between particles caused by stress-dilatancy behavior also gradually decreases until it disappears, so the phenomenon of stress reduction occurs.

The stress-strain behavior of the specimens under the dry condition, the deviator stresses were smaller in the specimen after cyclic loading than in those without cyclic loading, except a case at a confining pressure of 29.4 kPa.

In the dry condition, the confining pressure on 29.4 kPa indicates that after cyclic loading of the specimen, the particles are in closer contact, the compaction improves, and the strength increases. However, the case after cyclic loading decrease on the both confining pressures of 49.0 and 68.6 kPa. There are two possible reasons for this decrease in peak strength, i.e. change of packing state and reason of particle characteristics. The specimen without cyclic loading possesses a relatively loose packing state, which results in a larger strain hardening potential than the specimen with a dense packing state. In addition, since most of the particles are nearly spherical in shape. This would lead to a weaker interlocking and easier relative movement between soil particles, so the strength decreases (Wood, 1990; Chen et al., 2020).

**Fig.3.2 (b)** and **3.3 (b)** show that the deviator stress and axial strain relations (axial strain to 0.1%). **Fig.3.2 (c)** and **3.3 (c)** show that the deviator stress and axial strain relations (axial strain to 0.02%). **Fig.3.3 (c)** shows that when the confining pressure is 49.0 and 68.6 kPa, the stress-strain curve after cyclic loading appears S-shaped before the deviator stress 60 kPa in the dry condition. In general, the granular materials after cyclic loading and then monotonic triaxial compression test, the stress-strain curve appears S-shaped before the upper limit of stress amplitude of cyclic loading, the S-shape will appear on the stress-strain curve in the stress's range amplitude of the cyclic loading. This may be since the elastic deformation becomes better after cyclic loading (Kohata and Jiang, 1998; Kohata and Wakatsuki, 2019), it is easier to recover the original state when the test

specimen is compressed by external force in the elastic deformation range.

It was also found that the deviator stress increased with the increase of the confining pressure at the same axial strain  $\epsilon_a$  condition. It can indicate that granular materials monotonically loaded at higher confining pressures are stiffer and able to support larger loads failure (Bishop, 1966; Charles and Watts, 1980; Indraratna et al., 1998). The reason may be that the lateral constraint on the specimen enhanced with the increase of the confining pressure, which increases the contact area of the particles and makes the particle contact closer, producing a tightening effect on the specimen and playing the role of limiting the specimen deformation, so the strength of the specimen increases.

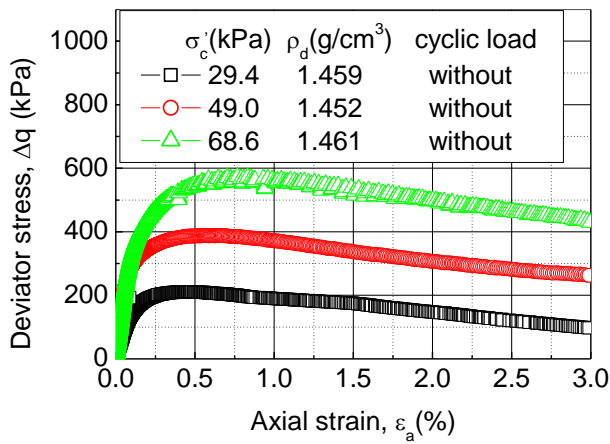


**Fig.3.2 (a)** Axial strain to 3 %, without cyclic loading

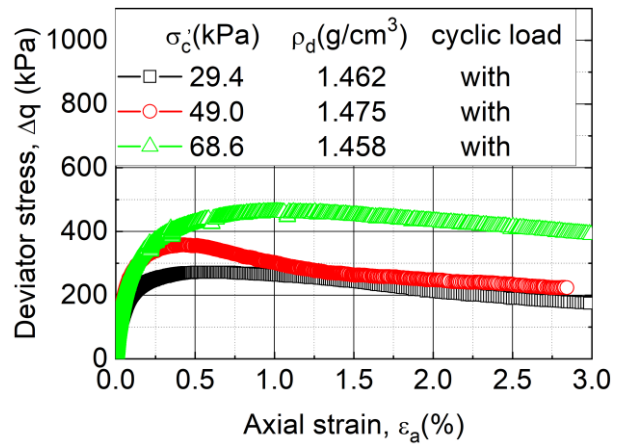


**Fig.3.3 (a)** Axial strain to 3 %, after cyclic loading

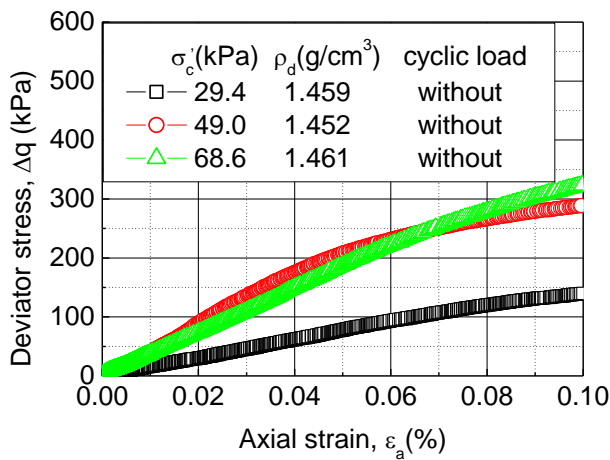


**Fig.3.2 (b)** Axial strain to 0.1 %, without cyclic loading

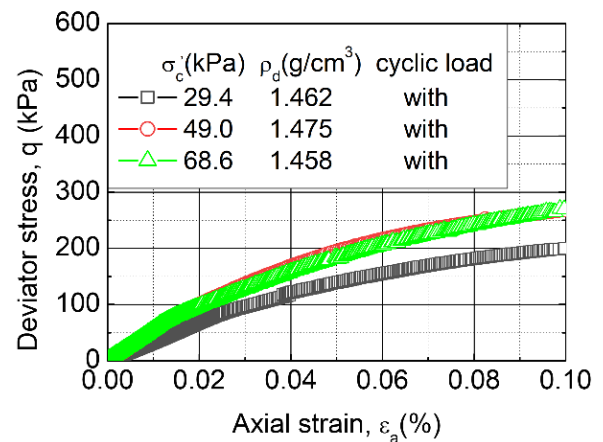


**Fig.3.3 (b)** Axial strain to 0.1 %, after cyclic loading

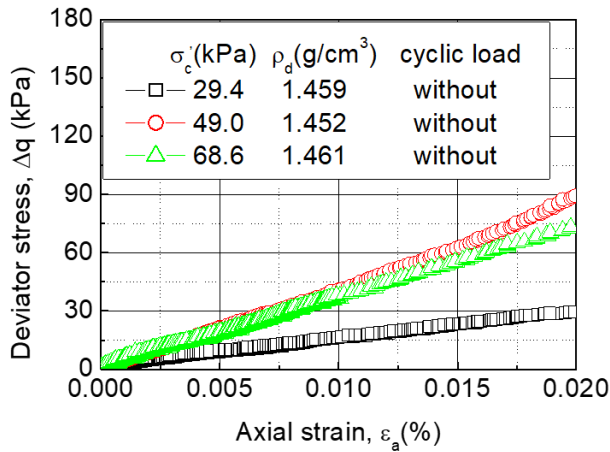


**Fig.3.2 (c)** Axial strain to 0.0.2 %, without cyclic loading

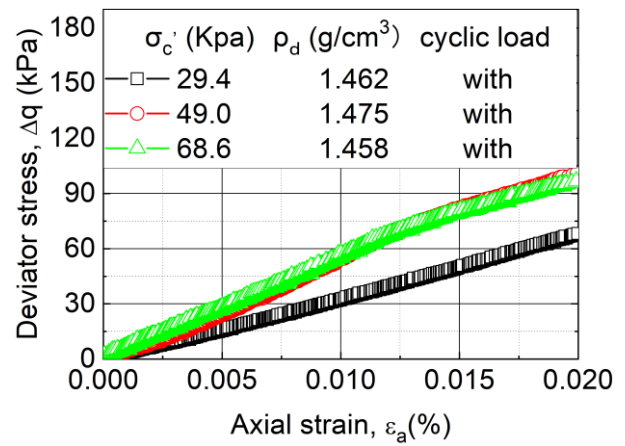


**Fig.3.3 (c)** Axial strain to 0.02 %, after cyclic loading

**Fig. 3.2 and Fig. 3.3** The stress-strain behavior of the specimens under the dry condition

### 3.3.2 Under optimum moisture content condition

**Fig.3.4 (a)** and **3.5 (a)** show that the deviator stress and axial strain relations are also strain softening under optimum moisture content condition. The deviator stress remains essentially unchanged with or without cyclic loading. It was found that cyclic loading does not have a significant effect on the strength of the specimen in the optimum moisture content condition. **Fig.3.4 (b)** and **3.5 (b)** show that the deviator stress and axial strain relations (axial strain to 0.1%). **Fig.3.4 (c)** and **3.5 (c)** show that the deviator stress and axial strain relations (axial strain to 0.02%). **Fig.3.5 (c)** shows that when the confining pressure is 29.4 and 49.0kPa, the stress-strain curve after cyclic loading appears S-shaped before the deviator stress 60 kPa in the optimum moisture content condition. It was also found that the deviator stress increased with the increase of the confining pressure at the same axial strain  $\epsilon_a$  condition.

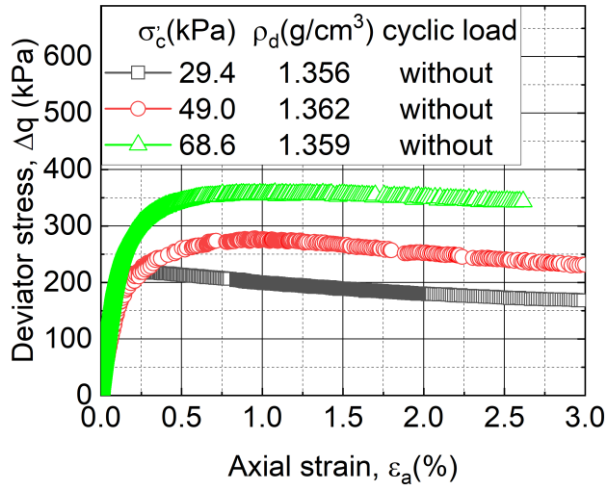


**Fig.3.4 (a)** Axial strain to 3 %, without cyclic loading

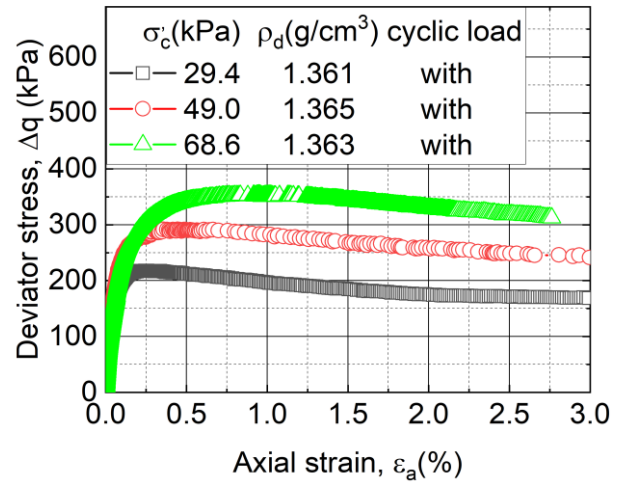


**Fig.3.5 (a)** Axial strain to 3 %, after cyclic loading

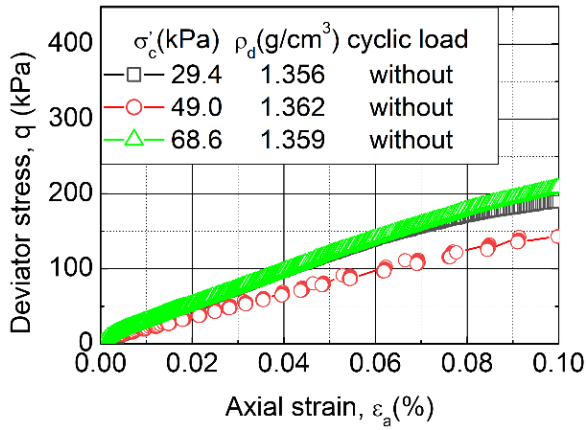


**Fig.3.4 (b)** Axial strain to 0.1 %, without cyclic loading

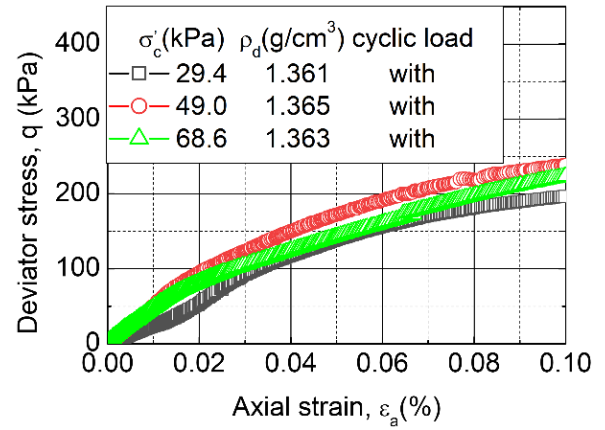


**Fig.3.5 (b)** Axial strain to 0.1 %, after cyclic loading

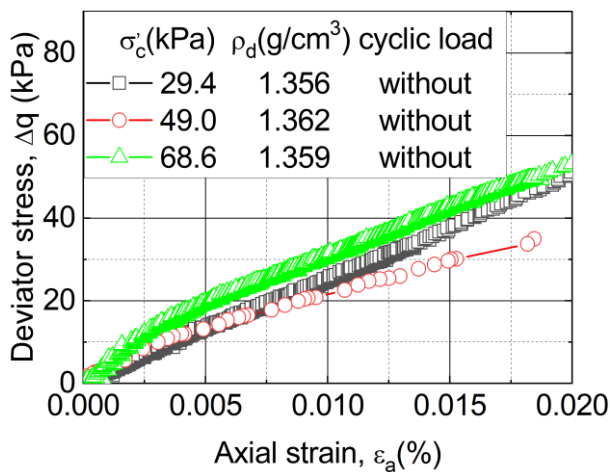


**Fig.3.4 (c)** Axial strain to 0.02 %, without cyclic loading

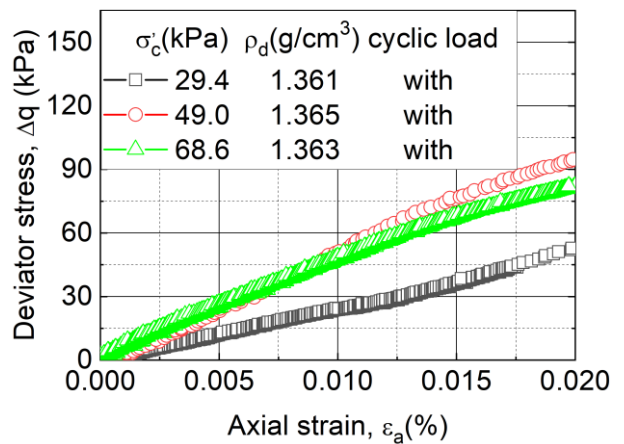


**Fig.3.5 (c)** Axial strain to 0.02 %, after cyclic loading

**Fig. 3.4 and Fig. 3.5** The stress-strain behavior of specimens under the optimum moisture content condition

### 3.4 The maximum deviator stress and Mohr's circle

#### 3.4.1 Under dry condition

It can be seen from Fig. 3.6 that the peak strength increases with increasing confining pressure, regardless of the stress history, which is due to the granular materials monotonically loaded at higher confining pressures are stiffer and able to support larger loads before failure. The peak strength were smaller in the specimen with cyclic loading than in those without cyclic loading. Only at a confining pressure of 29.4 kPa, after cyclic loading, the peak strength is greater than that without cyclic loading.

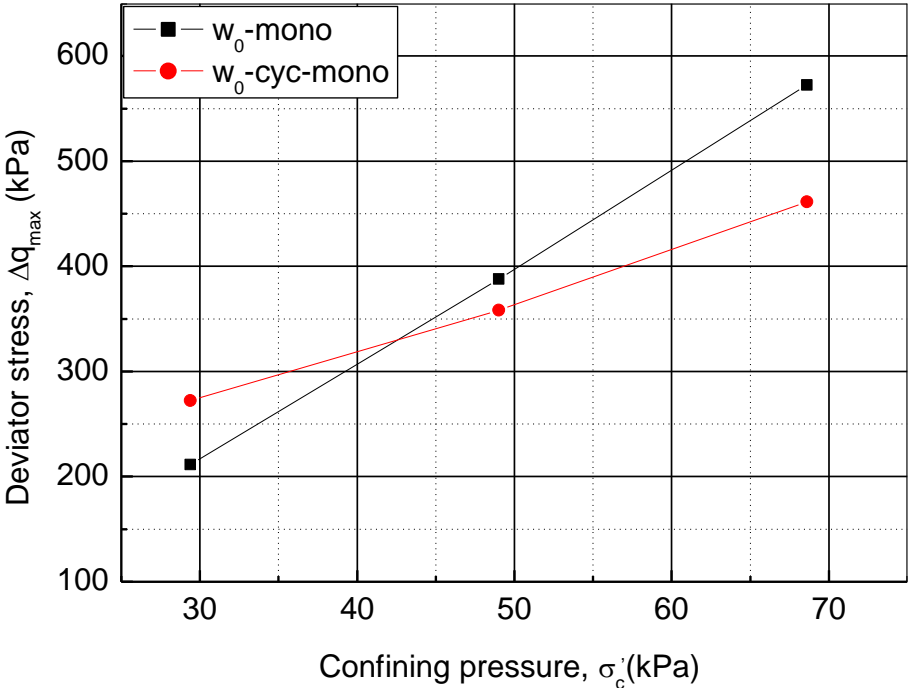


Fig. 3.6 The peak strength-confining pressure behavior of the specimens under dry condition

The peak strength of noncohesive granular materials in triaxial compression is often interpreted by means of a Mohr-Coulomb criterion (Lambe and Whitman, 1969; Wood, 1990; Vardoulakis and Sulem, 1995).

As shown in Fig. 3.7, it can be seen that the friction angle decreases after cyclic loading in the absolute dry condition; the cohesive force increases from 0 to 29 kPa after cyclic loading. It may be that after cyclic loading

the coarse particles underwent some sliding and were filled with fine material between them, which in turn reduced the occlusal force between the coarse particles, so the friction angle decreased the cohesive force is increased. The shear strength characteristics of coarse aggregates can be described by the Mohr-Coulomb criterion, while as a non-cohesive bulk material, there is no cohesive force between particles, only frictional resistance, but a large number of test results show that if the linear strength criterion is used to represent the shear strength of coarse aggregates ( $\tau$ ), the linear intercept representing the cohesive force  $c$  is not 0 kPa. Many scholars (Thom and Brown, 1989; Chen, 1994; Cao et al., 2016) believe that the value of  $c$  at this point is not explained by cohesion, but should be another manifestation of the occlusal force between coarse particles.

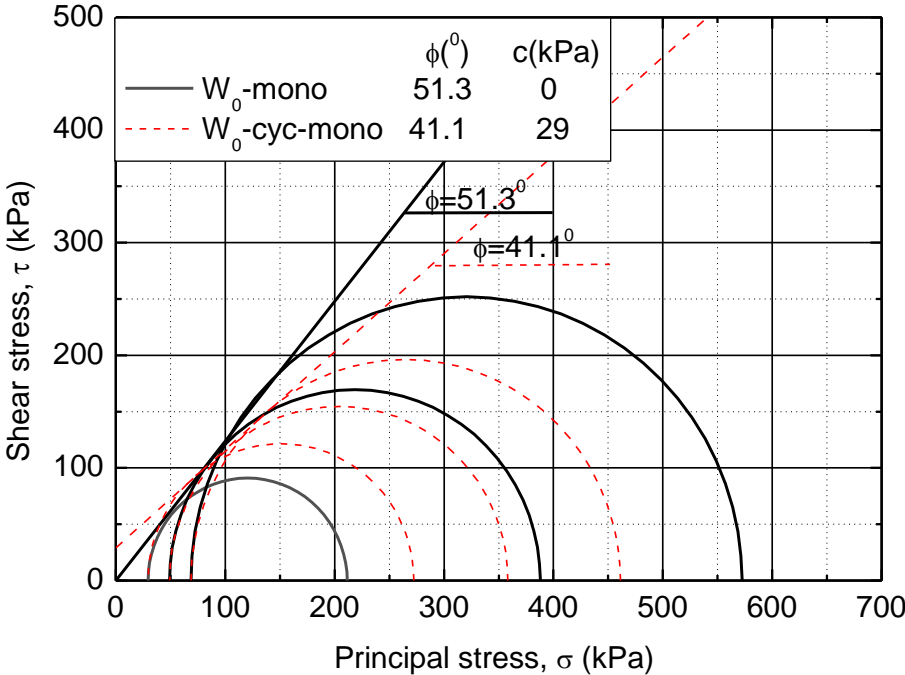


Fig. 3.7 The Mohr's circles in peak stress state under dry condition

**3.4.2 Under optimum moisture content condition**

After cyclic loading, it can be seen from Fig.3.8 that the peak strength is essentially unchanged at the same confining pressure. Only at a confining pressure of 49 kPa, after cyclic loading, the peak strength is greater than

that without cyclic loading.

The  $q_{max}$  after cyclic loading is essentially unchanged at the same confining pressure. According to the previous study (Kohata and Wakatsuki, 2019), the  $q_{max}$  of the common subbase course material is 225-300 kPa without cyclic loading under the optimum moisture content at confining pressure of 29.4 kPa, and the case after cyclic loading is 150-275 kPa. The  $q_{max}$  of the material of this study is about 225 kPa under the same conditions, which is about 80 % of the common subbase course material. **Fig.3.8** also shows that the maximum deviator stress increased with increase of the confining pressure.

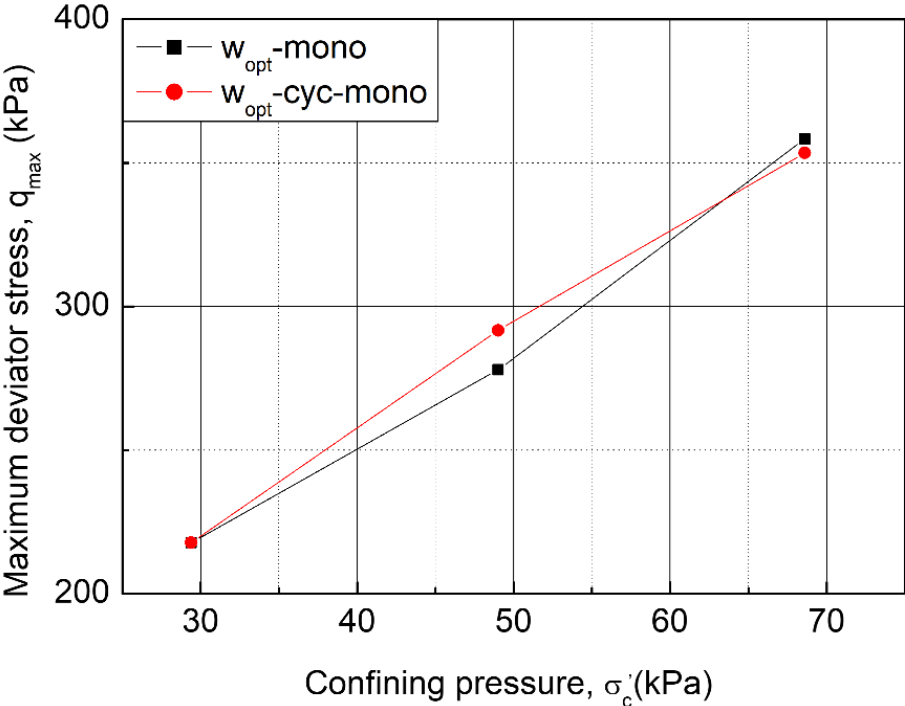


**Fig. 3.8** The peak strength-confining pressure behavior of the specimens under optimum moisture content condition

From **Fig. 3.9**, it can also be seen that the friction angle decreases and the cohesive force increases after cyclic loading in the optimum moisture content condition, but the increase and decrease are very small. It was found that cyclic loading has not a significant effect on the friction angle and the cohesive force of the specimen in the optimum moisture content condition.

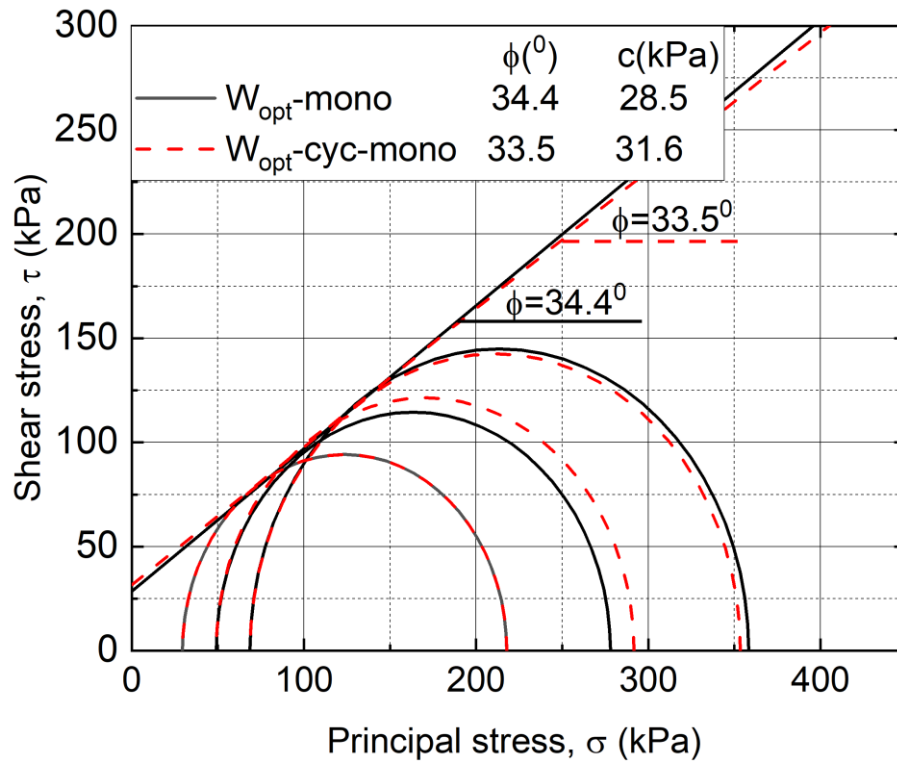


**Fig. 3.9** The Mohr's circles in peak stress state under optimum moisture content condition

### 3.5 Initial Young's modulus and Tangent Young's modulus

#### 3.5.1 Definition of the Young's modulus

In the **Fig. 3.10**, the definition of different Young's modulus is indicated. The initial Young's modulus  $E_0$  is often used to characterize the stiffness of the geomaterials. It is determined as the slope of the tangent line to the origin of the stress–strain curve. An example of determination is shown in **Fig. 3.11**. Coarse-grained soils exhibit linear elastic characteristics when the axial strain is less than  $10^{-5}$  under static or dynamic loading conditions according to the past research (Shibuya et al., 1992). In this study, small unloading and reloading is performed at the initial portion during monotonic loading. The initial deformation modulus  $E_0$  is defined as a slope of stress–strain relations at small strain level,  $\epsilon_a = 10^{-6} \sim 10^{-5}$ .

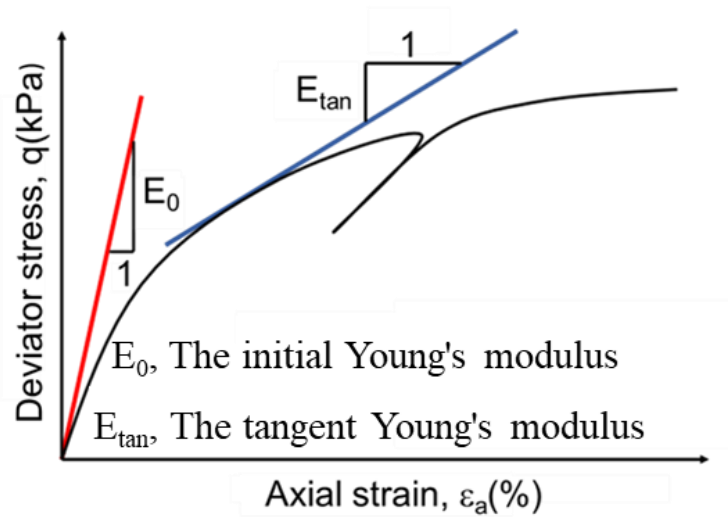


Fig.3.10 Definition of different Young's modulus

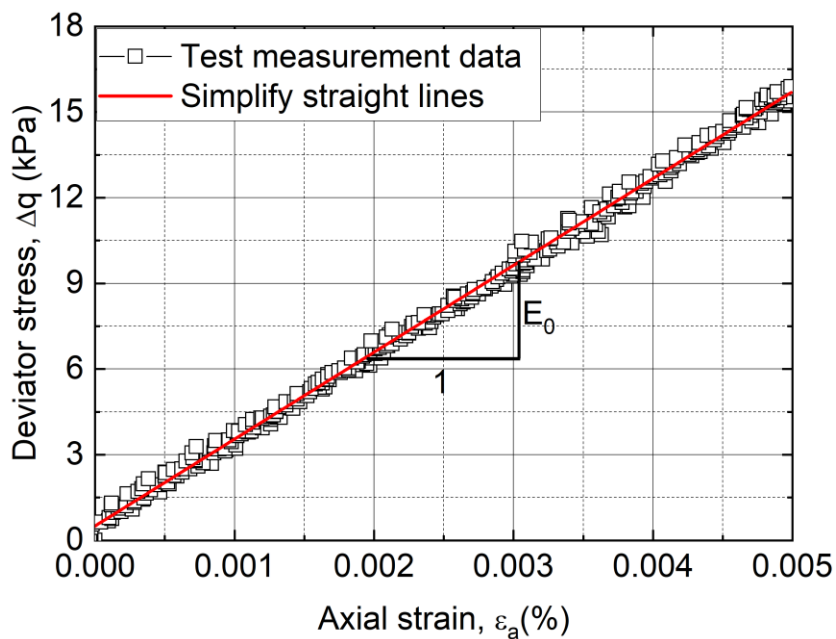


Fig. 3.11 Initial Young's modulus calculation method

### 3.5.2 Under dry condition

Fig.3.12 shows the relationship between the confining pressure and the initial deformation modulus  $E_0$  increases with the increase of the confining pressure. This is because the confining pressure plays a certain lateral restraint effect, when the confining pressure is small, the resistance to particle movement is small, and the

deformation resistance of specimen is weak. When the confining pressure is relatively large, the resistance to particle movement is large, and the deformation resistance of specimen is strong.

The initial modulus of the pre-straining compression curve is much higher than the case without cyclic loading. It is widely accepted that increase under stress level, a decrease in soil porosity or increase in the over-consolidation ratio would increase the stiffness of soils (Hardin and Richart, 1992; Gu et al., 2014; Chen et al., 2020). In this study, the increase in the pre-straining elastic modulus is mainly because of the decrease in the void ratio of the specimen, which is induced by the densification effect of cyclic loading, and the increase in the over-consolidation ratio, which is resulted from the release of cyclic deviator stress. At the particle scale, after the soil specimen experiences large stress, the average distance between the centers of adjacent particles becomes smaller and the number of particle contacts per particle increases, so decreasing the average contact stress corresponding to a certain external load. Hence, the deformation in particle contacts decreases, and the stiffness of soil increases.

**Fig. 3.13** and **Fig. 3.14** show that the relationship between axial strain and tangential deformation modulus  $E_{tan}$  under the dry condition, the general trend of the  $E_{tan}$  with the increase in strain is a slow increase followed by a sharp decrease. However, it is found that when the confining pressure is 68.6 kPa, there is a sharp decrease followed by an increase in the initial strain at the beginning. Therefore, it can be inferred that the stiffness at the initial stage of cyclic loading increases when the specimen is subjected to cyclic loading. In general, when granular materials are subjected to cyclic loading, the elastic component of strain becomes dominant and the stiffness at the initial stage of cyclic loading increases, and the same tendency can be considered for the mixed material used in this study.

Compared of the **Fig. 3.13** and **Fig. 3.14**, the laboratory test results prove that the  $E_{tan}$  of specimens after cyclic loading were larger than those without cyclic loading. After cyclic loading, the stiffness of specimen increases (Lenart et al., 2014).

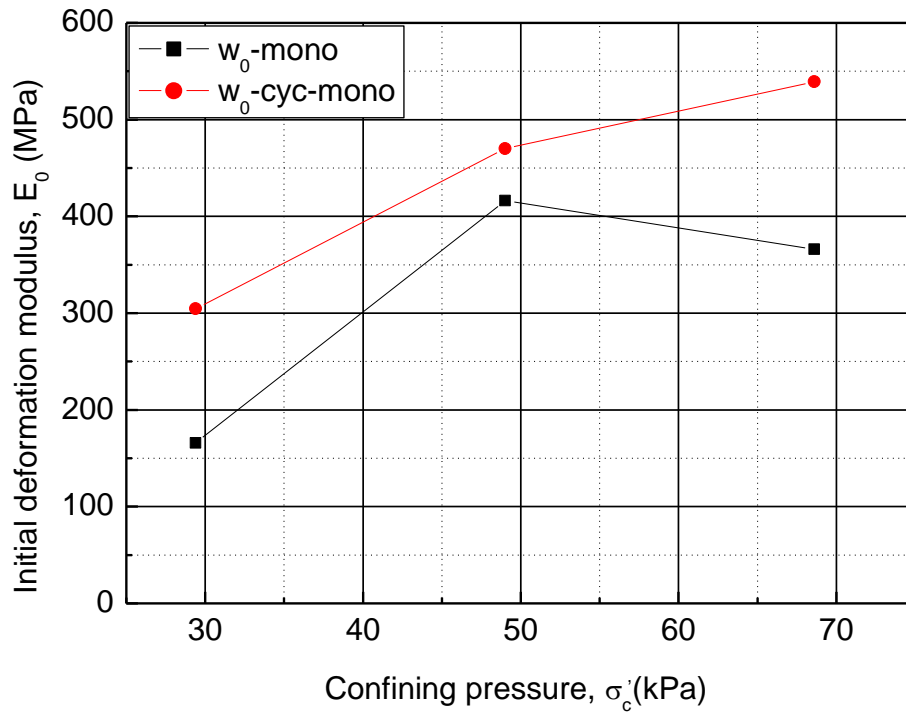


**Fig. 3.12** The relationship between confining pressure and initial deformation modulus under dry condition

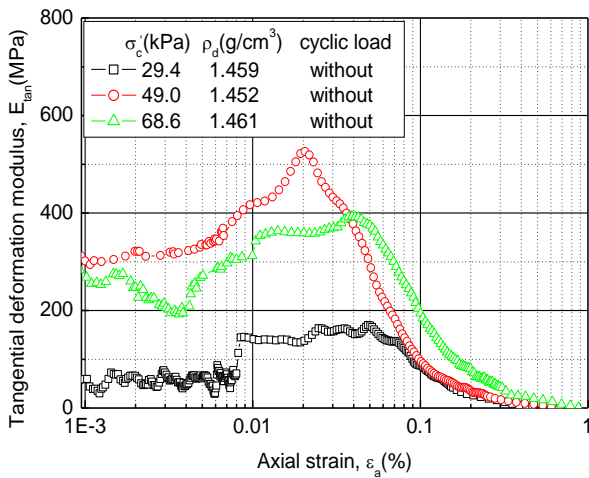


**Fig. 3.13** The relationship between axial strain and tangential deformation modulus without cyclic loading

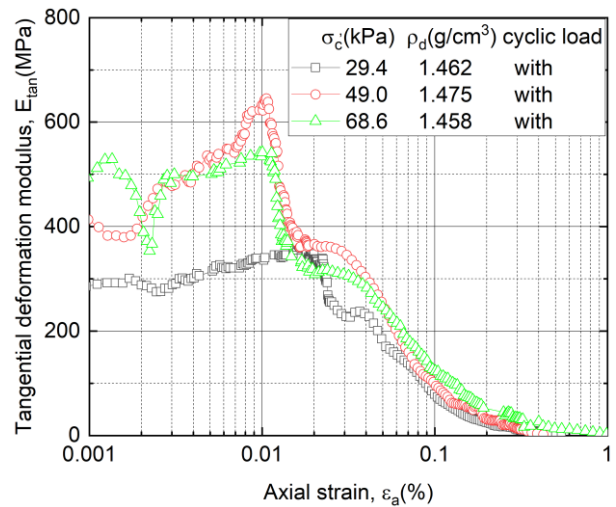


**Fig. 3.14** The relationship between axial strain and tangential deformation modulus after cyclic loading

### 3.5.3 Under optimum moisture content condition

Fig. 3.15 also shows the relationship between the confining pressure and the initial deformation modulus  $E_0$  increases with the increase of the confining pressure. The reason is the same as the case in dry condition.

Fig. 3.16 and Fig. 3.17 show that the relationship between the axial strain and the  $E_{tan}$  under the optimum moisture content condition, the general trend of the  $E_{tan}$  with the increase of strain is that it first goes through slowing down, then increasing, and finally dropping sharply.

Compared Fig. 3.16 and Fig. 3.17, the laboratory test results prove that the  $E_{tan}$  of specimens after cyclic loading were larger than those without cyclic loading.

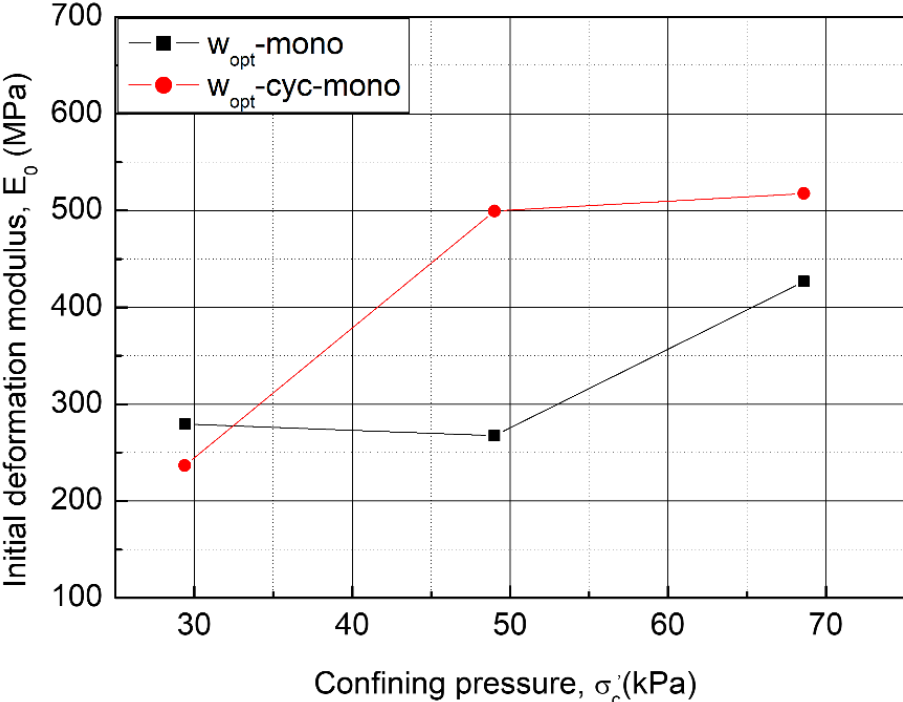
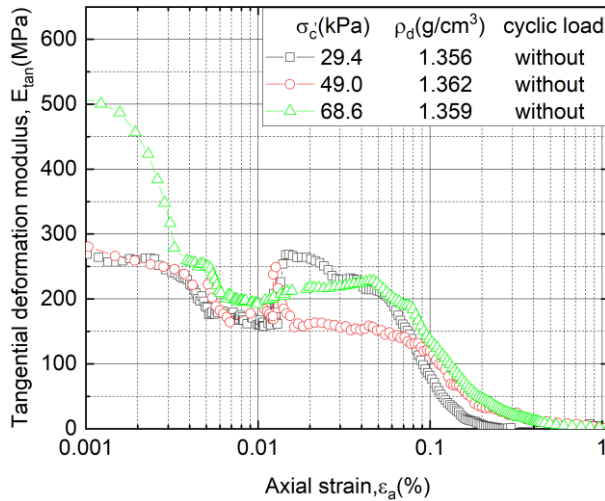
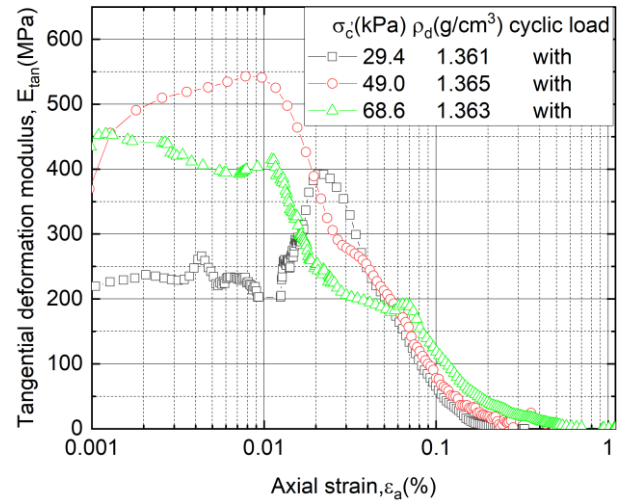


Fig. 3.15 The relationship between confining pressure and initial deformation modulus under optimum moisture content condition



**Fig. 3.16** The relationship between axial strain and tangential deformation modulus without cyclic loading



**Fig. 3.17** The relationship between axial strain and tangential deformation modulus after cyclic loading

### 3.6 Summary

The following understandings can be noted after we analyzed the static triaxial test results of specimen derived. In this chapter, the effects of cyclic loading on the strength and deformation of specimens are analyzed by the static triaxial test. The changes of deviator stress - axial strain relationship, Mohr circle, initial elastic modulus and tangent deformation modulus under dry and wet condition are compared. The following conclusions can be derived.

- (1) All specimens show an increase in  $q_{max}$  with increasing confining pressure and are characterized by strain softening.
- (2) The deviator stress- axial strain curve after cyclic loading appears S-shaped before the deviator stress 60 kPa.
- (3) It was found that the  $q_{max}$  was smaller in the specimen after cyclic loading than in those without cyclic loading in the dry condition, while cyclic loading does not have a significant effect on the  $q_{max}$  of the specimen in the optimum moisture content condition.
- (4) It can be seen that the angle of shear resistance decreases after cyclic loading in the dry condition, and the cohesion increases from 0 to 29 kPa, while the cohesion and the angle of shear resistance are stable in the

optimum moisture content condition.

(5) The angle of shear resistance of the light-weight subbase course material after cyclic loading is  $41.1^\circ$  and  $33.5^\circ$  under the dry condition and the optimum moisture content. It is considered that the requirement of the angle of shear resistance as road subbase course material is satisfied.

(6) The initial deformation modulus  $E_0$  increases with the increase of confining pressure.

(7) The initial stiffness after cyclic loading is much higher than that of the specimen compressed under the same pressure without cyclic loading.

(8) The tangent deformation modulus  $E_{tan}$  after cyclic loading were all larger than those without cyclic loading.

(9) In the case with cyclic loading, the  $E_{tan}$  tends to increase with the progress of shear, and then it turns to decrease.

(10) These findings show that the testing material, after cyclic loading, gains its stiffness while degrades in terms of peak strength. Therefore, the stability problem, which is mainly governed by the strength parameters of material, should take the effect of cyclic loading into consideration to avoid that the design is on the unsafe side.

## References:

Akke,S.J.S., Ernest,T.S. and Raymond,F., 2005. Static and Cyclic Triaxial Testing of Ballast and Subballast, *Journal of Geotechnical and Geoenvironmental Engineering*,Vol.131, Issue 6, pp. 771-782.

Bishop,A.W., 1966. "The Strength of Soils as Engineering Materials." *Geotechnique*, 16, pp. 91-128.

Cao,W., Huang,W.J., Wang,J.Y. and Zhai,Y.C., 2016. Large-scale triaxial test study on deformation and intensity characteristics of soil-rock aggregate mixture (in Chinese).

Charles,J.A. and Watts,K.S., 1980. "The Influence of Confining Pressure on the Shear Strength of Compacted Rockfill." *Geotechnique*, 30 (4), pp. 353-367.

Chen,W.B., Liu,K., Feng,W.Q. and Yin,J.H., 2020. Partially drained cyclic behavior of granular fill material in triaxial condition, *Soil Dynamics and Earthquake Engineering*, Vol. 139.

Chen,X.Z.,1994. Research on the strength of the coarse grained soil and the interlocking force (in Chinese).

Gu,C., Wang,J., Cai,Y. and Guo,L., 2014. Influence of cyclic loading history on small strain shear modulus of saturated clays, *Soil Dynam Eartha Eng*, Vol. 66, pp. 1-12.

Hardin,B.O. and Richart,J.F., 1963. Elastic wave velocities in granular soils, *Soil Mech Found Div ASCE*, Vol. 89, Issue 1, pp. 33-65.

- Hyde,A.F.L., Yasuhara,K. and Hirao,K., 1993. Stability criteria for marine clay under one-way cyclic loading. *J Geotech Eng*, pp. 1771-1789.
- Indraratna,B., Ionescu,D. and Christie,H.D., 1998. "Shear Behavior of Railway Ballast Based on Large-Scale Triaxial Tests." *Journal of Geotechnical and Geoenvironmental Engineering*, 124 (5), pp. 439-449.
- Kohata,Y. and Jiang,G.L., 1998. Triaxial shear deformation properties of a wellgraded crushed gravel subjected to cyclic loading, *RTRI REPORT*, Vol.12, Issue 4, pp. 43-48(in Japanese).
- Kohata,Y. and Wakatsuki,H., 2019. Triaxial shear property of man-made lightweight geomaterials clinker soil, *The 59th of Japanese Geotechnical Society Hokkaido Branch Technical Report Collection*, (in Japanese).
- Lambe,T.W. and Whitman,R.V., 1969. *Soil Mechanics*, New York, Wiley.
- Lenartab,S., Kosekib,J., Miyashitab,Y. and Satoc,T., 2014. Large-scale triaxial tests of dense gravel material at low confining pressures, *Soils and Foundations*, Volume 54, Issue 1, Pages 45-55.
- Moses,G.G. and Rao,S.N., 2003. Degradation in cemented marine clay subjected to cyclic compressive loading. *Mar Georesour Geotechnol*, pp. 37-62.
- Seed,H.B. and Mcneill,R.L.,1956. Soil deformation in normal compression and repeated loading test. *Highway Res Board Bull* 141, pp. 44-53.
- Shibuya,S., Tatsuoka,F., Teachavorasinskun,S., Kong,X.J., Abe,F., Kim,Y.S. and Park,C.S., 1992. Elastic deformation properties of geomaterials [J], *Soils and Foundations*, Vol. 32, Issue 3, pp. 26-46.
- Thom,N.H. and Brown,S.F., 1989. The mechanical properties of unbound aggregates from various sources. *UNBAR* 3, Nottingham, pp130-142.
- Van,G E. and Borst R., 1998. "Introduction to material instabilities in solids." *Material instabilities in solids*, R. de Borst, and E. van der Giessen, eds., Wiley, Chichester.
- Vardoulakis,I. and Sulem,J., 1995. *Bifurcation analysis in geomechanics*, Blackie, London.
- Wang,J., Cai,Y.Q. and Yang,F., 2013. Effects of initial shear stress on cyclic behavior of saturated soft clay. *Marine Georesources & Geotechnology*, Volume 31, 2013 - Issue 1, pp. 86-106.
- Wood,D.M., 1990. *Soil behaviour and critical state soil mechanics*, Cambridge University Press, Cambridge, U.K.



## **CHAPTER 4**

### **EFFECT OF MOISTURE ON STRENGTH DEFORMATION OF SPECIMEN**



## 4.1 Introduction

Among the various factors, it is known that moisture has a significant impact on the deformation behavior of Unbound Granular Materials (UGMs), which in turn significantly affects the performance of the pavement structure (Ekblad, 2007; Erlingsson, 2010; Cary and Zapata, 2011; Ebrahim et al, 2019). Water can enter pavement structures by many methods, such as rain and groundwater (Dempsey and Elzeftawy, 1976). Ridgeway (1976) concluded, based on field measurements, that cracks can be a significant source of free water for both flexible and rigid pavements. Hassan and White (1997) reached the same conclusion performing laboratory and field experiments and stated that surface infiltration is the primary source of water in pavements. Dempsey (1979), on the other hand, predicted, from regression analysis of precipitation and drainage outflow, considerably lower infiltration rates. Simulation of pavement response by Markow (1982) and Liu and Lytton (1984) indicated decreased pavement life and reduced pavement strength as a consequence of water infiltration through cracks and joints.

The cracks in the asphalt layers lead to the ingress of water in the rainy season and cause the moisture fluctuations within the base and base layers. In addition, seasonal fluctuations in the groundwater level also cause changes in the water content in the road substructure (Inam et al., 2012). With regard to the studies on the moisture content, Cerni et al. (2012) compared the permanent deformation behavior of two unbound granular materials between the optimal moisture state and the saturated state under cyclic loading and found that samples under optimal moisture conditions had a higher plastic shakedown and plastic creep limit than those under a saturated state. Duong et al. (2013) investigated the effects of fine and water contents on the intermediate floors and showed that higher fineness levels lead to greater permanent axial expansions in an almost saturated state, while the opposite trend was observed with lower water contents. Inam et al. (2012) carried out a series of laboratory tests on granular base course materials at different moisture contents and found that the moisture content for maximum deformation varied depending on the loading method. Cao et al. (2017) and Cerni et al. (2012) compared the permanent deformation behavior of two UGMs under the optimal moisture state and the saturated state and highlighted the moisture susceptibility of the mixture of UGMs. Trinh et al. (2012) performed monotonous and cyclic triaxial tests under three moisture content conditions and found that a higher moisture

content led to a greater permanent axial strain. The authors in (Dawson et al., 1996; Uthus, 2007) reported that too much water trapped in the pavement structure combined with the repeated loading from traffic may cause decrease in effective stress and due to excessive pore pressure occurrence in the material. The consequence is reduction in bearing capacity in the base and subbase leading to cracking and rutting of the asphalt pavement. The moisture content of most untreated granular materials has been found to affect the resilient response characteristics of the material in laboratory and in situ conditions (Kancherla, 2004). Thom and Brown, (1987) reported that increased moisture content may decrease the resilient modulus of a wet aggregate base material to approximately 10% of the value corresponding to the dry condition.

In general, water causes changes in the properties of the UGMs. What effect water has on the strength deformation of the mixes is a question worthy of in-depth study. In this chapter, the effect of wetting on the strength-deformation properties of the mixes is analyzed by comparing the results of triaxial tests of the mixes in the dry condition and the wet condition.

## **4.2 Relationship between deviator stress and axial strain**

### **4.2.1 Without loading history**

Many scholars (Coronado et al., 2005; Ekblad and Isacsson, 2008; Ng et al., 2013) indicated that the moisture of the specimen has a considerable influence on the strength characteristics of unbound granular material in the monotonic triaxial compression tests. Karube and Kato (1994) found the volume change initially decreases, and then the specimen shows the trend of dilatancy regardless of the degree of saturation. In this case, the positive dilatancy tends to be stronger in the order of saturated, optimum, simulated, and air-dried specimens. This phenomenon is thought to be caused by the capillary force between particles which attempts to maintain the soil skeleton structure of the unsaturated soils. Zhan and Ng (2006) studied the shear strength characteristics of an expansive clay, and discussed the contribution of the matric suction to the shear strength. Oka et al. (2010) found that the initial matric suction strongly influenced the stress-strain behavior of the unsaturated silt.

**Fig. 4.1 (a)** and **4.2 (a)** show that the deviator stress and axial strain relations of all test case without loading history in this study. As shown in Figure, with the increase of the axial strain, the deviator stress sharply increases

to the peak stress at an axial strain of about 0.5 % under both conditions, and then it gradually decreases. **Fig. 4.1 (b)** and **4.2 (b)** show that the deviator stress and axial strain relations (axial strain to 0.1%). **Fig. 4.1 (c)** and **4.2 (c)** show that the deviator stress and axial strain relations (axial strain to 0.02%). From the stress-strain behavior of the specimens without loading history, it can be seen that the deviator stresses were smaller in the specimen under wet condition than in those under dry condition, except a case at a confining pressure of 29.4 kPa.

It can be seen that moisture improves the shear strength of the specimen under confining pressure of 29.4 kPa. The reason may be the matrix suction plays a certain role. The resistance of soils to plastic deformation is strongly influenced by shear resistance between grain contact points. The matric suction here is presented in the capillary force, which acts perpendicularly on grain contact points and attracts soil particles together. Then this force restrains relative small sliding between soil particles (Kohgo et al., 2007b).

However, the shear strength of the specimen under wet condition decrease on the both confining pressures of 49.0 and 68.6 kPa, the reason may be that the shear resistance of cohesionless soils is considered to be the result of interparticle friction and dilation. The interparticle locking could restrain sliding and rotation between particles and the dilation tends to degrade the interparticle locking. Therefore, large shear stress is required to break the interlocking between particles. The volumetric strain under dry condition is larger than that of wet condition, which implies that more stress is needed to break the interlocking between dry particles (Guo and Su, 2007).

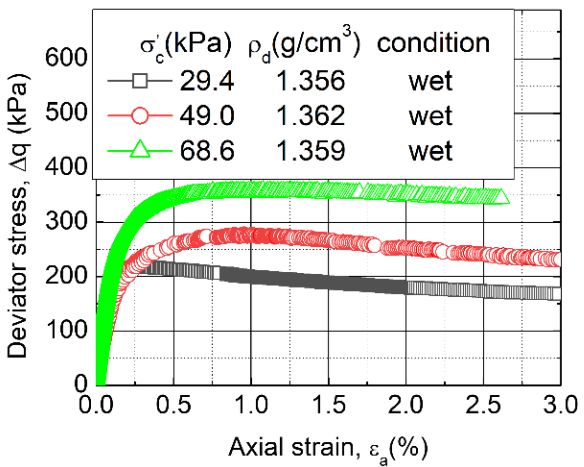
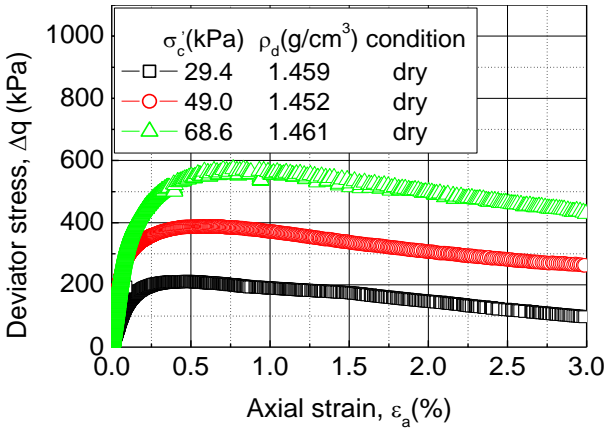


**Fig. 4.1 (a)** Axial strain to 3 %, under dry condition    **Fig. 4.2 (a)** Axial strain to 3 %, under wet condition

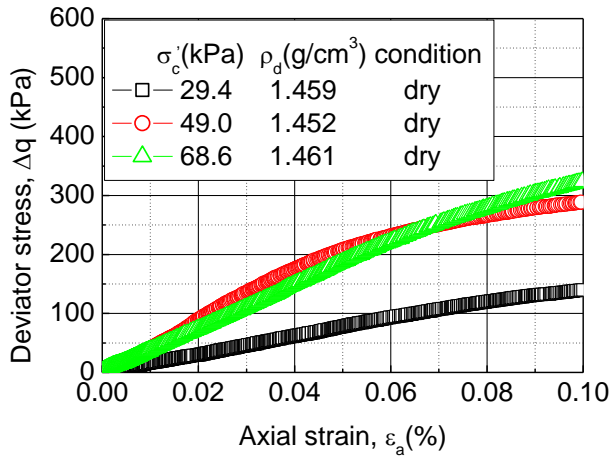


Fig. 4.1 (b) Axial strain to 0.1 %, under dry condition

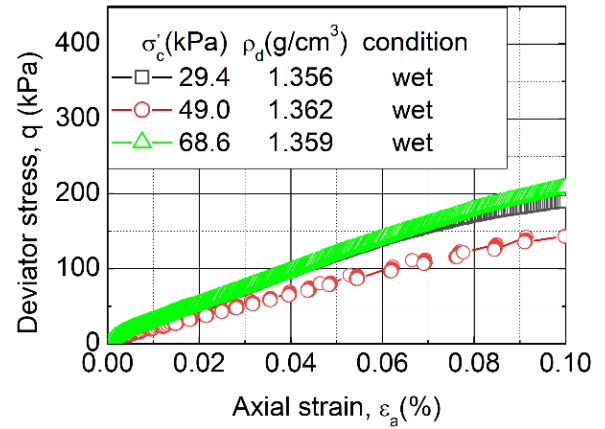


Fig. 4.2 (b) Axial strain to 0.1 %, under wet condition

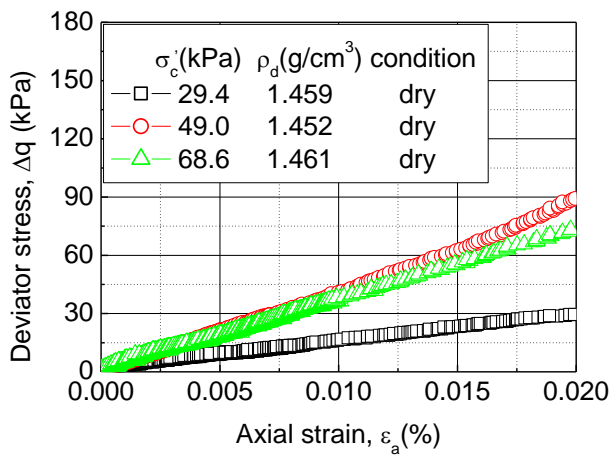


Fig.4.1(c) Axial strain to 0.02 %, under dry condition

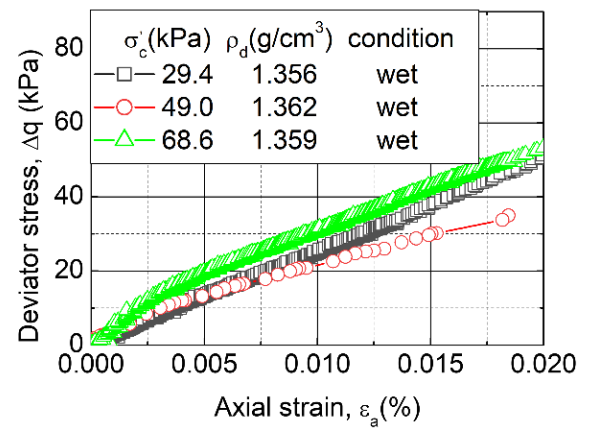


Fig. 4.2(c) Axial strain to 0.02 %, under wet condition

Fig. 4.1 and Fig. 4.2 The stress-strain behavior of the specimens without loading history

#### 4.2.2 With loading history

Fig. 4.3 (a) and 4.4 (a) show that the deviator stress and axial strain relations of all test case with loading history in this study. As shown in Figure, with the increase of the axial strain, the deviator stress sharply also increases to the peak stress at an axial strain of about 0.5 % under both conditions, and then it gradually decreases. Fig. 4.3 (b) and 4.4 (b) show that the deviator stress and axial strain relations (axial strain to 0.1%). Fig. 4.3 (c) and 4.4 (c) show that the deviator stress and axial strain relations (axial strain to 0.02%). From the stress-strain behavior of the specimens with loading history, it can be seen that the deviator stresses were smaller in the specimen under wet condition than in those under dry condition.

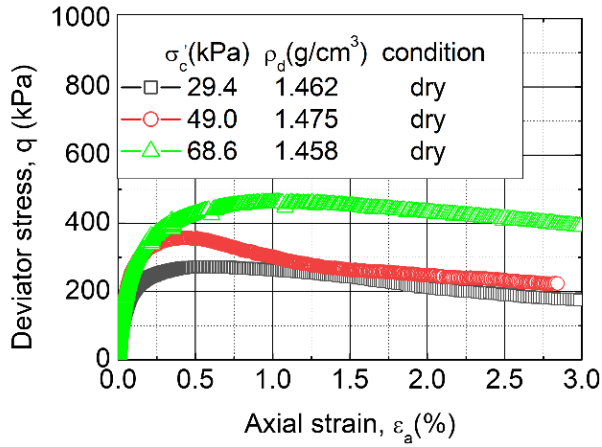


Fig. 4.3 (a) Axial strain to 3 %, under dry condition

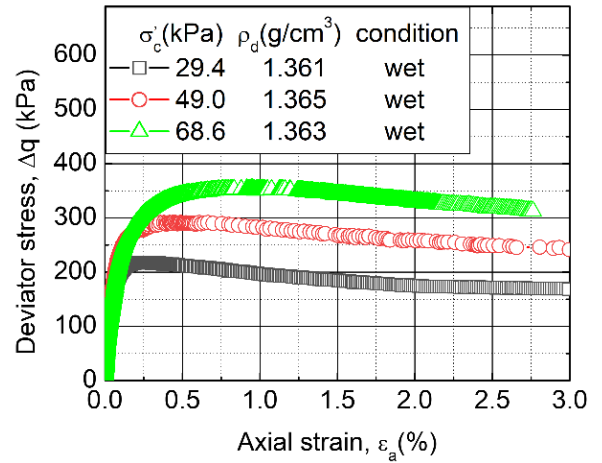


Fig. 4.4(c) Axial strain to 3 %, under wet condition

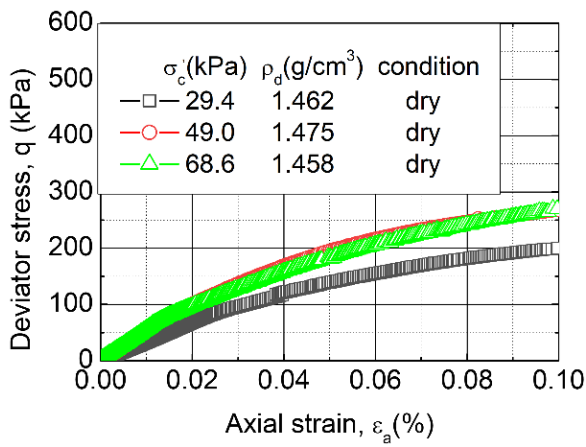


Fig. 4.3 (b) Axial strain to 0.1 %, under dry condition

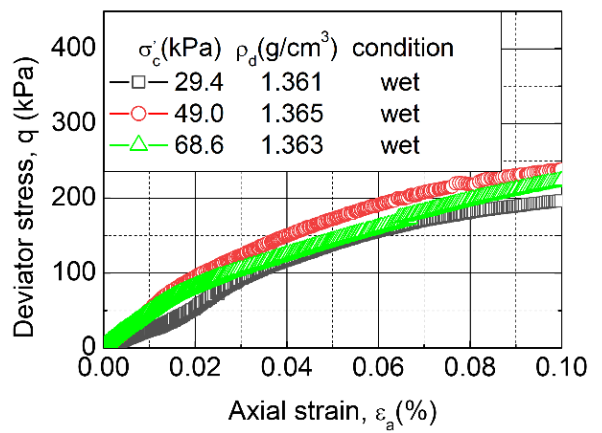


Fig. 4.4(c) Axial strain to 0.1 %, under wet condition

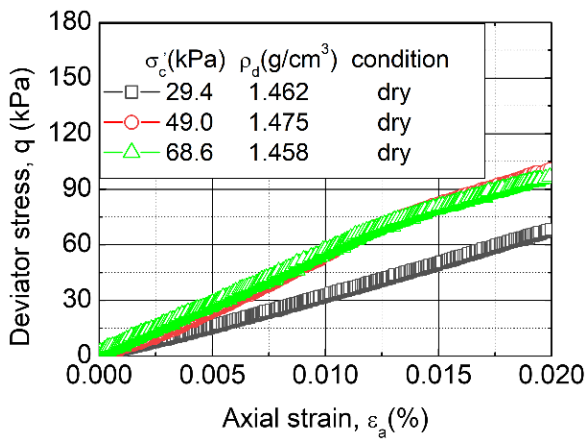


Fig. 4.3 (c) Axial strain to 0.02 %, under dry condition

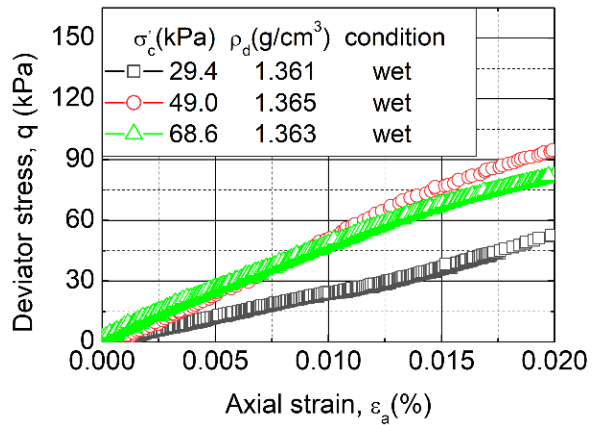


Fig. 4.4 (c) Axial strain to 0.02 %, under dry condition

Fig. 4.3 and Fig. 4.4 The stress-strain behavior of the specimens with loading history

### 4.3 The maximum deviator stress and Mohr's circle

#### 4.3.1 Without loading history

It can be seen from Fig. 4.5 that the peak strength increases with increasing confining pressure under both conditions. The peak strength were smaller in the specimen under wet condition than in those under dry condition. Only at an confining pressure of 29.4 kPa, the peak strength of specimen under wet condition is greater than that under dry condition. The increase of maximum deviator stresses in the specimen had an almost linear relationship with confining pressure. The lubrication of water leads to lower friction between particles, which leads to greater deformation of aggregate combination and subsequent reduction of stiffness, weakening the connection between soil particles. Classical water film theory (Zhao et al., 2007) believes that too high or too low moisture content is not conducive to the tight arrangement of the granular materials, squeeze each other, and adversely affect the strength of the mixture.

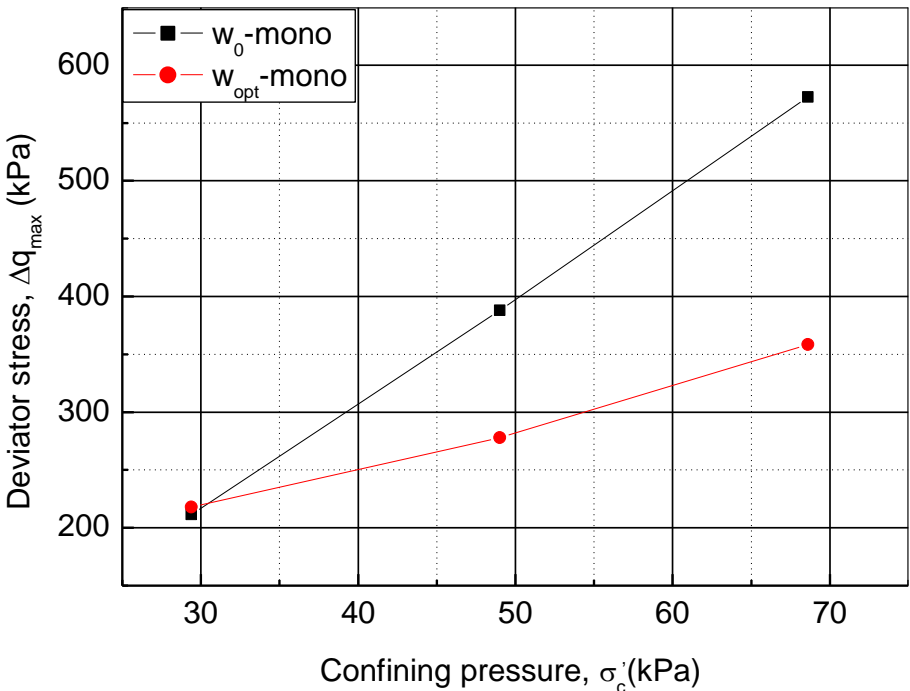


Fig. 4.5 The peak strength-confining pressure behavior of the specimens without loading history

Mohr circles together with the Mohr-Coulomb failure envelope of the specimen without loading history are presented in Fig. 4.6. The specimen under dry condition had angle of friction of 51.3°, which was greater than

34.4° that of wet condition. It can be seen that moisture is the reason for reduction of friction between particles. This also explained the greater shear strengths of dry condition compared to those of wet condition. Fig. 4.6 also shows that the failure envelope of specimen had an intercept with the shear axis indicating cohesion for specimen under wet condition, which is 28.5 kPa. Because water will form a capillary tension on the particle surface, which leads to the increase of cohesion. Classical soil mechanics believes that sand-like non-cohesive soil does not have cohesion, but when there is water in the sand, the internal pores will shrink due to the negative pressure of capillary water, which creates cohesion for the sand. But this cohesion gradually disappears with the gradual increase of moisture as the capillary water gradually turns into free water, so it is also called “fake cohesion” or “apparent cohesion”. The change of the moisture in the sand has a significant effect on the content and distribution of capillary water in the sand, so the moisture has a greater influence on the apparent cohesion of coral gravelly sand in the triaxial shear test. A similar observation about the decrease of internal friction angle when increasing water content was made by Seif El Dine et al. (2010), Selig and Waters (1994) and Fortunato et al. (2010).

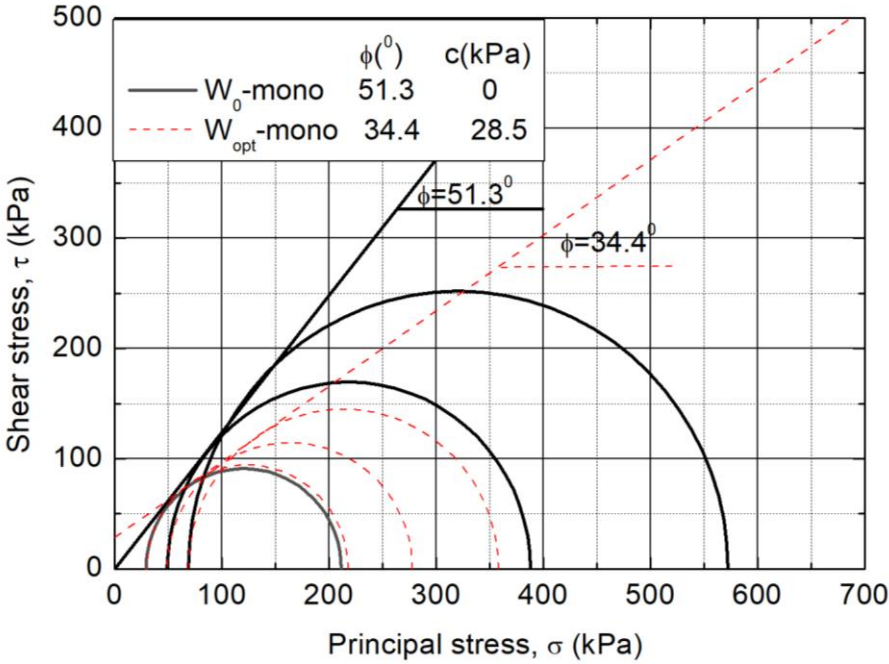


Fig. 4.6 The Mohr's circles in peak stress state without loading history

### 4.3.2 With loading history

It can be seen from Fig. 4.7 that the peak strength increases with increasing confining pressure under both conditions. The peak strength were smaller in the specimen under wet condition than in those under dry condition. The increase of maximum deviator stresses in the specimen also had an almost linear relationship with confining pressure.

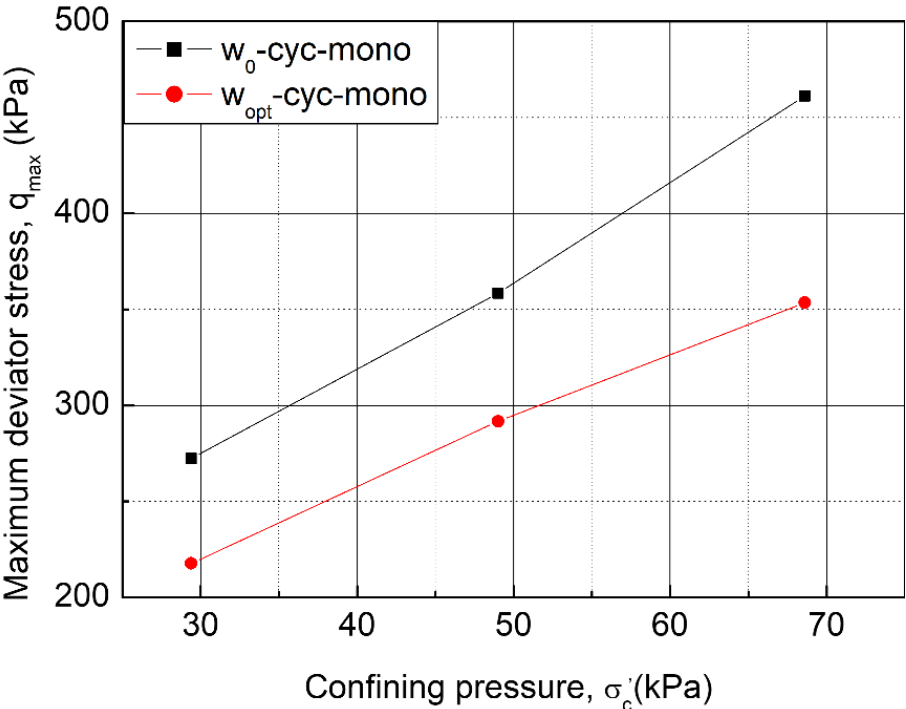


Fig. 4.7 The peak strength-confining pressure behavior of the specimens with loading history

Mohr circles together with the Mohr-Coulomb failure envelope of the specimen with loading history are presented in Fig. 4.8. The specimen under dry condition had angle of friction of  $41.1^\circ$ , which was greater than  $33.5^\circ$  that of wet condition. Fig. 4.8 also shows that the failure envelope of specimen had an intercept with the shear axis indicating cohesion for specimen under wet condition. The cohesion of the specimen in the dry state is 29 kPa and that in the wet state is 31.6 kPa. Due to moisture, the friction angle decreases and the cohesion increases, but the variation range is less than that without cyclic load.

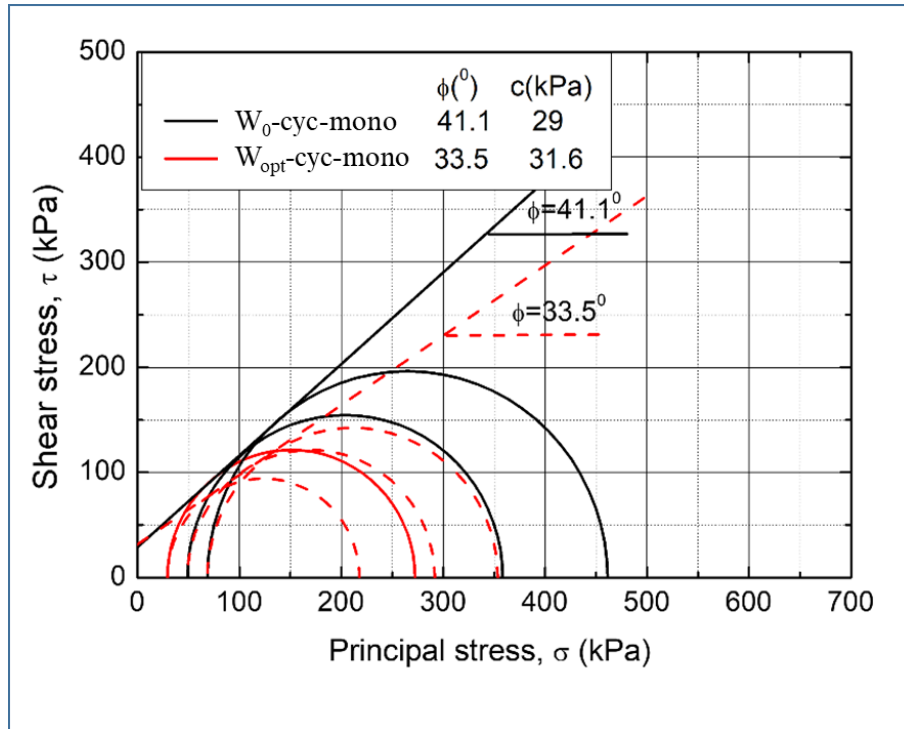


Fig. 4.8 The Mohr's circles in peak stress state with loading history

#### 4.4 The Initial deformation modulus and Tangent deformation modulus

##### 4.4.1 Without loading history

Fig. 4.9 shows the relationship between the confining pressure and the initial deformation modulus  $E_0$  without loading history. It can be seen that the initial deformation modulus of the sample in the dry state increases and then decreases with the increase of the confining pressure; the sample in wet state decreases slightly and then increases with the increase of the confining pressure. When the confining pressure of the dry specimen is 68.8 kPa, the particles may be broken, resulting in the decrease of the initial deformation modulus. The initial deformation modulus of the specimen in the dry state is less than that in the wet state, except for the case when the confining pressure is 49.0 kPa.

Fig.4.10 shows that the relationship between axial strain and tangential deformation modulus  $E_{\text{tan}}$  under dry condition, the general trend of the  $E_{\text{tan}}$  with the increase in strain is a slow increase followed by a sharp decrease.

Fig.4.11 shows that the relationship between axial strain and tangential deformation modulus  $E_{\text{tan}}$  under wet condition, the general trend of the  $E_{\text{tan}}$  with the increase in strain is a sharp decrease followed by a sharp increase

and lastly decreases. When the confining pressure of the sample is 29.4 kPa, the  $E_{tan}$  of the specimen in the dry state is less than that in the wet state. However, when the confining pressure of the sample is 49.0 kPa and 68.6 kPa, the  $E_{tan}$  of the specimen in the dry state is more than that in the wet state.

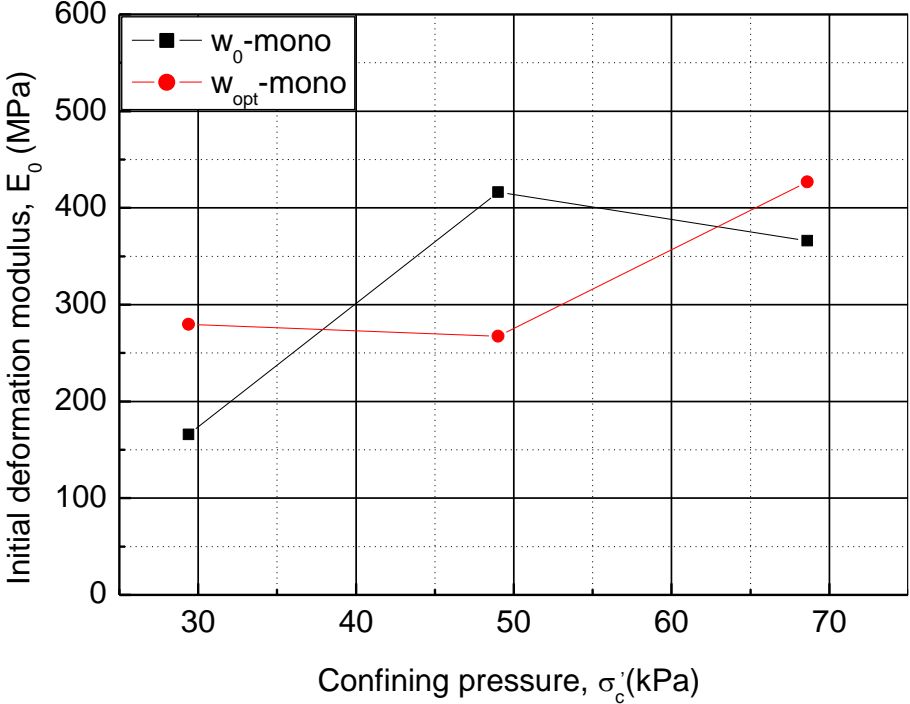


Fig. 4.9 The relationship between confining pressure and initial deformation modulus without loading history

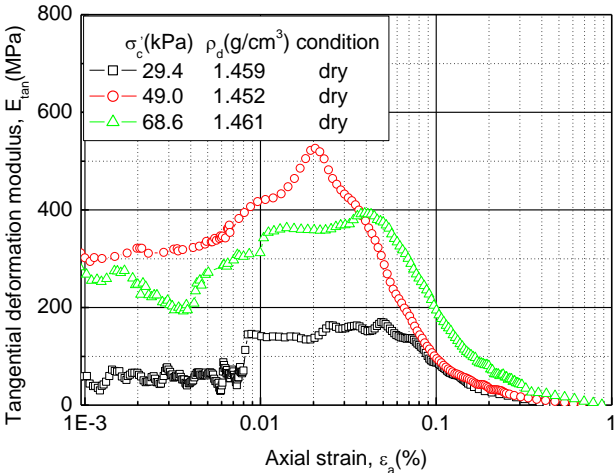


Fig. 4.10 The relationship between axial strain and tangential deformation modulus under dry condition

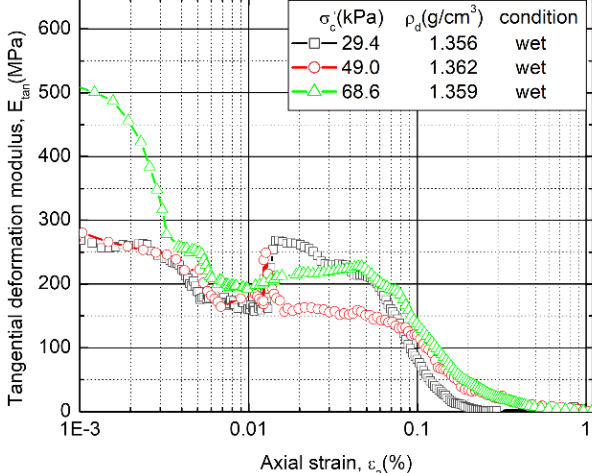


Fig. 4.11 The relationship between axial strain and tangential deformation modulus under wet condition

### 4.4.2 With loading history

Fig. 4.12 shows the relationship between the confining pressure and the initial deformation modulus  $E_0$  with loading history. It can be seen that the initial deformation modulus of the sample in the dry state increases with the increase of the confining pressure. The initial deformation modulus of the specimen in the dry state is more than that in the wet state, except for the case when the confining pressure is 49.0 kPa.

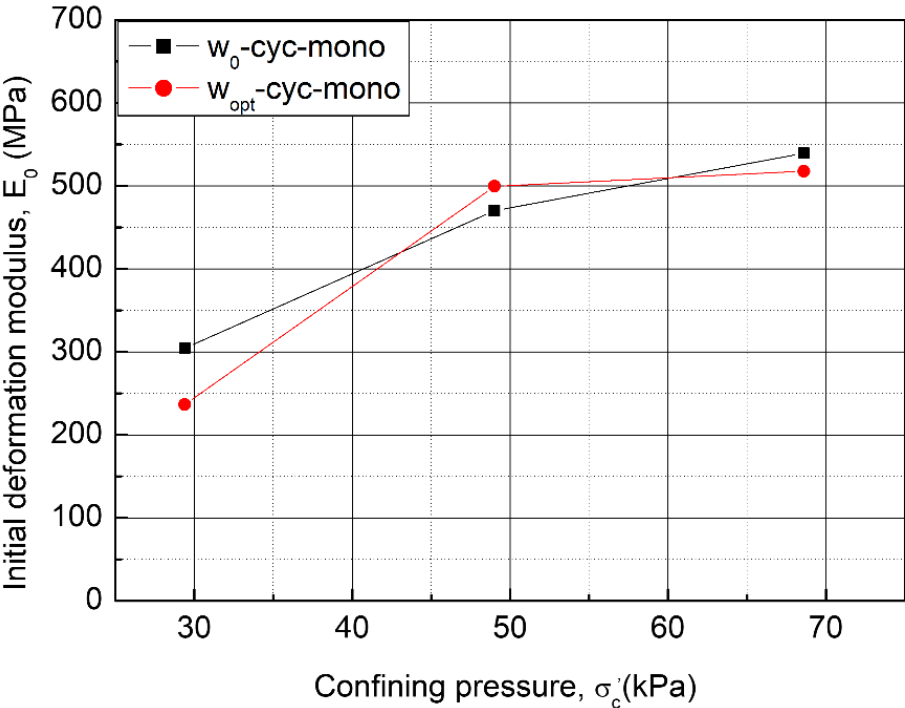
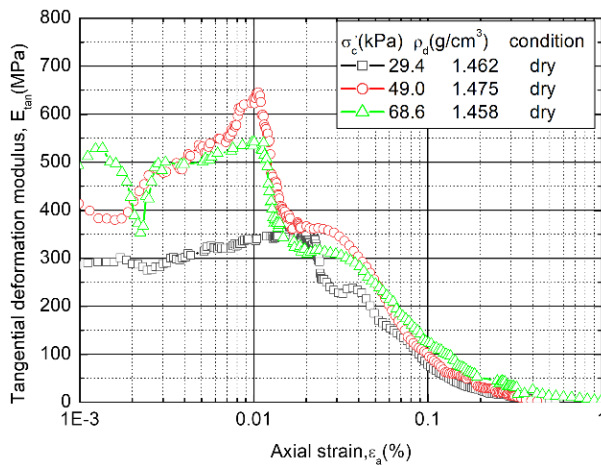
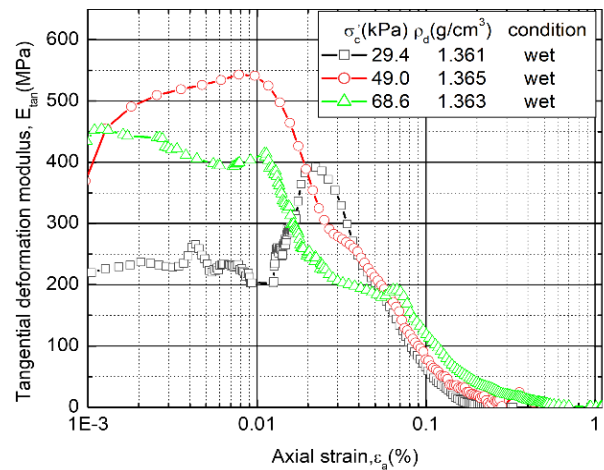


Fig. 4.12 The relationship between confining pressure and initial deformation modulus with loading history

Fig. 4.13 and Fig. 4.14 show that the relationship between axial strain and tangential deformation modulus  $E_{tan}$  with loading history, the general trend of the  $E_{tan}$  with the increase in strain is a slow increase followed by a sharp decrease. Before the strain is 0.01 %, the tangential deformation modulus of the sample in dry state is greater than that in wet state. After the strain is 0.01 %, the tangential deformation modulus in the two states is basically the same.



**Fig. 4.13** The relationship between axial strain and tangential deformation modulus under dry condition



**Fig. 4.14** The relationship between axial strain and tangential deformation modulus under wet condition

## 4.5 Summary

In this chapter, the effects of moisture on the strength and deformation of specimens are analyzed by the static triaxial test. The changes of deviator stress - axial strain relationship, Mohr circle, initial elastic modulus and tangent deformation modulus under dry and wet condition are compared. The following conclusions can be derived.

(1) With the increase of the axial strain, the deviator stress sharply also increases to the peak stress at an axial strain of about 0.5 %, and then it gradually decreases. It was found that the deviator stress was greater in the specimen under dry condition than in those under wet condition.

(2) It was found that the maximum deviator stress  $q_{max}$  was greater in the specimen under dry condition than the case under wet condition.

(3) The angle of friction of specimen under dry condition was greater than the case under wet condition. The cohesion of specimen under dry condition was less than the case under wet condition.

(4) The initial deformation modulus  $E_0$  increases with the increase of confining pressure. When the confining pressure of the dry specimen is 68.8 kPa, the particles may be broken, resulting in the decrease of the initial deformation modulus.

(5) The tangential deformation modulus of the specimen in dry state is greater than that in wet state.

(6) The increase of maximum deviator stresses in the specimen had an almost linear relationship with confining pressure.

(7) The existence of water reduces the friction angle, increases the cohesion of particles, and reduces the strength and deformation modulus.

## References:

Cao,Z., Chen,J., Cai,Y., Gu,C. and Wang,J., 2017. "Effects of moisture content on the cyclic behavior of crushed tuff aggregates by large-scale tri-axial test." *Soil Dyn. Earthquake Eng.*, 95, pp. 1-8.

Cary,C.E. and Zapata,E.C., 2011. Resilient modulus for unsaturated unbound materials. *Road Materials and Pavement Design*, 12 (3), 615–638.

Cerni,G., Cardone,F., Virgili,A. and Camilli,S., 2012. "Characterisation of permanent deformation behaviour of unbound granular materials under repeated triaxial loading." *Constr. Build.Mater.*, 28(1), pp. 79-87.

Coronado,O., Fleureau,J., Correia,A. and Caicedo,B., 2005. Influence of suction on the properties of two granular road materials, In: I. Horvli (Ed.), *Proceedings of the 7th International Conference on the Bearing Capacity of Roads, Railways and Air-fields*, Trondheim, pp. 27-29.

Dawson,A.R., Thom,N.H. and Paute,J.L., 1996. Mechanical Characteristics of Unbound Materials as A function of Condition," *Flexible Pavements, Proceedings, European Symposium Euroflex 1993*, A.G.Corria,ed., Balkema, Rotterdam, The Netherlands, pp.35-44.

Dempsey,B.J. and Elzeftawy,A., 1976. Mathematical model for predicting moisture movement in pavement systems. *Transportation Research Record* 612, pp. 48-55.

Dempsey,B.J., 1979. Influence of precipitation, joints and sealing on pavement drainage. *Transportation Research Record* 705, pp. 13-23.

Duong,T.V., Tang,A.M., Cui,Y.J., Trinh,V.N., Dupla,J.C., Calon,N., Canou, J. and Robinet, A., 2013. Effects of fines and water contents on the mechanical behavior of interlayer soil in ancient railway sub-structure, *Soils Found*, 53 (6), pp. 868-878.

Ebrahim,S., Douglas,J.W., Tam,J.L. and Philippa,M.B., 2019. The Role of Water in Unbound Granular Pavement Layers: a Review, *Transportation Infrastructure Geotechnology* volume 6, pp. 289-317.

Ekblad,J., 2007. Influence of water on coarse granular road material properties. Doctoral thesis. KTH Royal Institute of Technology, Stockholm.

Ekblad,J. and Isacsson,U., 2008. Water in coarse granular materials: Resilient and retentive properties. In: Ellis, Yu, McDowell, Dawson, Thom (Eds.), *Proceedings of the International Conference on Advances in Transportation Geotechnics*, Nottigham, pp. 117-123.

Erlingsson,S., 2010. Impact of water on the response and performance of a pavement structure in an accelerated test. *Road Materials and Pavement Design*, 11 (4), 863-880.

Fortunato,E., Pinelo,A. and Fernandes,M.M., 2010. Characterization of the fouled ballast layer in the sub-structure of a 19th century railway track under renewal, *Soils Found.*, 50 (1), pp. 55-62.

- Guo,P.J. and Su,X.B., 2007. Shear strength, inter particle locking, and dilatancy of granular material, *Canadian Geotechnical Journal*, Vol. 44, No. 5, pp. 579-591.
- Hassan,H.F. and White,T.D., 1997. Laboratory and field moisture conditions for flexible pavements. *Transportation Research Record* 1568, pp. 96-105.
- Inam,A., Ishikawa,T. and Miura,S., 2012. Effect of principal stress axis rotation on cyclic plastic deformation characteristics of unsaturated base course material, *Soils Found*, 52 (3), pp. 465-480.
- Kancherla,A., 2004. Resilient Modulus and Permanent Deformation Testing of Unbound Granular Materials, MSc Thesis Submitted to the Office of Graduate Studies of Texas A & M University.
- Karube,D., Kato,S., 1994. An ideal unsaturated soil and the Bishop's soil. In: *Proceedings of the 13th International Conference on Soil Mechanics and Foundation Engineering*, New Delhi, India, 5-10 January, Taylor and Francis, New York, vol.1, pp. 43-46.
- Kohgo,Y., Asano,I. and Hayashida,Y., 2007. Mechanical properties of unsaturated low quality rockfills, *Soils and Foundations*, Vol. 47, No. 5, pp. 947-959.
- Liu,S.J. and Lytton,R.L., 1984. Rainfall Infiltration, Drainage, and Load-Carrying Capacity of Pavements. *Transportation Research Record* 993, pp. 28-35.
- Markow,M.J., 1982. Simulating pavement performance under various moisture conditions. *Transportation Research Record* 849, pp. 24-29.
- Ng,C.W.W., Zhou,C., Yuan,Q. and Xu,J., 2013. Resilient modulus of unsaturated subgrade soil: experimental and theoretical investigations, *Canadian Geotechnical Journal*, Vol. 50, pp. 223-232.
- Oka,F., Kodaka,T. and Suzuki,H., 2010. Experimental study on the behavior of unsaturated compacted silt under triaxial compression, *Soils and Foundations*, Vol. 50, No. 1, pp. 27-44.
- Ridgeway,H.H., 1976. Infiltration of water through the pavement surface. *Transportation Research Record* 616, pp. 98-100.
- Seif El Dine,S., Dupla,J., Frank,R., Canou,J. and Kazan,Y., 2010. Mechanical characterization of matrix coarse-grained soils with a large-sized triaxial device, *Can. Geotech. J.*, 47 (4), pp. 425-438.
- Selig,E. and Waters,J., 1994. *Track Geotechnology and Sub-structure Management*, Thomas Telford, London, UK.
- Thom,N.H. and Brown,S.F., 1987. Effect of Moisture on the Structural Performance of a Crushed-Limestone Road Base. In *Transportation Research Record* 1121, TRB, National Research Council, Washington, DC, pp. 50-56.
- Trinh,V.N., Tang,A.M., Cui, Y.J., Dupla,J.C., Canou,J., Calon,N., Lambert,L., Robinet,A. and Schoen,O., 2012. "Mechanical characterisation of the fouled ballast in ancient railway track substructure by large-scale triaxial tests." *Soils Found.*, 52(3), pp. 511-523.
- Uthus,L., 2007 *Deformation properties of Unbound Granular Aggregates*, Doctoral Thesis, Norwegian University of Science and Technology, Faculty of Engineering, Department of civil Transport Engineering.
- Zhan,T.L.T. and Ng,C.W.W., 2006. Shear strength characteristics of an unsaturated expansive clay, *Canadian Geotechnical Journal*, Vol. 43, pp. 751-763.
- Zhao,M.H., Liu,X.P. and Peng,W.X., 2007. Application of aqueous film theory to study of unsaturated soil's suction, *Fundamental Theory and Experimental Research*, Vol. 28, Issue (7), pp. 1323-1327.

## **CHAPTER 5**

### **DEFORMATION CHARACTERISTICS OF SPECIMEN UNDER CYCLIC LOADING**



### 5.1 Introduction

In the Chapter 3 and Chapter 4, the static triaxial test of lightweight geo-materials has been carried out, and the effects of confining pressure, moisture and loading history on its strength and deformation have been analyzed.

When used in practical engineering, lightweight geo-materials may undergo various dynamic load induced by earthquake, vehicle, ocean wave, etc.; so it is necessary to investigate its behavior under cyclic loading. **Fig. 5.1** shows the compressive forces, tensile forces, shear stresses and strains exerted by the wheels to the road layers along with time.

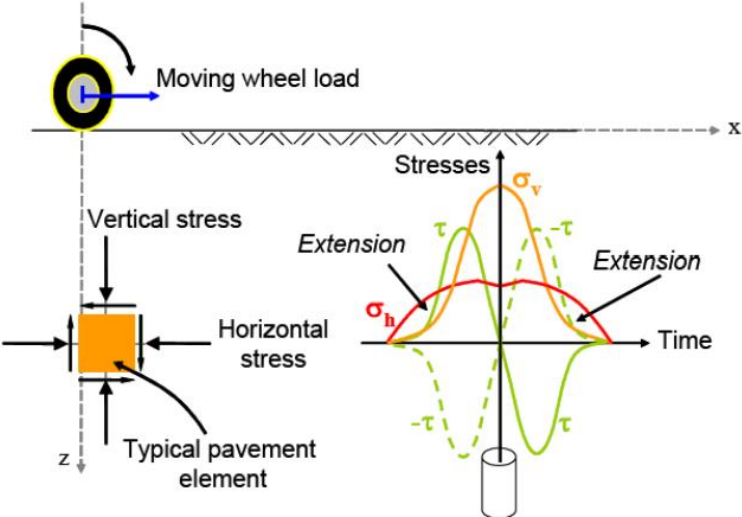


**Fig. 5.1** Stress regimes experienced by a pavement element under a moving wheel load

Barksdale (1971) found that the cyclic triaxial test more closely simulate the stress conditions in flexible pavements than other available test methods like e.g. CBR. So the cyclic triaxial testing is currently the most useful laboratory method for determination of the deformation behavior of unbound aggregates under traffic loading (Barksdale, 1972; Bennert et al., 2000). This procedure is to be preferred to the static ones, which are considered as inadequate for determining the behavior of aggregate mixtures subjected to the impulse-type repeated loading representative of moving wheel loads (The Aggregate Handbook, 1993). The cyclic load triaxial test provides a means of studying the deformational response of granular layers under traffic-type loading, which

is conveniently characterized by a recoverable (resilient) deformation and a residual deformation (Lekarp et al., 2000; Cerni et al., 2015; Alnedawi et al., 2018 ). Granular materials in a pavement behave as non-linear elastic material after a larger number of cycles of traffic loading. The elastic modulus under such condition depends on stress state and time of loading and is termed as resilient modulus.

There are some reports about the behavior of granular materials during cyclic loading (Ishihara and Towhata, 1983 ; Tokimatsual, 1986 ; Sagaseta et al., 1991 ; Kohata et al., 1997 ), but study on the effect of stress amplitude of repeated loads is still very limited . Some researchers have reported that small Young's modulus did not change noticeably after a large number of cyclic loading ( TeachavorasinSkun et al., 1994; Dong et al ., 1994), white the others have reported opposite trends of behavior ( Hoque et al., 1996; Correia et al., 2001). It is also reported that resilient behavior of granular materials is affected by stress level, density, grading, fines content, maximum grain size, aggregate type, particle shape, moisture content, stress history and number of load applications (Seed et al., 1967; Smith and Nair, 1973; Lekarp et al., 2000). Resilient modulus increases significantly with confining pressure and sum of principal stresses, and marginally with deviator stress. Increasing moisture content, particularly at high degrees of saturation, has shown a significant reduction of resilient modulus as well as Poisson's ratio. The modulus also increases with increasing density. It also increases with increase in maximum particle size, because the transmission of the load via coarser particles with smaller number of particle contacts results in less total deformation and consequently results in higher stiffness (e.g., Hicks and Monismith, 1971; Lekarp et al., 2000, Araya, 2011; Ba et al., 2011; Behiry, 2014).

In general as for uniform geo-materials such as graded crushed stone, sand or clay, it is well known that the deformation characteristics are nonlinear and shear modulus and damping ratio vary significantly with shear strain amplitude under cyclic loading (Hardin and Drnevich, 1972; Alarcon, 1986). However, lightweight geo-materials is non-homogeneous, consisting of two mixtures with different properties; so whether there are any differences in behavior of lightweight geo-materials under cyclic loading comparing to that of uniform geo-materials is worth to research. In this chapter, the effects of confining pressure, moisture and loading numbers on the deformation characteristics of light geo-materials under cyclic loading are analyzed through cyclic triaxial tests.

## 5.2 Test principle

The cyclic load triaxial compression test is currently the most commonly used method to measure the resilient (elastic) deformation characteristics of aggregates for use in pavement design (Tutumlu and Seyhan, 1999). The resilient deformation test is performed on a cylindrical specimen subjected to a cyclic axial compressive stress,  $\sigma_a$ , and a constant all-around confining stress,  $\sigma_c$ . A schematic representation of the triaxial loading system is shown in **Fig. 5.2**. The resilient properties, equivalent young's modulus  $E_{eq}$  and Poisson's ratio  $\nu$ , describe the relation between the resilient deformation of a specimen,  $\epsilon_a$  and  $\epsilon_r$ , and the applied stresses,  $q$  and  $\sigma_c$ , (equations 5.1 and 5.2):

$$\Delta\epsilon_a = \frac{\Delta q - 2\nu * \Delta\sigma_c}{E_{eq}} \quad (5.1)$$

$$\Delta\epsilon_r = \frac{\Delta\sigma_c * (1 - \nu) - \nu * \Delta q}{E_{eq}} \quad (5.2)$$

For a cylindrical axial symmetrical triaxial specimen the lateral (radial) confining stress ( $\sigma_c$ ) and strain ( $\epsilon_r$ ) are the minor principal stress and strain and the vertical axial stress ( $q$ ) and strain ( $\epsilon_a$ ) are the major principal stress and strain. For a constant confining pressure resilient deformation test, at any applied stress combination  $\sigma_c = \text{constant}$  and thus  $\Delta\sigma_c = 0$ . Equations 5.3 to 5.4 can therefore be simplified to:

$$\Delta\epsilon_a = \frac{\Delta q}{E_{eq}} \quad (5.3)$$

$$\Delta\epsilon_r = \frac{-\nu * \Delta q}{E_{eq}} = -\nu * \Delta\epsilon_a \quad (5.4)$$

From equations 5.3 and 5.4 the  $E_{eq}$  and  $\nu$  can thus be expressed as equations 5.5 and 5.6. The  $E_{eq}$  determined in this way is in line with the European standard EN 13286-7 (2004) for the case:

$$E_{eq} = \frac{\Delta q}{\Delta \varepsilon_a} \quad (5.5)$$

$$\nu = \frac{\Delta \varepsilon_r}{\Delta \varepsilon_a} \quad (5.6)$$

The volumetric strain is computed by the following equation 5.7.

$$\varepsilon_v = \varepsilon_a + 2 * \varepsilon_r \quad (5.7)$$

The Local Displacement Transducer (LDT) was used to precisely measure the axial strain  $\varepsilon_a$  without the effect of bending errors from less than 0.001% to about 2%. The axial strain measurement range beyond 2% is supplemented by a dial gauge. A non-contact displacement transducer was used to measure the lateral strain  $\varepsilon_r$  of the specimen. It is introduced in detail in the 2 chapter.

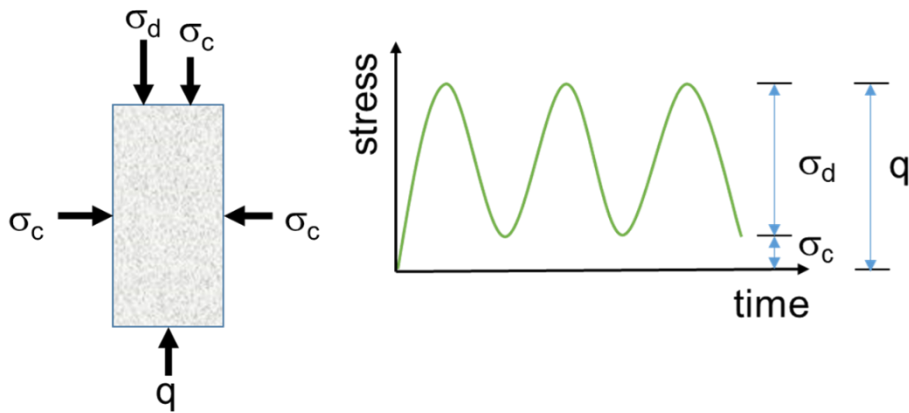
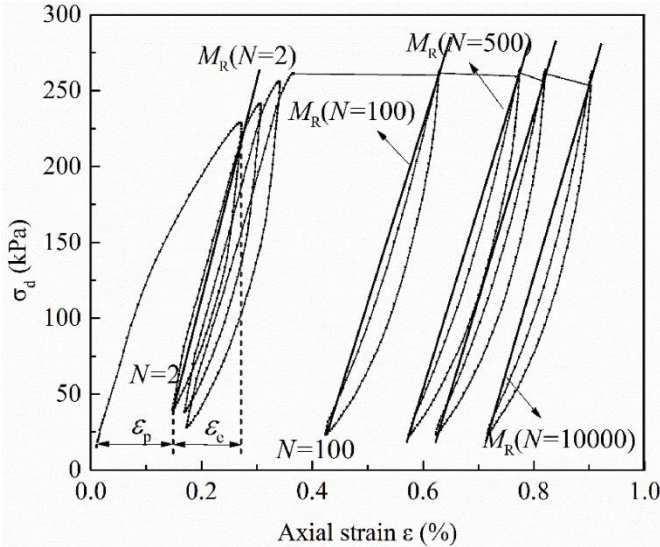


Fig. 5.2 Schematic representation of triaxial stress system

### 5.3 The deformation under cyclic loading

The geometric meaning of the resilient modulus is the slope of the line connecting the two ends of the hysteresis loop in the stress-strain curve (Nie et al., 2021). **Fig. 5.3** is a schematic diagram of determining a resilient modulus according to a dynamic stress-strain relationship curve. Hysteresis loop is not closed at the initial stage of loading, and it is difficult to determine the resilient modulus of the soil from a single hysteresis

loop. Therefore, in the initial stage of loading, two adjacent hysteresis loops are used to determine the resilient modulus of the soil. These two hysteresis loops have two intersections which form a new closed hysteresis loop. The resilient modulus can be determined based on the new closed hysteresis loop (the slope of the black straight line in the figure is the resilient modulus). As the number of loading cycles increases, the hysteresis loop gradually closes, the resilient modulus is obtained from the slope of the line between the lowest point and the highest point.



**Fig. 5.3** Hysteresis loop of different number of loading cycles

The response of an UGM specimen under repeated loading is divided into a resilient (recoverable) strain and a permanent (unrecoverable) strain. The recoverable behavior is characterized by the resilient modulus of UGM, as shown in **Fig 5.4**. The permanent strain accumulated under load repetitions is used to describe the permanent deformation behavior (Gu et al., 2015). To evaluate the permanent deformation properties of UGM, the shakedown theory has been widely used by pavement design practitioners (Werkmeister et al., 2001; Tao et al., 2010; Erlingsson et al., 2013). According to this theory, the UGMs are categorized as three groups:

Range A -plastic shakedown range: For relatively low stress levels, permanent strain accumulates up to a finite number of load applications after which the response becomes entirely resilient and there is no further permanent strain. At this stage, the post-compaction is completed and the material is stabilized.

Range B -intermediate response (plastic creep): For stress levels higher than that for range A, and up to a certain level, the accumulation of permanent strain continues with load applications. In this case, permanent strain rate (per cycle) decreases from high to a low and nearly constant level during the first load cycles.

Range C -incremental collapse: When the stress levels are higher than that for range B, the permanent strain accumulates at a much faster rate compared to range A or B. In this case the permanent rate decreases very slowly or not at all. This may eventually lead to failure.

In pavement design, the pavement must be able to resist permanent deformation. To ensure that pavement has desirable rutting resistance, the pavement design guide suggests to select the base materials from Range A and Range B, and avoid using the base materials from Range C. To define the shakedown range boundaries, Werkmeister (2003) proposed the following criteria:

$$\text{Range A: } \varepsilon_{p,5000} - \varepsilon_{p,3000} < 4.5 \times 10^{-5}$$

$$\text{Range B: } 4.5 \times 10^{-5} < \varepsilon_{p,5000} - \varepsilon_{p,3000} < 4.0 \times 10^{-4}$$

$$\text{Range C: } \varepsilon_{p,5000} - \varepsilon_{p,3000} > 4.0 \times 10^{-4}$$

where,  $\varepsilon_{p,5000}$  is the accumulated plastic strain at the 5000<sup>th</sup> load cycle, and  $\varepsilon_{p,3000}$  is the accumulated plastic strain at the 3000<sup>th</sup> load cycle.

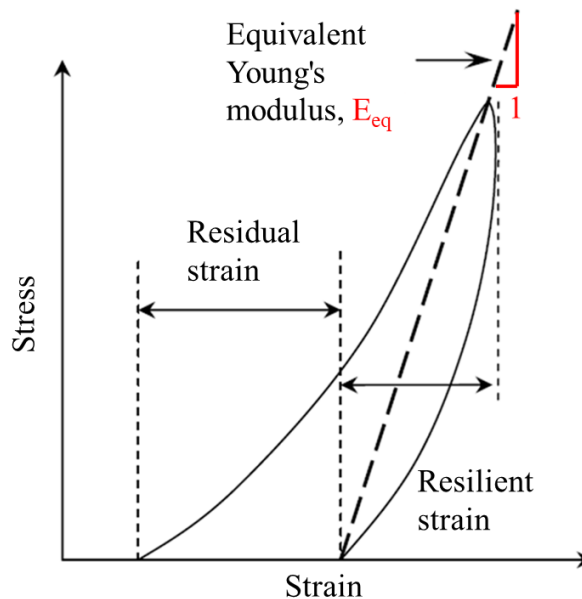


**Fig.5.4** Strains in the testing materials during one load cycle

## 5.4 Relationship between deviator stress and axial strain

### 5.4.1 Under dry condition

**Fig. 5.5(a)-(c)** shows the stress-strain behavior of the specimens in the dry condition under different confining pressure. In general, under the action of dynamic loads, the stress-strain curves of the specimen show hysteresis loops with loading cycles. As the number of loading cycle increases, hysteresis loops move horizontally to the right along the strain axis, indicating that the strain induced by the dynamic load includes plastic and elastic strain and the plastic strain accumulates with the increasing number of loading cycles, as shown in **Fig.5.3**. According to the development trend of the accumulated plastic strain, the state of the specimen under the dynamic load can be divided into three categories: stable, destructive and critical.

As shown in **Fig. 5.5(a)** and **(c)**, hysteresis loops move horizontally to the right along the strain axis and become increasingly intensive as the number of loading cycle increases. When the number of loading cycle reaches about 5000, hysteresis loops gradually overlap. This phenomenon means that the accumulated plastic strain increment gradually decreases or even becomes zero. This type of specimen is stable. As shown in **Fig. 5.5(b)**, hysteresis loops move horizontally to the left along the strain axis from the number of loading cycles 500. It may be that the particles cross each other, and the cyclic loading leads to the dilatancy.

In this study, the axial strain of the load cycle 1000th and 5000th are compared. According to the shakedown theory, it can be seen that the shakedown range boundaries of the dry specimen under three confining pressures all belongs to Range A.

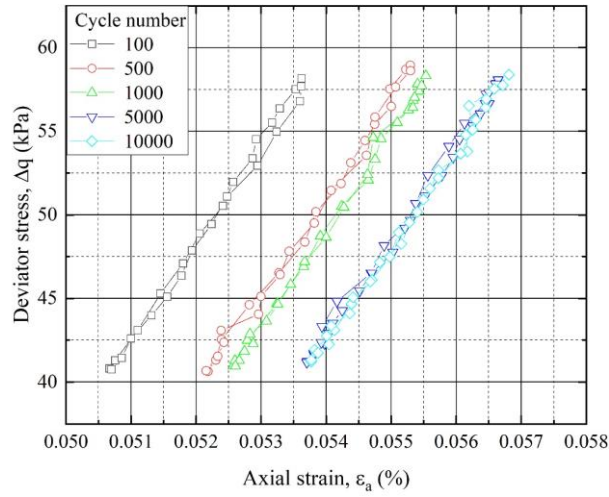


**Fig. 5.5(a)** Confining pressure, 29.4 kPa

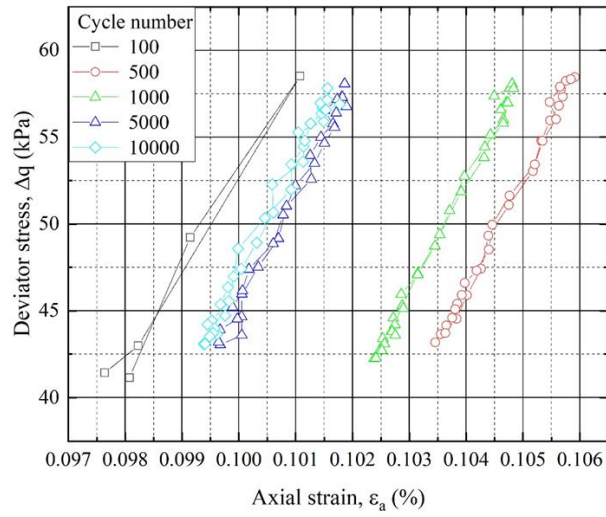


**Fig. 5.5(b)** Confining pressure, 49.0 kPa

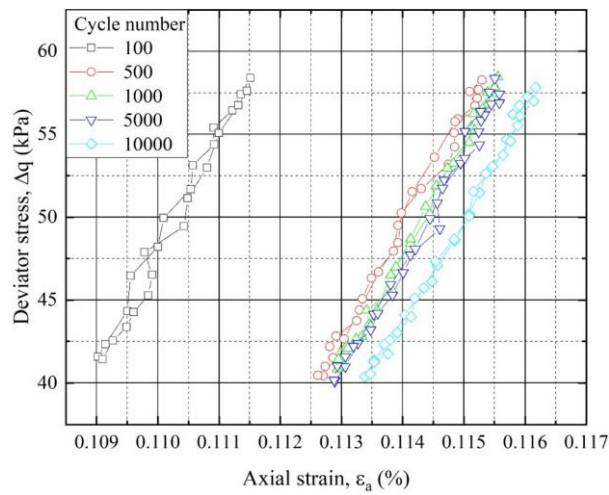


**Fig.5.5 (c)** Confining pressure, 68.6 kPa

**Fig. 5.5 (a) ~ (c)** The stress-strain behavior of the specimens in the dry condition under different confining pressure

### 5.4.2 Under optimum moisture content condition

Fig. 5.6 (a)-(c) shows the stress-strain behavior of the specimens in the wet condition under different confining pressure. As shown in Fig. 5.6 (a) and (b), hysteresis loops move horizontally to the right along the strain axis and become increasingly intensive as the number of loading cycle increases. As shown in Fig. 5.6 (c), hysteresis loops move horizontally to the left along the strain axis from the number of loading cycles 1000. It also may be that the particles cross each other, and the cyclic loading leads to the dilatancy.

According to the shakedown theory, it also can be seen that the shakedown range boundaries of the specimen under three confining pressures all belongs to Range A.

Generally, the axial strain of the wet specimen decreases with the increase of confining pressure. This is not the case for the specimen found in this study. Since it is difficult to control the uniformity and consistency of the specimen in the process of specimen making, and the local unevenness of the specimen will have an impact on the test results.

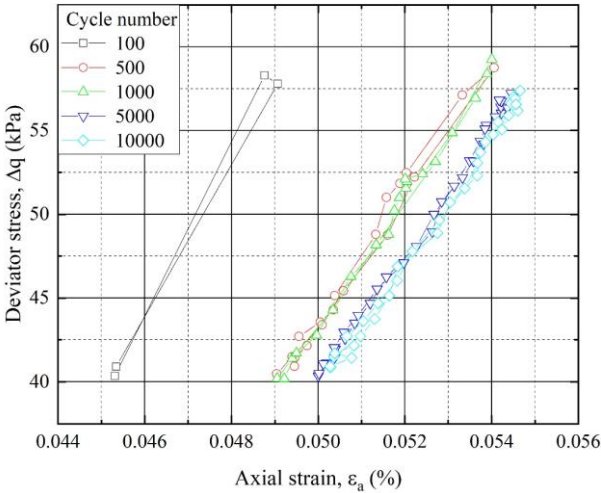
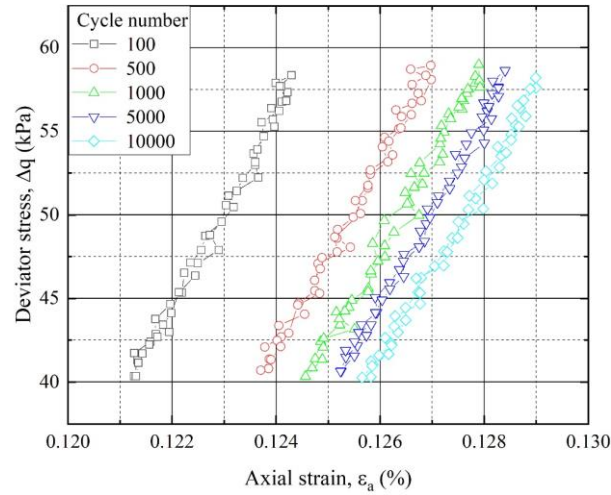
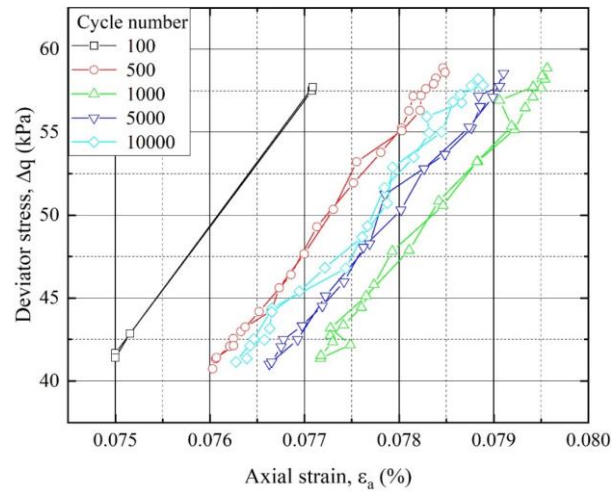


Fig. 5.6 (a) Confining pressure, 29.4 kPa



**Fig. 5.6 (b)** Confining pressure, 49.0 kPa



**Fig. 5.6 (c)** Confining pressure, 68.6 kPa

**Fig. 5.6 (a) ~ (c)** The stress-strain behavior of the specimens in optimum moisture content condition under different confining pressure

## 5.5 Equivalent young's modulus and number of loading cycles

The equivalent Young's modulus  $E_{eq}$  was obtained from the secant gradient of peak to peak on the loop of deviator stress - axial strain relations in this study.

**Fig.5.7** shows the relationship between number of loading cycles and equivalent young's modulus. The equivalent young's modulus of specimen increases with the increase of confining pressure, a phenomenon that is called “stiffening”. Monismith et al., (1967) reported an increase as great as 500 % in resilient modulus for a change in confining pressure from 20 kPa to 200 kPa. An increase of about 50 % in resilient modulus was

observed by Smith and Nair (1973), when the sum of principal stresses increased from 70 kPa to 140 kPa. For dry specimens in this study, when the confining pressure increases from 29.4 kPa to 49 kPa, the equivalent young's modulus increases by 11 %. When the confining pressure increases from 49 kPa to 68.6 kPa, the equivalent young's modulus increases by 18 %. For wet specimens, when the confining pressure increases from 29.4 kPa to 49 kPa, the equivalent young's modulus increases by 41.5 %. When the confining pressure increases from 49 kPa to 68.6 kPa, the equivalent young's modulus increases by 27.4 %. For specimen in this study, confining pressure has a greater impact on the resilient modulus. The increase of confining pressure makes the void ratio of soil smaller, the cohesion and friction force between soil particles increase, and the relative slip between particles becomes more difficult, thus improving the ability of the specimen to resist deformation and damage and increasing the resilient modulus. On the other hand, the influence of confining pressure on the equivalent young's modulus in the wet specimen is greater than the case in the dry specimen.

It also can be seen that the equivalent young's modulus of dry specimen is greater than the wet specimen. Since the moisture leads to the lubrication between the particles, which reduces the friction between the particles and the skeleton structure becomes unstable, so that lead to a greater deformation in the assemblage of aggregate and a consequent decrease in the stiffness. When the confining pressure is 29.4 kPa, Due to the influence of moisture, the equivalent young's modulus value decreases by 31.3 %. When the confining pressure is 49.4 kPa, the resilient modulus value decreases by 12.6 %. When the confining pressure is 68.6 kPa, the resilient modulus value decreases by 5.6 %. Therefore, as the confining pressure of specimen increases, the influence of moisture content on the equivalent young's modulus becomes more reduced. At the same time, the increase of moisture content makes the water film bound by soil particles thicken, the cohesion decreases, and its shear strength also decreases. Leng et al. (2016) found that when the confining pressure is 150 kPa, the shear strength of the coarse-grained soil decreases more than when the confining pressure is 100 kPa (Leng et al., 2016). In actual engineering, due to the influence of rainfall, the subbase course often has water. Therefore, the reduction of resilient modulus caused by the moisture content should be properly considered in the design process to improve the design level of subgrade.

The relationship curves between equivalent young's modulus and number of loading cycles of the specimens

are shown in Fig. 5.7. The equivalent young's modulus maintains stable at the first 5000 cycles and then slightly decreases at the 10000 cycles. With the increase of number of loading cycles, the particles in the specimen rearrange to form a new structure. However, most of the particles are nearly spherical in shape, which would lead to a weaker interlocking and easier relative movement between soil particles under cyclic loading, so the equivalent young's modulus decreases with the increase of loading numbers. Hicks (1970) reported that the resilient properties of the granular materials tested were virtually the same after 50th - 100th load cycle as after 25000th load cycle. Allen and Thompson (1974) also found that the equivalent young's modulus was independent of the number of loading cycles, as they achieved the same equivalent young's modulus after 250th load cycle as after several thousand cycles.

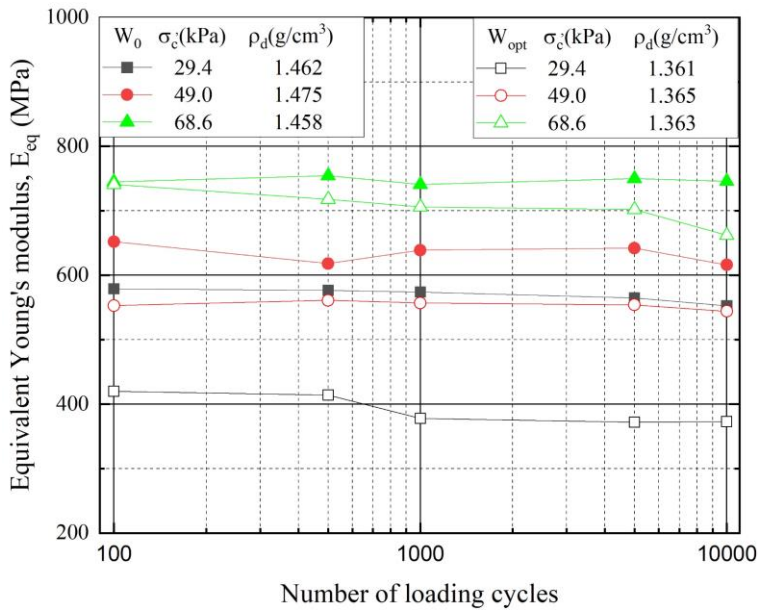


Fig. 5.7 The relationship between number of loading cycles and equivalent young's modulus

## 5.6 Relationship between radial strain and axial strain

### 5.6.1 Under dry condition

The lateral strain  $\epsilon_r$  as well as the axial strain  $\epsilon_a$  is important to discuss the strength and deformation properties of materials under the triaxial condition.

Fig. 5.8 (a)-(c) show the lateral strain-axial strain behavior of the specimens in dry condition under different

confining pressure. As Poisson's ratio is an elastic parameter, it can only be determined when the soil specimen is deforming in an elastic region. From Fig. 5.8 (a)-(c), it can be seen that under different loading cycles, the relationship between lateral strain and axial strain is close to linear response, except that 100th load cycle under confining pressure 49.0 kPa . This is because the structure formed by compaction of the remolded specimen in the initial loading stage is disturbed to a certain extent.

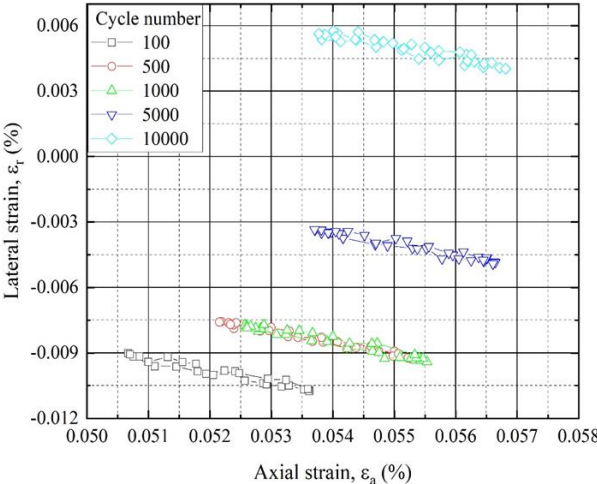


Fig. 5.8 (a) Confining pressure, 29.4 kPa

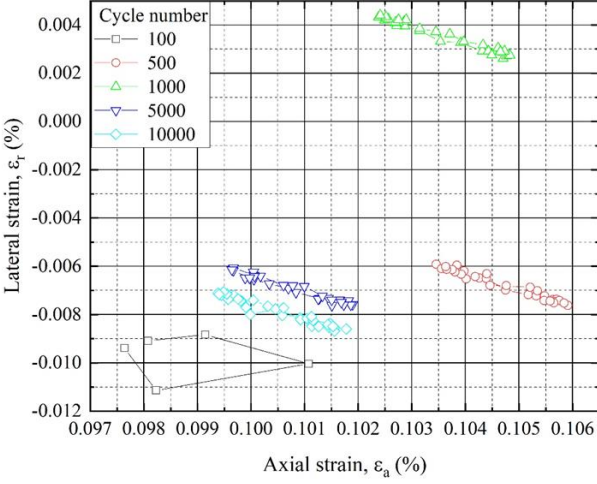
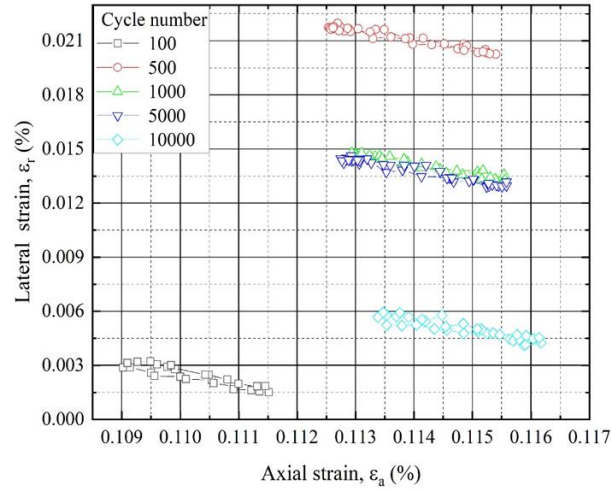


Fig. 5.8 (b) Confining pressure, 49.0 kPa



**Fig. 5.8 (c)** Confining pressure, 68.6 kPa

**Fig. 5.8 (a) ~ (c)** The lateral strain-axial strain behavior of the specimens in dry condition under different confining pressure

### 5.6.2 Under optimum moisture content condition

**Fig. 5.9 (a)-(c)** shows the lateral strain-axial strain behavior of the specimens in wet condition under different confining pressure. From **Fig. 5.9 (a)-(c)**, it can be seen that under different loading cycles, the relationship between lateral strain and axial strain is also close to linear response, except that 100<sup>th</sup> load cycle under confining pressure 29.4 kPa and 68.6 kPa.

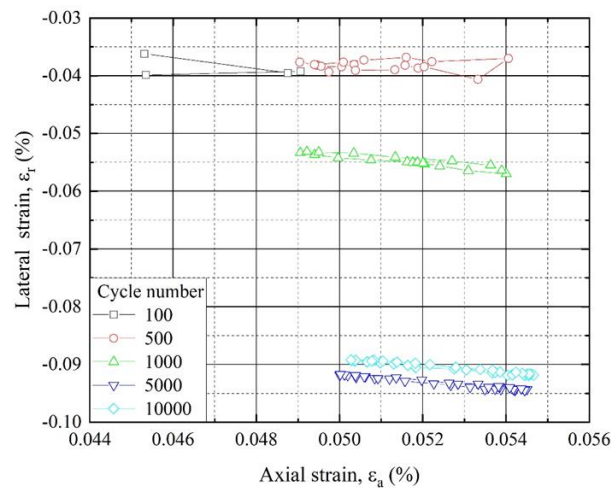


**Fig. 5.9 (a)** Confining pressure, 29.4 kPa

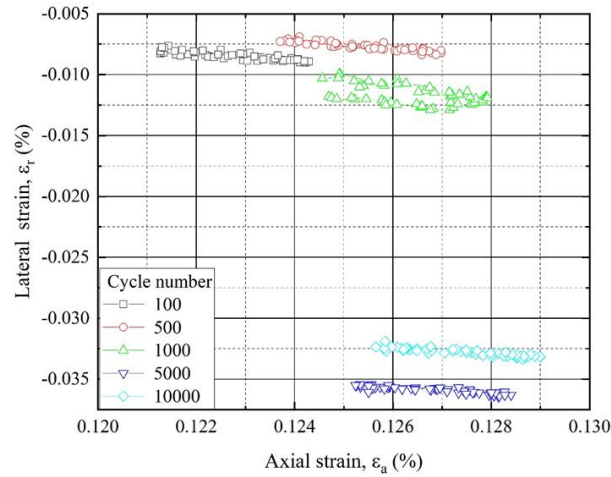


**Fig. 5.9 (b)** Confining pressure, 49.0 kPa

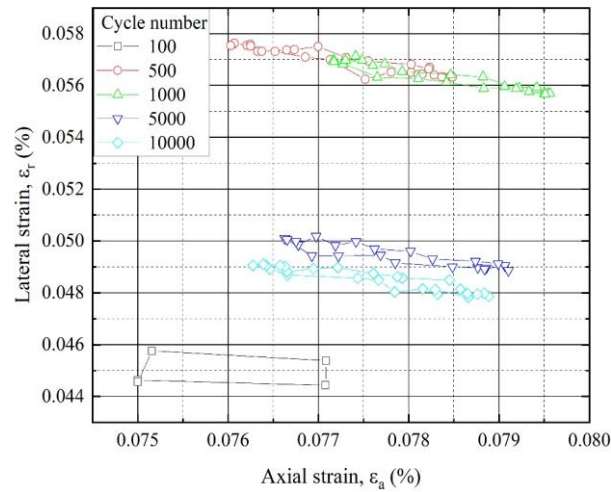


**Fig. 5.9 (c)** Confining pressure, 68.6 kPa

**Fig. 5.9 (a) ~ (c)** The lateral strain-axial strain behavior of the specimens in optimum moisture content condition under different confining pressure

## 5.7 Poisson's ratios and number of loading cycles

Poisson's ratio is defined as the lateral deformation due to the application of a load along the longitudinal direction, which is obtained as the ratio of radial to axial strains of a loaded specimen. It is a foundation mental elastic parameter characterizing the mechanical properties of materials. It is considered as a constant in many kinds of analyses and designs, but in fact its values are not strictly constant. Generally, for soils, Poisson's ratio ranges from 0.1 to 0.4. For granular materials, Poisson's ratios have not been well investigated. The few earlier studies on the subject include that of a square-prismatic triaxial specimen with dimensions of 57 cm × 23 cm × 23

cm on a large triaxial apparatus employed to evaluate Poisson's ratio of Toyoura sand and Hime gravel statically (Hoque and Tatsuoka, 1998). In addition, a medium-sized hollow cylinder apparatus measuring strains in vertical and torsional directions was employed to evaluate Poisson's ratio of Hime gravel (De Silva, 2004). Precise local strain measurement is essential in evaluating Poisson's ratio, in order to minimize the effects of bedding errors and system compliance (Goto et al., 1991; Tatsuoka and Shibuya, 1992; Lo Presti et al., 1993; Tatsuoka and Kohata, 1995). A non-contact displacement transducer was used to measure the lateral strain  $\epsilon_r$  of the specimen in this study.

The Poisson's ratio was obtained from the secant gradient of peak to peak on the loop of the lateral strain - axial strain relations in this study. **Fig.5.10** shows the relationship between number of loading cycles and Poisson's ratio. It can be seen that Poisson's ratio fluctuates with the increase of loading cycles. The fluctuation range is within 0.05 at the same condition. At 100th load cycle, Poisson's ratio decreased, which may be due to the sliding between particles in the specimen in the initial loading stage, resulting in the change of axial strain greater than lateral strain.

As shown **Fig.5.10**, the Poisson's ratio is about 0.38 when confining pressure of the dry specimen is 29.4 kPa. The Poisson's ratio are about 0.52 when confining pressure of the dry specimen are 49.4 kPa and 68.6 kPa. The Poisson's ratio is about 0.45 when confining pressure of the wet specimen is 29.4 kPa. The Poisson's ratio is about 0.33 when confining pressure of the wet specimen is 49.0 kPa. The Poisson's ratio is about 0.37 when confining pressure of the wet specimen is 68.6 kPa. In general, it is reported that the Poisson's ratio of granular crushed stone during cyclic loading is about 0.15~0.2, and that of single granular crushed stone is about 0.2~0.5 (Kohata and Jiang, 1998; Kohata et al., 2001; Kohata et al., 2003). **Fig. 5.10** shows that the Poisson's ratio of all the specimens are generally above 0.2, which is relatively large. This may be attributed to applied large cyclic loading stress levels, which leads to the relatively large axial strain.

The Poisson's ratio of dry specimen is greater than that of wet specimen at the same confining pressure, except that when the confining pressure is 29.4kPa.

It can be seen from the above that the factor affecting (confining pressure, moisture, number of loading cyclic) Poisson's ratio under dynamic load is not single, it may be affected by a variety of factors.

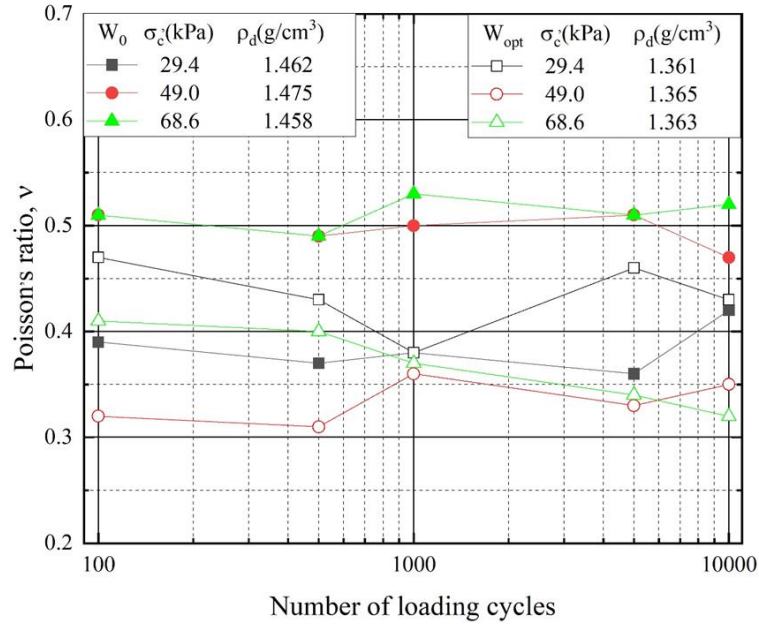


**Fig. 5.10** The relationship between number of loading cycles and Poisson's ratios

## 5.8 Relationship between volumetric strain and axial strain

### 5.8.1 Under dry condition

Dilatancy is the volume change observed in granular materials when they are subjected to shear deformations (Nedderman, 2005; Pouliquen et al., 2013). This effect was first described scientifically by Osborne Reynolds (Reynolds, 1886) and is also known as Reynolds dilatancy. Unlike most other solid materials, the tendency of a compacted dense granular material is to dilate (expand in volume) as it is sheared. This occurs because the grains in a compacted state are interlocking and therefore do not have the freedom to move around one another. When stressed, a lever motion occurs between neighboring grains, which produces a bulk expansion of the material. On the other hand, when a granular material starts in a very loose state it may continuously compact instead of dilating under shear. A sample of a material is called dilative if its volume increases with increasing shear and contractive if the volume decreases with increasing shear (Casagrande et al., 1964; Poulos, 1971).

Some scholars (Tatsuoka et al., 1990; Mitchell, 1993; Wu et al., 2008) based on investigations of shear bands in granular materials, concluded that disturbance of the shear zone accounts for the bulk of the observed volume changes.

**Fig. 5.11 (a)-(c)** show the volumetric strain-axial strain behavior of the specimens in dry condition under different confining pressure. From **Fig. 5.11 (a)-(c)**, it can be seen that under different loading cycles, the relationship between lateral strain and axial strain is close to linear response, except that 100th load cycle under confining pressure 49.0 kPa . This is also because the structure formed by compaction of the remolded specimen in the initial loading stage is disturbed to a certain extent.

As shown in **Fig. 5.11 (a)**, when the cycle number increases from 100 to 500, the specimen shows contractive tendency. When the cycle number increases from 500 to 1000, the specimen shows constant tendency. When the cycle number increases from 1000 to 5000, the specimen shows contractive tendency. When the cycle number increases from 5000 to 10000, the specimen shows contractive tendency.

As shown in **Fig. 5.11 (b)**, when the cycle number increases from 100 to 500, the specimen shows contractive tendency. When the cycle number increases from 500 to 1000, the specimen shows contractive tendency. When the cycle number increases from 1000 to 5000, the specimen shows dilative tendency. When the cycle number increases from 5000 to 10000, the specimen shows dilative tendency.

As shown in **Fig. 5.11 (c)**, when the cycle number increases from 100 to 500, the specimen shows contractive tendency. When the cycle number increases from 500 to 1000, the specimen shows dilative tendency. When the cycle number increases from 1000 to 5000, the specimen shows constant tendency. When the cycle number increases from 5000 to 10000, the specimen shows dilative tendency.

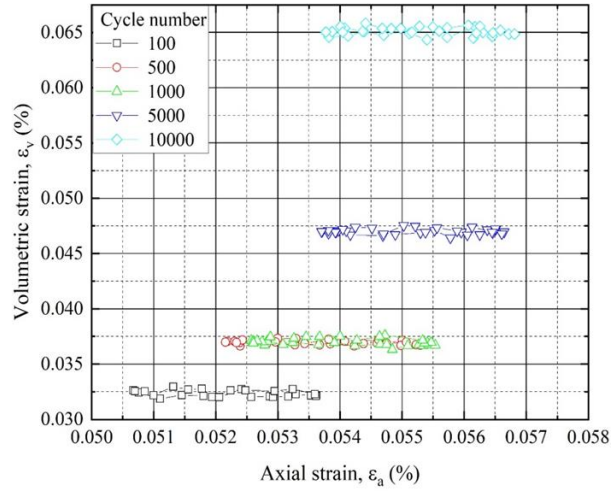


**Fig. 5.11 (a)** Confining pressure, 29.4 kPa

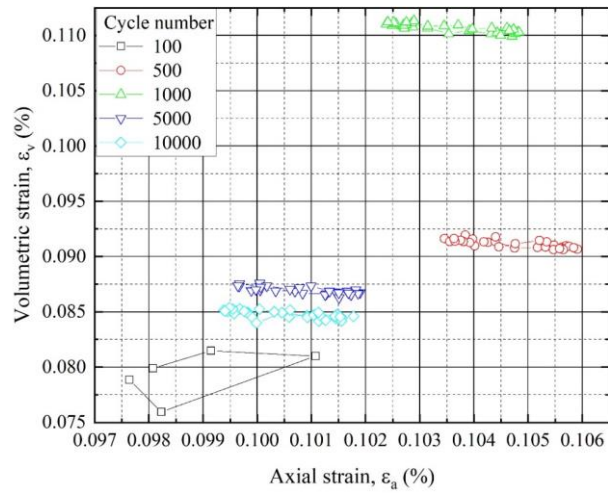


**Fig.5.11 (b)** Confining pressure, 49.0 kPa

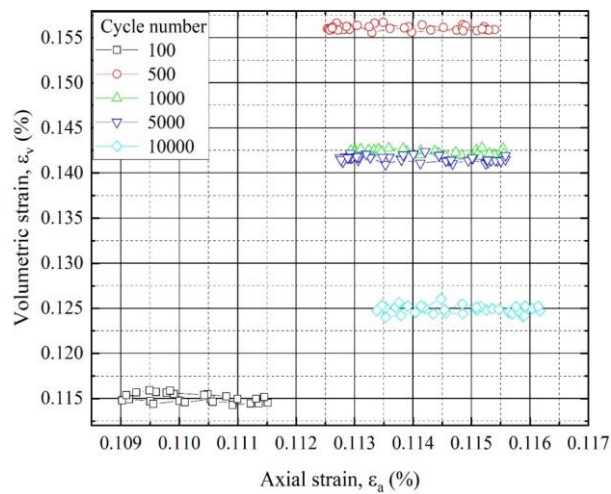


**Fig.5.11 (c)** Confining pressure, 68.6 kPa

**Fig.5.11 (a) ~ (c)** The volumetric strain-axial strain behavior of the specimens in dry condition under different confining pressure

## 5.8.2 Under optimum moisture content condition

**Fig. 5.12 (a)-(c)** show the lateral strain-axial strain behavior of the specimens in wet condition under different confining pressure. From **Fig. 5.12 (a)-(c)**, it can be seen that under different loading cycles, the relationship between lateral strain and axial strain is also close to linear response, except that 100th load cycle under confining pressure 29.4 kPa and 68.6 kPa.

As shown in **Fig. 5.12 (a)**, when the cycle number increases from 100 to 500, the specimen shows dilative tendency. When the cycle number increases from 500 to 1000, the specimen shows dilative dilative tendency. When the cycle number increases from 1000 to 5000, the specimen shows dilative tendency. When the cycle number increases from 5000 to 10000, the specimen shows dilative tendency.

As shown in **Fig. 5.12 (b)**, when the cycle number increases from 100 to 500, the specimen shows contractive tendency. When the cycle number increases from 500 to 1000, the specimen shows dilative constant tendency. When the cycle number increases from 1000 to 5000, the specimen shows dilative tendency. When the cycle number increases from 5000 to 10000, the specimen shows dilative tendency.

As shown in **Fig. 5.12 (c)**, when the cycle number increases from 100 to 500, the specimen shows contractive tendency. When the cycle number increases from 500 to 1000, the specimen shows constant tendency. When the cycle number increases from 1000 to 5000, the specimen shows dilative tendency. When the cycle number increases from 5000 to 10000, the specimen shows contractive tendency.

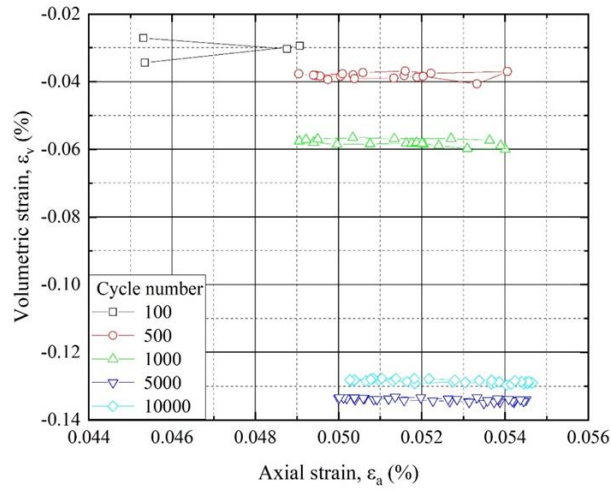


**Fig. 5.12 (a)** Confining pressure, 29.4 kPa

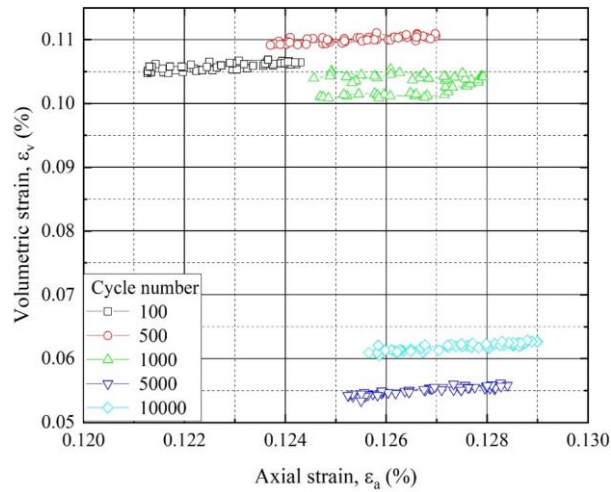


**Fig. 5.12 (b)** Confining pressure, 49.0 kPa

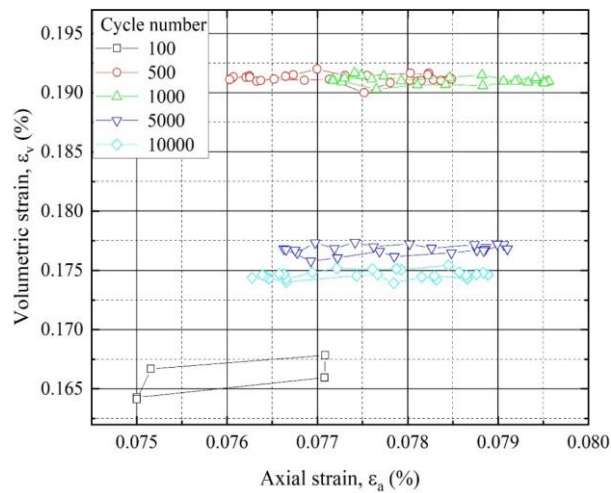


**Fig. 5.12 (c)** Confining pressure, 49.0 kPa

**Fig. 5.12 (a) ~ (c)** The volumetric strain-axial strain behavior of the specimens in optimum moisture content condition under different confining pressure

## 5.9 Dilatancy properties under cyclic loading

Dilatancy properties of all specimens were compared based on their relationship between volumetric strain and axial strain, as shown in **Table 5.1**. When the cycle number increases from 500 to 5000, the wet specimens show dilative tendency under three confining pressure. When the cycle number increases from 0 to 1000, the wet specimens show dilative tendency under three confining pressure.

With the increase of confining pressure under both condition, the volume strain of specimen increases and the contractive tendency also increases. The reason may be that under high confining pressure, particles are broken under loading cyclic, resulting in specimen compression.

It is found that all specimens were loaded after 10000 cycles and showed contractive tendency under the cyclic loading, except that the wet specimen is at confining pressure 29.4 kPa, which shows dilative tendency.

**Table. 5.1** The dilatancy properties under different numbers of cyclic loading

Specimen material state	Confining pressure (kPa)	Number of loading cyclic					
		0-100	100-500	500-1000	1000-5000	5000-10000	After testing
W <sub>0</sub>	29.4	contractive tendency	contractive tendency	constant	contractive tendency	contractive tendency	contractive tendency
	49	contractive tendency	contractive tendency	contractive tendency	dilative tendency	dilative tendency	contractive tendency
	68.6	contractive tendency	contractive tendency	contractive tendency	constant	dilative tendency	contractive tendency
W <sub>opt</sub>	29.4	dilative tendency	dilative tendency	dilative tendency	dilative tendency	contractive tendency	dilative tendency
	49	contractive tendency	contractive tendency	dilative tendency	dilative tendency	contractive tendency	contractive tendency
	68.6	contractive tendency	contractive tendency	constant	dilative tendency	dilative tendency	contractive tendency

## 5.10 Summary

In this chapter, the effects of moisture, confining pressure and number of the cyclic loading on the deformation characteristics of specimen during cyclic loading were analyzed by the cyclic triaxial test. The relationship between deviator stress and axial strain, Equivalent Young's modulus, the relationship between radial strain and axial strain, Poisson's ratios, the relationship between volumetric strain and axial strain, and dilatancy properties under cyclic loading were discussed in detail. The following conclusions can be derived.

(1) For specimen in this study, the confining pressure has a greater impact on the equivalent young's modulus. The equivalent young's modulus of specimen increases with the increase of confining pressure. The influence of confining pressure on the equivalent young's modulus in the wet specimen is greater than the case in the dry specimen.

(2) Since the moisture leads to the lubrication between the particles, which reduces the friction between the particles and the skeleton structure becomes unstable. The equivalent young's modulus of dry specimen is greater than the case in the wet specimen. As the confining pressure of specimen increases, the influence of moisture content on the equivalent young's modulus becomes more reduced.

(3) For specimen in this study, the number of loading cycles has not greater impact on the equivalent young's modulus. The equivalent young's modulus maintains stable with number of loading cycles of the specimens. According to the shakedown theory, it also can be seen that the shakedown range boundaries of the specimen under three confining pressures all belong to Range A.

(4) The Poisson's ratio fluctuates with the increase of loading cycles and the fluctuation range is within 0.05 at the same condition.

(5) The relationship between lateral strain and axial strain is close to linear response under different loading cycles.

(6) The Poisson's ratio of dry specimen is greater than that of wet specimen at the same confining pressure, except that when the confining pressure is 29.4kPa.

(7) It is found that after all specimens were loaded 10000 cycles and showed contractive tendency under the cyclic loading, except that the wet specimen is at confining pressure 29.4 kPa, which shows dilative tendency.

## References:

- Alarcon,G.A., 1986. Cyclic stress–strain and liquefaction characteristics of sands. PhD dissertations. Purdue University, West Lafayette, Indiana.
- Allen,J.J. and Thompson,M.R., 1974. Resilient response of granular material subjected to time-dependent lateral stresses. Trans -portation Research Record 510. Transportation Research Board, Washington, D.C. pp. 1-13.
- Alnedawi,A., Nepal,K.P. and Al-Ameri,R., 2018. Mechanistic behavior of open and dense graded unbound granular materials under traffic loads, Int. J. Geomate, 14 (45), pp. 124-129.
- Araya,A.A., 2011. Characterization of unbound granular materials for pavements [PhD Thesis]. Delft University of Technology.
- Ba,M., Fall,M., Samb,F., Sarr,D. and Ndiaye,M., 2011. Resilient modulus of unbound aggregate base courses from Senegal (West Africa), J Civil Eng, 1 (1), pp. 1-6.
- Barksdale,R., 1971. Compressive Stress Pulse Times in Flexible Pavements for Use in Dynamic Testing. Highway Research Record 345, Highway Research Board, Washington, DC, USA, pp 32-44.
- Barksdale,R.D., 1972. Repeated load test evaluation of base coarse materials, Georgia Highway Department Research Project 7002, Georgia Institute of Technology, Atlanta.
- Behiry,A.E., 2014. Characterization of layered pavement by modeling and calibration of resilient modulus, Am J Civil Eng, 2 (3), pp. 74-86.
- Bennert,T., Papp, W.J., Maher,A. and Gucunski,N., 2000. Utilization of construction and demolition debris under traffic-type loading in base and subbase applications, Transp. Res. Rec., 1714, pp. 33-39.
- Casagrande,A., Hirschfeld,R.C. and Poulos,S.J., 1964. Fourth Report: Investigation of Stress-Deformation and Strength Characteristics of Compacted Clays. HARVARD UNIV CAMBRIDGE MA SOIL MECHANICS LAB.
- CEN, Unbound and hydraulically bound mixtures - Part 7: Cyclic load triaxial test for unbound mixtures, in EN 13286-7., 2004. European Committee for Standardization (CEN): Brussels.
- Cerni,G., Corradini,A., Pasquini,E. and Cardone,F., 2015. Resilient behaviour of unbound granular materials through repeated load triaxial test: influence of the conditioning stress, Road Mater. Pavement Design, 16 (1), pp. 70-88.

Correia,G.A., AnhDan,L.Q., Shinoda,M., Tatsuoka,F. and Koseki,J., 2001. Small strain stiffness under different isotropic and anisotropic stress conditions of two granular granite materials, *Advanced Laboratory Stress-Strain Testing of Geomaterials* (eds. by Tatsuoka et al.), Swets and Zeitlinger Publishers, pp. 209-216.

De Silva,L.I.N., 2004. “Locally Measured Quasi-Elastic Deformation Properties of Geomaterials under Torsional Shear and Triaxial Loadings,” M.S. dissertation, The Univ. of Tokyo, Japan.

Dong,J., Nakamura,K., Tatsuoka,F. and Kohata,Y., 1994. Deformation characteristics of gravels in triaxial compression tests and cyclic triaxial tests, *Pre-failure Deformation of Geomaterials*, Balkema, pp.17-24.

Erlingsson,S. and Rahman,M.S., 2013. Evaluation of permanent deformation characteristics of unbound granular materials by means of multistage repeated-load triaxial tests. *Transp. Res. Rec.*, pp. 11-19.

Goto,S., Tatsuoka,F., Shibuya,S., Kim,Y.S. and Sato,T., 1991. “A Simple Gauge for Local Small Strain Measurements in the Laboratory,” *Soils Found.*, Vol. 31, No. 1, pp. 169-180.

Gu,F, Sahin,H, Luo,X., Luo,R. and Lytton,R.L., 2015. Estimation of resilient modulus of unbound aggregates using performance-related base course properties. *J. Mater. Civ. Eng.*

Hardin,B.O. and Drnevich,V.P., 1972. Shear modulus and damping in soils: design equations and curves, *Journal of the Soil Mechanics and Foundations Division, ASCE*, 98 (7), pp. 667-692.

Hicks,R.G., 1970. “Factors influencing the resilient properties of granular materials,” PhD thesis, University of California, Berkeley, Berkeley, Calif.

Hicks,R.G. and Monismith,C.L., 1971. Factors influencing the resilient properties of granular materials. *Transportation research record no. 345*, Transport Res Board, pp. 15-31.

Hoque,E., Tatsuoka,F. and Sato,T., 1996. Measuring anisotropic elastic properties of sand using a large triaxial specimen, *Geotechnical Testing Journal, ASTM*, 19(4), pp. 411-420.

Hoque,E. and Tatsuoka,F., 1998, “Anisotropy in Elastic Deformation of Granular Materials,” *Soils Found.*, Vol. 38, No. 1, pp. 163-179.

Ishihara,K. and Towhata,I., 1983. Cyclic behaviour of sand during rotation of principal stress axes, *Mechanic of Granular Material: New Models and Constitutive Equations*, (eds. By Jenkins, J. T. and Satake, M.), pp. 53-73.

- Kohata,Y., Tatsuoka,F., Wang,L., Jiang,G.L., Hoque,E. and Kodaka,T., 1997. Modelling the non-linear deformation properties of stiff geomaterials, *Geotechnique*, 47(3), pp. 563-580.
- Kohata,Y. and Jiang,G.L., 1998. Triaxial shear deformation properties of a well-graded crushed gravel subjected to cyclic loading, *RTRI REPORT*, Vol.12, Issue 4, pp. 43-48 (in Japanese).
- Kohata,Y., Tadano,N., Sekin,E., 2001. Deformation properties of single granite subjected to cyclic hysteretic loading, *Journal of railway mechanics*, JSCE No.5, pp. 61-65 (In Japanese).
- Kohata,Y., Miura,K., Iguch,M. and Etsekine,E., 2003. The strength and deformation properties of the single-graind crushed stones on the similar grain size distribution, *Journal of railway mechanics*, JSCE , NO.7, pp. 25-30 (In Japanese).
- Lekarp,F., Isacsson,U. and Dawson, A., 2000. State of the art. I: Resilient response of unbound aggregates, *J. Transp. Eng.*, 126 (1), pp. 66-75.
- Leng,W.M., Mei,H.H. and Nie,R.S., 2016.. Static characteristic research on coarse grained soil filling in heavy haul railway subgrade bed. *J Railw Eng Soc* pp. 23-28.
- Lo Presti,D., Pallara,O., Lancelotta,R., Amandi,M. and Maniscalco,R., 1993. “Monotonic and Cyclic Loading Behavior of Two Sands at Small Strains,” *Geotech. Test. J.*, Vol. 16, No. 4, pp. 409-424.
- Mitchell,J.K., 1993. *Fundamentals of soil behavior*, 2nd edn. Wiley.
- Monismith,C.L., Seed,H.B., Mitry,F.G. and Chan.C.K., 1967. Prediction of Pavement Deflections from Laboratory Tests. *Proceedings of the 2nd International Conference on Structural Design of Asphalt Pavements*, Ann Arbor, Mich., pp. 109-140.
- Nedderman,R.M., 2005. *Statics and kinematics of granular materials* (Digitally printed 1st pbk. version. ed.). Cambridge, UK: Cambridge University.
- Nie,R.S., Sun,B. L., Leng,W.M., Li,Y.F. and Ruan,B., 2021. Resilient modulus of coarse-grained subgrade soil for heavy-haul railway: An experimental study. *Soil Dynamics and Earthquake Engineering*, Volume 150.
- Pouliquen,B., Andreotti,Y. and Forterre,O., 2013. *Granular media : between fluid and solid*. Cambridge: Cambridge University.
- Poulos,S.J., 1971. *The stress-strain curves of soils*. Geotechnical Engineers Incorporated. Chicago.

Reynolds,O., 1886. "Experiments showing dilatancy, a property of granular material, possibly connected with gravitation," Proc. Royal Institution of Great Britain, Read.

Sagaseta,C., Cuellar,V. and Pastor,M., 1991. Cyclic loading, Proc. European Conference on Soil Mechanics and Foundation Engineering, Florence, 3, pp. 981-999.

Seed,H., Mitry,F., Monismith,C. and Chan,C., 1967. Prediction of flexible pavement deflections from laboratory repeated-load tests, NCHRP Report, 35.

Smith,W.S., and Nair,K.,1973. Development of Procedures for Characterization of Untreated Granular Base Coarse and Asphalt Treated Base Course Materials.Report No.FhWA-RD-74-61,Federal Highway Administration, Washington, D.C.

Tao,M., Mohammad,L.N., Nazzal,M., Zhang,Z. and Wu,Z., 2010. Application of shakedown theory in characterizing traditional and recycled pavement base materials. J. Transp. Eng.,136(3), pp. 214-222.

Tatsuoka,F., Nakamura,S., Huang,C.C. and Tani.K., 1990. Strength anisotropy and shear band direction in plane strain tests of sand. Soils Found 30(1), pp. 35-56.

Tatsuoka,F. and Shibuya,S., 1992, "Deformation Characteristics of Soils and Rocks From Field and Laboratory Tests," Proceedings of 9th Asian Regional Conference of SMFE, Vol. 2, Bangkok, Thailand, pp. 101-170.

Tatsuoka,F. and Kohata,Y., 1995. "Stiffness of Hard Soils and Soft Rocks in Engineering Applications," Proceedings of International Symposium on Pre-failure Deformation of Geomaterials, S. Shibuya, T. Mitachi and S. Miura, Eds., Balkema, Rotterdam, The Netherlands, pp. 947-1063.

Teachavorasinskun,S., Tatsuoka,F. and Lo Presti,D. C. F., 1994. Effects of the cyclic prestraining on dilatancy characteristics and liquefaction strength of sand, Pre-failure Deformation of Geomaterials, Balkema, pp. 75-80.

The Aggregate Handbook, 1993. National Stone Association, Washington, D.C.

Tokimatsu,K., Yamazaki,T. and Yoshimi,Y., 1986. Soil liquefaction evaluations by elastic shear moduli, Soils and Foundations, 26(1), pp. 25-35.

Tutumluer,E. and Seyhan,U., 1999. Laboratory Determination of Anisotropic, Aggregate Resilient Moduli Using a New Innovative Test Device in 78th Annual, Meeting of the Transportation Research Board Specialty Session on "Determination of Resilient Modulus for Pavement Design". Washington DC.

Werkmeister,S., 2003. Permanent deformation behavior of unbound granular materials. Ph.D. Dissertation, University of Technology, Dresden, Germany.

Werkmeister,S., Dawson,A.R. and Wellner,F.,2001. Permanent deformation behavior of granular materials and the shakedown concept. Transp. Res. Rec., pp. 75-81.

Wu,P.K., Matsushima,K. and Tatsuoka,F., 2008. Effects of specimen size and some other factors on the strength and deformation of granular soil in direct shear tests. Geotech Test J 31(1), pp. 1-20

**CHAPTER 6**  
**CONCLUSIONS**



## 6.1 Introduction

This research focuses on an attempt to use a new lightweight geo-material to replace the traditional upper subbase material. The cause of the out-of-trend data of the testing is not test variability or test error because of 1 specimen in 1 test condition. Based on the results and discussion, the following conclusions and recommendations were drawn.

## 6.2 Effect of cyclic loading on strength deformation of specimen (Chapter 3)

This chapter analyzed the effects of cyclic loading on the strength and deformation of specimens by the monotonic triaxial test.

- (1) The behavior of deviator stress- axial strain shows a characterized as strain softening.
- (2) The deviator stress- axial strain curve after cyclic loading appears S-shaped before the deviator stress 60 kPa.
- (3) The cyclic loading increases the  $q_{max}$  in the dry specimen. However, it has little effect on wet samples.
- (4) The cyclic loading increases the cohesion and decreases the friction angle in the specimen.
- (5) The cyclic loading increases the  $E_0$  and  $E_{tan}$  in the specimen.
- (6) The  $E_0$  increases with the increase of confining pressure.
- (7) In the case with cyclic loading, the  $E_{tan}$  tends to increase with the progress of shear, and then it turns to decrease.

## 6.3 Effect of dry and wet state on strength deformation of specimen (Chapter 4)

This chapter analyzed the effects of moisture on the strength and deformation of specimens by the monotonic triaxial test.

- (1) The deviator stress sharply also increases to the peak stress at an axial strain of about 0.5 % with the increase of the axial strain, and then it decreased slowly.
- (2) The deviator stress of dry specimen was greater than the case in the wet specimen.
- (3) The increase of the  $q_{max}$  in the specimen had an almost linear relationship with confining pressure.

(4) The  $E_{tan}$  of dry specimen was greater than the case in the wet specimen.

(5) The existence of water reduces the friction angle, increases the cohesion of particles, and reduces the strength and deformation modulus.

## 6.4 Deformation characteristics of specimen under cyclic loading (Chapter 5)

This chapter analyzed the effects of moisture, confining pressure and number of the cyclic loading on the deformation characteristics of specimen during cyclic loading by the cyclic triaxial test.

(1) The  $E_{eq}$  of specimen increases with the increase of confining pressure. The influence of confining pressure on the equivalent young's modulus in the wet specimen is greater than the case in the dry specimen.

(2) The  $E_{eq}$  of dry specimen is greater than the case in the wet specimen. As the confining pressure of specimen increases, the influence of moisture content on the equivalent young's modulus becomes more reduced.

(3) The number of loading cycles has not greater impact on the  $E_{eq}$  in this study. The shakedown range boundaries of the specimen under all conditions belong to range A.

(4) The relationship between lateral strain and axial strain is close to linear response under different loading cycles.

(5) All specimens showed contractive tendency under the cyclic loading, except that the wet specimen is at confining pressure 29.4 kPa, which shows dilative tendency.

## 6.5 Recommendations

Based on the testing and conclusions, the following recommendation are made:

(1) The test material for this study was composed of artificial lightweight coarse aggregate and standard sand mixed at a mass ratio of 1: 1. The next research experiment can adjust the mass ratio, optimize the grain-size distribution and reduce the weight of the mixture.

(2) Resilient characteristics of lightweight geo-materials during cyclic loading are basically insensitive to stress history. Therefore, large numbers of resilient tests can be carried out sequentially on the same specimen to determine the resilient parameters of the material. Such as, performing three confining pressures on the same

specimen to analyze the deformation characteristics under cyclic loading. In this way, the data error caused by different specimens can be solved.

(3) In order to more clearly study the dilatancy of the specimen, the dilatancy of the specimen also should be analyzed on monotonic triaxial test.

(4) The next work can consider the relationship between static parameters and dynamic parameters.